Tampere University

Vilma Lampinen

WET BONDING OF SOFT ELASTOMERIC MICROCHANNELS

Master of Science Thesis
Faculty of Medicine and Health Technology
Examiners: Prof. Pasi Kallio,
Assoc. Prof. Veikko Sariola
November 2022

ABSTRACT

Vilma Lampinen: Wet Bonding of Soft Elastomeric Microchannels
Master of Science Thesis
Tampere University
Master's Programme in Biotechnology and Biomedical Engineering
November 2022

In microfluidics small amounts of fluids are circulating in channels with maximum dimensions in hundreds of micrometers. Poly(dimethylsiloxane) (PDMS) elastomers and especially commercial Sylgard 184 (Dow Corning) is widely used for fabrication of microfluidic devices due to its advantageous chemical and mechanical properties. As stretchability and softness of Sylgard 184 are limited, softer elastomers from Dragon Skin and Ecoflex product families (Smooth-On) are commonly used in applications that demand more deformability from the material. Fabrication of soft microchannels from these silicone elastomers is conducted with cast molding and layer-by-layer stacking. To create closed channels, the open channels are sealed to a flat elastomer substrate. Sylgard 184 can be sealed with oxygen plasma bonding where the increased number of functional groups form the bond between oxygen plasma treated surfaces. This method is not applicable for most softer elastomers due to silicone oils that are diffusing to the surface preventing the bonding. As an alternative, a thin layer of uncured elastomer can be used as adhesive between the layers. This bonding technique is relatively unreliable as the uncured elastomer easily flows to the open channels blocking the channel. The capillary action can be reduced by decreasing the thickness of the layer and partially curing it before bonding. Softness of the elastomer also effects on the dimensions of producible microchannels. The ceiling of the channel can collapse, or the channel walls can pair before bonding if the dimensions are not suitable for the elastomer.

In this work, the soft microchannels are fabricated from commercial elastomers Dragon Skin 30, Ecoflex 00-50 and Ecoflex 00-20 by bonding the elastomer substrates with the adhesive layer to enhance reliability and reproducibility of the fabrication technique. The adhesive layer is spread evenly with a spin coater. Thus, spin speed and spin time together with viscosity of the elastomer are determining the thickness of the layer. The layer is partially cured in an oven at elevated temperature. Different spin speeds and pre-curing times are tested to find suitable parameters for each elastomer for the reliable fabrication process. Different channel widths and separations are used to discover the range of producible microchannel dimensions for these soft elastomers. The study revealed that the capillary action can be decreased but not totally prevented. Based on the results, 2000 RPM spin speed and 20-40 seconds pre-curing in oven at 60°C are proposed for the reliable and reproducible fabrication process with Ecoflex 00-50 and Ecoflex 00-20. The same spin speed is recommended for Dragon Skin 30, but pre-curing the layer is not required. Microchannels with 50 µm width are producible with Dragon Skin 30 as well as 50 µm thick channel walls. That narrow and dense channels were unfeasible with softer Ecoflex 00-50 and Ecofelx 00-20.

In addition, a soft pneumatic strain sensor was fabricated from Ecoflex 00-50 to show a practical example of the studied bonding technique. The sensor changes its pneumatic resistance as response to deformation of the embedded microchannel while external force is applied. The fabricated soft strain sensor can tolerate at least 300% strain, has negligible hysteresis, and can be used to measure large strains with gauge factor close to 1.

Keywords: soft microfluidics, silicone elastomers, wet bonding, soft strain sensor

TIIVISTELMÄ

Vilma Lampinen: Pehmeiden elastomeeristen mikrokanavien märkäliimaus
Diplomityö
Tampereen yliopisto
Bioteknologian ja biolääketieteen tekniikan maisteriohjelma
Marraskuu 2022

Mikrofluidistiikassa pieniä määriä nesteitä ja kaasuja kiertää kanavissa, joiden halkaisijat ovat korkeintaan satoja mikrometrejä. Erityisesti kaupallista Sylgard 184 -silikonielastomeeriä (Dow Corning) on käytetty paljon mikrofluidististen laitteiden valmistuksessa sen kemiallisten ja mekaanisten ominaisuuksien takia. Pehmeämpiä elastomeerejä Dragon Skin ja Ecoflex -tuoteperheistä (Smooth-On) hyödynnetään sovelluksissa, joiden vaatimuksiin Sylgard 184:n venyvyys ja pehmeys ei riitä. Pehmeät mikrokokoiset kanavat valmistetaan tällaisista materiaaleista valamalla nestemäinen elastomeeri muottiin sekä kasaamalla kovettuneet valokset yhteen kerros kerrokselta, jolloin muotteihin valetut avoimet kanavat suljetaan tasaista elastomeeripalasta vasten. Sylgard 184 -tuotteesta valmistetut kerrokset voidaan liimata yhteen pintakäsittelemällä valettu elastomeeri happiplasmalla. Pintakäsittely kasvattaa elastomeerin pinnan funktionaalisten ryhmien määrää. Kun plasmakäsitellyt pinnat tuodaan yhteen, funktionaaliset ryhmät muodostavat vahvoja kovalenttisia sidoksia pintojen välille kiinnittäen ne yhteen. Pehmeämmät silikonielastomeerit sisältävät silikoniöljyä, joka diffundoituu elastomeerin pinnalle estäen sidoksien muodostumisen. Vaihtoehtoinen tapa sitoa kerrokset yhteen, on käyttää samaa elastomeeriä liimana kerrosten välissä. Menetelmä on kuitenkin verrattain epäluotettava, sillä nestemäinen elastomeeri nousee helposti kapillaarivoimien avulla avoimeen kanavaan tukkien sen. Kapillaari-ilmiö voidaan välttää tekemällä liimakerroksesta mahdollisimman ohut sekä osittain kovettamalla nestemäistä elastomeeriä. Lisäksi elastomeerin pehmeys rajoittaa valmistettavien kanavien kokoa: vierekkäisten kanavien seinämät voivat alkaa nojata toisiinsa muotista irrottamisen jälkeen tai valmiin kanavan katto voi romahtaa, jos kanavien mitat ovat kyseiselle elastomeerille epäsopivat.

Tässä työssä valmistetaan kaupallisista Dragon Skin 30, Ecoflex 00-20 ja Ecoflex 00-50 -elastomeereistä pehmeitä mikrokanavia kiinnittäen elastomeerikerrokset yhteen käyttäen samaa elastomeeriä liimana kerrosten välissä. Työn tarkoituksena on parantaa menetelmän luotettavuutta ja toistettavuutta. Liimakerros levitetään tasaisesti pyörimispinnoitus-menetelmällä, jossa pyörimisnopeus, pyörimisaika sekä nestemäisen elastomeerin viskositeetti määrittävät liimakerroksen paksuuden. Kerros kovetetaan osittain 60 asteisessa uunissa levityksen jälkeen. Työssä testataan eri pyörimisnopeuksia, kovettamisaikoja sekä kanavakokoja, jotta löydetään luotettavan valmistuksen takaavat parametrit työssä käytetyille elastomeereille. Tulokset osoittavat, ettei kapillaari-ilmiötä voida täysin välttää, mutta sitä pystytään vähentämään riittävästi valmistustavan luotettavuuden parantamiseksi. Tulosten perusteella luotettavaan ja toistettavaan valmistukseen suositellaan 2000 RPM:n pyörimisnopeutta sekä 20–40 sekunnin kovetusta 60 asteisessa uunissa Ecoflex 00-50 ja Ecoflex 00-20 -elastomeereille. Samaa pyörimisnopeutta suositellaan käytettäväksi Dragon Skin 30 kanssa, mutta se ei vaadi liimakerroksen osittaista kovettamista. Mikrokanavia, joiden leveys tai seinämän paksuus oli 50 µm, pystyttiin valmistamaan Dragon Skin 30:ta, muttei pehmeämmistä Ecoflex 00-50 ja Ecoflex 00-20 -elastomeereistä.

Lopuksi tässä työssä tutkitulle valmistustekniikalle esitellään käytännön esimerkki. Ecoflex 00-50 -elastomeeristä valetaan pehmeä venymäanturi, jonka sisältämän mikrokanavan pneumaattinen resistanssi muuttuu anturia venyttäessä. Valmistettu pehmeä venymäanturi kestää ainakin 300 %:n venytystä. Anturin hystereesi on olematon, ja se sopii vakauskertoimensa (~1) perusteella suurten venymien mittaamiseen.

Avainsanat: pehmeä mikrofluidistiikka, silikonielastomeeri, märkäliimaus, pehmeä venymäanturi

PREFACE

This work was done in the Bioinspired Materials and Robotics group in the Faculty of Medicine and Health Technology in Tampere University. I would like to thank my supervisor and examiner, Assoc. Prof. Veikko Sariola for the opportunity, guidance, and support. I am grateful to my other supervisor, Dr. Anastasia Koivikko for mentoring me and also for all the help, motivation, and inspiration with the thesis work and outside of that. In addition, I would like to thank Dr. Vipul Sharma for performing the SEM imaging of my microchannels.

Lastly, I would like to thank my family and friends for endless support during this work and over the years.

Tampere, 18.11.2022

Vilma Lampinen

CONTENTS

1. INTRODUCTION 1
2. BACKGROUND 4
    2.1 Soft Silicone Elastomers for Soft Devices 4
    2.2 Soft Microfluidic Devices 8
    2.3 Soft Strain Sensors 14
3. AIMS OF THE STUDY 19
4. MATERIALS AND METHODS 21
    4.1 Soft Silicone Elastomers and Mold Design 21
    4.2 Mold Fabrication with Photolithography 23
    4.3 Fabrication of Soft Elastomeric Microchannels 24
    4.4 Evaluation of Fabricated Microchannels and Statistical Analysis 26
    4.5 Fabrication and Characterization of Soft Pneumatic Strain Sensor 27
5. RESULTS AND DISCUSSION 29
    5.1 Fabrication of Soft Elastomeric Microchannels with Wet Bonding 29
    5.2 Soft Pneumatic Strain Sensor 41
6. CONCLUSIONS AND FUTURE WORK 46
REFERENCES 49
APPENDIX: RESULTS OF THE MICROCHANNEL FABRICATION 55

LIST OF FIGURES

Figure 1. *Variables describing softness.* ***a*** *Approximate Young's modulus of selected biological tissues and materials used for microfluidics and sensor fabrication. Modified from [3], [14].* ***b*** *Rough estimation of the relation between Young's modulus and Shore hardness scales for silicones. Modified from [15].* *4*

Figure 2. *Schematic illustrations of a flexible microchannel.* ***a*** *Undeformed microchannel.* ***b*** *Cross-section of deformed microchannel perpendicularly to the flow.* ***c*** *Cross-section of deformed microchannel parallely to the flow. All modified from [3].* *9*

Figure 3. *Schematic illustrations.* ***a*** *Fabrication process of microchannels with silicone casting. Modified from [2].* ***b*** *Capillary action of uncured adhesive silicone layer. Modified from [53].* ***c*** *Channel dimensions (i) and related problems: lateral collapse or "pairing" (ii) and sagging (iii). Modified from [12].* *12*

Figure 4. *Parameters affecting the reliability of microchannel fabrication with wet bonding process.* *19*

Figure 5. *Pattern of channel networks used in this study: (i) 100 µm wide channels with 200 µm wall thickness and 50 µm wide channels with 100 µm wall thickness, (ii) 200 µm wide channels with 200 µm wall thickness and 100 µm wide channels with 100 µm wall thickness, (iii) 200 µm wide channels with 100 µm wall thickness and 100 µm wide channels with 50 µm wall thickness, and (iv) 400 µm wide channels with 400 µm wall thickness and 800 µm wide channels with 800 µm wall thickness.* *22*

Figure 6. *Microchannel fabrication with wet bonding process.* ***a*** *Fabrication of open microchannels with replica molding, curing and demolding.* ***b*** *Spin coating thin layer of uncured elastomer on top of fabricated flat elastomer substrate.* ***c*** *Partially curing the adhesive elastomer layer in the oven.* ***d*** *Placing the elastomer substrate with open channels on top of the adhesive layer.* ***e*** *After curing, cutting the microchannel network with open inlet and outlet from the substrate and filling with colorful liquid for visualiazation.* *25*

Figure 7. *Soft pneumatic strain sensor.* ***a*** *Schematic of the strain sensor and its pneumatic circuit containing pneumatic resistor R_c and the strain sensor R in series as the sensor is vented to atmospheric pressure P_{atm}. A pressure sensor measures the pressure P_{gauge} between the resistor and the strain sensor.* ***b*** *Electrical circuit corresponding to the pneumatic circuit.* ***c*** *Measurement setup for the strain sensor. All reported also in [10].* *27*

Figure 8. *Thickness of spin coated layer.* ***a*** *Thickness of the spin coated layer as function of spin speed for the soft silicone elastomers.* ***b*** *Cross-sectional micrographs of the spin coated layers with different spin speeds. Scale bar: 100 µm.* *29*

Figure 9. *Scanning electron micrographs of fabricated microchannels.* ***a*** *Open 200 µm wide channels from Ecoflex 00-50 with 300 µm wall thickness.* ***b*** *Open 50 µm and 100 µm wide channels from Dragon Skin 30 with 100 µm and 200 µm wall thickness respectively.* ***c & d*** *Cross-sectional micrographs of 200 µm high and 200 µm wide microchannels fabricated from Ecoflex 00-50 by wet bonding with 2500 RPM spin speed and 40 s pre-curing time at 60°C.* *30*

Figure 10. *Overview of the channel fabrication results.* ***a*** *Yields of channels grouped by material ($p < 0.0001$).* ***b*** *Micrograph of 200 µm and*

100 µm wide channels with AR (D/L) as 1 fabricated from Dragon Skin 30 with 2500 RPM spin speed and 40 s pre-curing time at 60°C. Channels are filled with pink liquid to visualize them. Scale bar: 500 µm. ***c*** *Yields of channels grouped based on spin speed ($p < 0.0001$).* ***d*** *Yields of channels grouped by pre-curing time ($p < 0.0001$).* **e** *Yields of channels grouped based on the geometry of the channel ($p < 0.0001$). 32*

Figure 11. *Yields of microchannels per soft silicone elastomers Dragon Skin 30 (DS30), Ecoflex 00-50 (EF50) and Ecoflex 00-20 (EF20).* ***a*** *Yields for spin speeds grouped by material.* ***b*** *Yields for pre-curing times grouped by material.* ***c*** *Yields for channel geometries grouped by material. 33*

Figure 12. *Micrographs of fabricated microchannels.* ***a*** *Undulation,* ***b*** *deformation, and* ***c*** *lateral collapse and undulation of 100 µm wide open channels with 50 µm wall thickness fabricated from Ecoflex 00-50.* **e**, ***d*** *Lateral collapse of 50 µm wide open channels with 100 µm wall thickness fabricated from Ecoflex 00-50 and Ecoflex 00-20 respectively.* ***f*** *Blocked 50 µm wide closed channels with 100 µm wall thickness fabricated from Ecoflex 00-20 without partially curing the adhesive layer applied with 1500 RPM spin speed.* ***g*** *Lateral collapse of 50 µm wide open channels with 200 µm wall thickness before and* ***h*** *after stretching (Ecoflex 00-20).* ***i*** *Unsuccessful 100 µm wide closed channels with 50 µm wall thickness fabricated from Ecoflex 00-20 with pre-curing the adhesive layer (1500 RPM spin speed) for 20 s. All scale bars: 500 µm. 35*

Figure 13. *Follow-up study for Ecoflex 00-20.* ***a*** *Yields for different channel geometries fabricated from Ecoflex 00-20.* ***b*** *Micrograph of 80 µm wide embedded channels with 140 µm wall thickness fabricated from Ecoflex 00-20 with wet bonding process (2000 RPM, 20 s at 60°C).* ***c*** *Micrograph of 50 µm wide embedded channels with 300 µm wall thickness fabricated from Ecoflex 00-20 by spin coating the adhesive layer with 2000 RPM and without partially curing it.* ***d*** *Micrograph of 50 µm wide closed channels with 200 µm wall thickness fabricated from Ecoflex 00-20 with wet bonding process (2000 RPM, 40 s at 60°C). Channels filled with colorful liquid to visualize them. All scale bars: 500 µm. 37*

Figure 14. *Soft pneumatic strain gauge.* ***a*** *Relative change in pneumatic resistance as function of engineering strain for five strain sensor samples. Each curve is an average of five measurements with one sample. Error bars represent standard deviation ($n = 5$).* ***b*** *Gauge factor (average of five strain gauges) calculated from the data of the measurement expressed in* ***a*** *with Equation 5. Shaded blue area represent standard deviation ($n = 5$).* ***c*** *Hysteric behavior of the strain sensor while stretching the sensor five times up to 50% engineering strain with 0.01 mm/s strain rate.* ***d*** *Pictures of the pneumatic strain sensor as relaxed (I), stretched (II), twisted (III) and bent (IV). Blue liquid is used to fill the microchannel for visualization. All scale bars: 1 cm. All reported also in [10]. 42*

LIST OF SYMBOLS AND ABBREVIATIONS

3D	Three-dimensional
AR	Aspect ratio
df	Degrees of freedom
DS30	Dragon Skin 30
EGaIn	eutectic Gallium-Indium
EF50	Ecoflex 00-50
EF20	Ecoflex 00-20
GF	Gauge factor
PDMS	Poly(dimethylsiloxane)
UV	Ultraviolet
A	Cross-sectional area of a microchannel
ε	Engineering strain
D	Width of a microchannel
E_i	Theoretical or expected value
H	Height of a microchannel
L	Wall thickness of a microchannel
O_i	Observed value
P_{atm}	Atmospheric pressure
P_{gauge}	Pressure inside the pneumatic strain gauge
P_{supply}	Supply pressure
Q	Initial flow rate
R	Pneumatic resistance of the strain gauge
R_c	Pneumatic resistance of the constant pneumatic resistor
$\Delta R/R_c$	Relative change in pneumatic resistance
Δp	Pressure drop

1. INTRODUCTION

Microchannels with maximum dimensions in hundreds of micrometers are the main components of microfluidic systems. In microfluidic devices, small amounts of fluids are circulating in a microchannel network containing valves, pumps, mixers, and other elements to control and process the fluid. Originally the microfluidic systems were fabricated from rigid materials—for example glass or silicon—with photolithography and related techniques adopted from the field of microelectronics. [1] Polymeric materials—in particular, poly(dimethylsiloxane) (PDMS)—have replaced the conventional materials due to relatively low costs, conventional fabrication processes, and attractive mechanical and chemical properties such as elasticity, nontoxicity, permeability to gases, optical transparency, low surface energy and chemically inert nature. As a silicone elastomer, PDMS has high compliance and can withstand large strains, it is used especially in applications that demand elasticity and deformability from the microfluidic construct (e.g., biomimetic cell culturing devices, microvalves, and micropumps). [2] Currently, elastomers of Sylgard product family manufactured by Dow Corning and especially Sylgard 184 (Shore A hardness 50) are the most implemented PDMS kits in the field of microfluidics. However, increased interest of soft devices such as soft microfluidic systems or soft electronics has created a need for even more compliant materials than Sylgard 184. Commercial Dragon Skin (Shore A hardness 10–30) and Ecoflex (Shore 00 hardness 10–50) series (Smooth-On) are widely used elastomers in applications that can withstand more strain than can be achieved with Sylgard 184 [3]. Even though the chemical structure or filler content of these silicones are not provided by the manufacturer, recent studies reveal that they are PDMS elastomers with silica fillers [4], [5].

Soft wearable microfluidic sensors have been used to continuously measure physiological state by analysing biofluids including sweat, saliva, and tears collected from the user. Soft microchannels are used in these devices to transport the fluidic samples to the sensing elements for chemical analysis. [6] Heartbeat, respiration and posture or movement of the body can be detected with wearable mechanical microfluidic sensors, fabricated from soft elastomers [7]. In addition, such sensors can be integrated into soft robots which are robots made from compliant materials. The sensors provide intelligence and perception to the robot, essential for the development of autonomous systems. [8] Soft

strain sensors are typically resistive sensors, made by filling soft elastomer microchannels with liquid metals or ionic liquids, or by integrating conductive fillers to the elastomer. Stretching or compressing the conductive matter changes its electrical resistance. This provides the ability to transduce external stimuli to electrical signals. Microchannels filled with conductive fluid can also be used to fulfil the soft electrical system as flexible and stretchable interconnections between circuit elements. [9] Another approach proposed in our recent work [10] is to use soft microchannels filled with pressurized air as the sensor. The operation is based on change in pneumatic resistance instead of electrical resistance as with typical microfluidic strain sensors made of liquid metals or ionic liquids. Stretching of the sensor deforms the dimensions of the microchannel changing the resistivity of the channel to fluid flow. [10]

Fabrication of microchannels from soft silicone elastomers—such as PDMS—is done with well-known cast molding method including casting the pre-mixed elastomer in liquid form to a mold to create an elastomer substrate with open microchannels and cavities. The substrate with open microchannels is then sealed against another elastomer substrate to form closed channels. The advantage of Sylgard 184 is that sealing it to itself and other materials including glass and silicon is relatively easy since it can be performed with plasma bonding [2]. Treating the surface of the Sylgard 184 substrates with oxygen plasma increases the number of silanol (SiOH) groups at the surface of the PDMS elastomer. When the surfaces treated with oxygen plasma are brought together, the functional groups form a strong irreversible seal between the surfaces. The same technique does not work with softer PDMS elastomers since silicone oils softening the elastomer diffuse to the surface preventing the plasma bonding [11]. Thus, alternative methods are needed for fabrication of softer devices.

One option to bond softer PDMS elastomers than Sylgard 184 is to use a thin layer of uncured elastomer as an adhesive between the layers. The layer can be spread evenly to the surface of the flat elastomer substrate with different techniques such as spin coating or bar coating. The problem of this bonding method is that the uncured layer of the elastomer easily flows into the open microchannels and cavities due to capillary forces, blocking the channels and decreasing the reliability of the fabrication process. This can be reduced by making the adhesive layer as thin as possible and by partially curing it before bonding. However, curing the adhesive layer too much can result in a weak seal. [11] In addition, softness of the elastomer limits the dimensions of channels that can be fabricated. The walls of open microchannels can collapse laterally and the ceiling of the bonded closed channel can sag, if the dimensions of the channels are unsuitable

for the elastomer. [12] These issues are reflected in the reliability of the fabricated microfluidic device.

In this work, microchannels in commercial soft PDMS elastomers (Dragon Skin 30, Ecoflex 00-50 and Ecoflex 00-20) are fabricated by using a thin adhesive layer of the elastomer to seal open microchannels to a flat elastomer substrate. The adhesive layer is the same PDMS elastomer as the rest of the device and it is spread evenly on the surface of the flat substrate with a spin coater. As the capillary action and blocking of the channels can be reduced by decreasing the thickness and by pre-curing the adhesive layer, different spin speeds and pre-curing times are tested. The pre-curing is done at elevated temperature, in an oven. In addition, varying channel widths and wall thicknesses are tested, to find out what are the ranges of channel dimensions that can be reliably produced using the studied method and materials. Based on this study, suitable parameters for the reliable and reproducible microchannel fabrication are proposed.

A practical application of the studied bonding method is given by fabricating a soft pneumatic strain sensor from Ecoflex 00-50 with the method. The response of the soft microfluidic strain sensor to varying strain rates is characterized to demonstrate that fabricated pneumatic microchannel meandering in soft elastomer can be used to measure large strains. The novel microfluidic strain sensor has recently been reported by Koivikko et al. [10]. The measurements and characterizations of the pneumatic strain sensor represented in this thesis are executed together with A. Koivikko.

2. BACKGROUND

2.1 Soft Silicone Elastomers for Soft Devices

The soft materials used in soft microfluidic devices, soft sensors, and soft robots are typically soft silicone elastomers, rubbers or thermoplastic polymers [13], [14]. These soft materials are viscoelastic and have low Young's modulus close to biological tissues such as human skin [14]. Young's modulus describes stiffness of the material when straining force is applied lengthwise. Higher modulus corresponds to stiffer material. Hence, devices made from soft materials with low modulus are reducing the mismatch between conventional rigid materials and biological matter or organisms as seen in the Young's modulus spectrum expressed in Figure 1a.

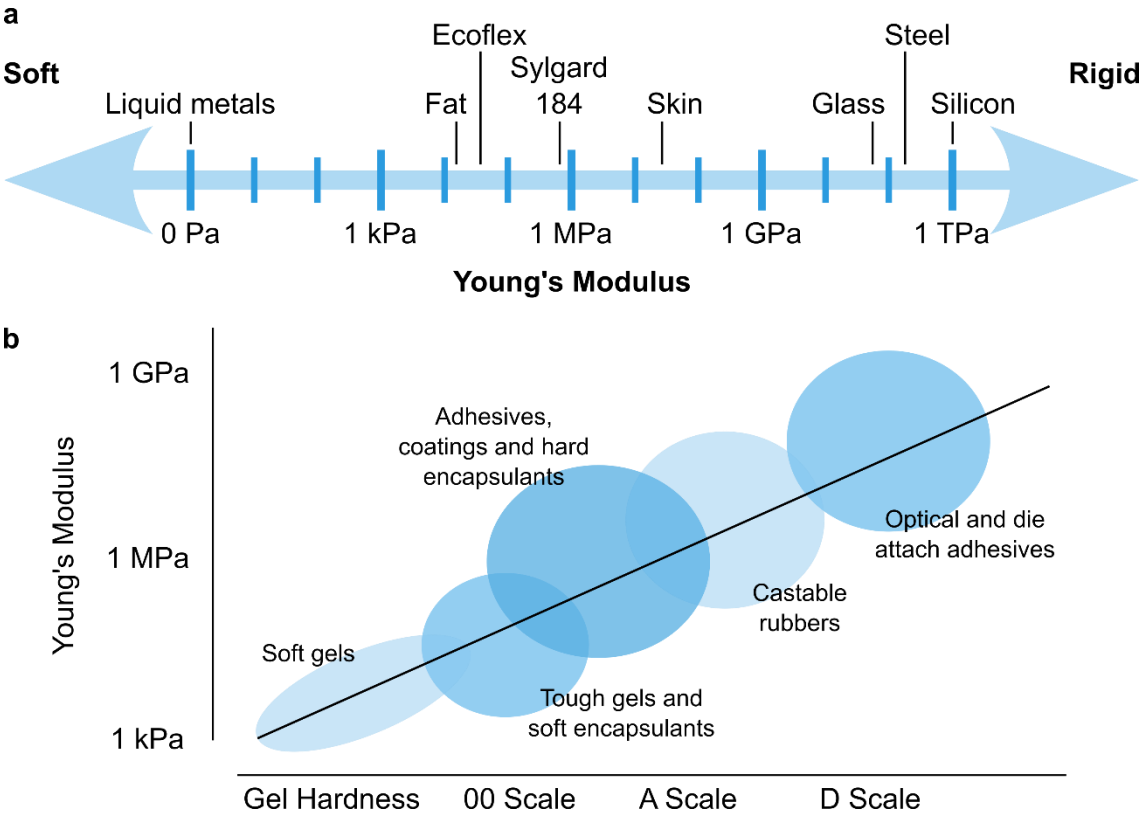

Figure 1. Variables describing softness. **a** Approximate Young's modulus of selected biological tissues and materials used for microfluidics and sensor fabrication. Modified from [3], [14]. **b** Rough estimation of the relation between Young's modulus and Shore hardness scales for silicones. Modified from [15].

Softness of elastomeric material can also be described with Shore hardness scales as Shore hardness value express the elastic behavior of the material. There is no straight relation between Young's modulus and Shore hardness value but rough estimations and approximate correlations exist as expressed in Figure 1b [15], [16]. Shore hardness test

is used in elastomer industry to evaluate resistance of the material to indentation. The material is compressed with a durometer by a constant force and depth of developed indentation is measured and defines the Shore hardness value that is a dimensionless number in range from 0 to 100. Lower value indicates softer material. The depth is dependent on the softness and viscoelasticity of the material, shape of the durometer's indenter, and duration of the test. ASTM D2240 standard includes seven durometer types: D, D0, B, C, A, 0, and 00 from harder to soft. [17] These durometer types are used for materials with different properties and correspond to Shore hardness scales. The scales are overlapping each other enabling comparison between Shore hardness values from different scales. In general, Shore A hardness scale is used for soft elastomers to hard and inflexible elastomers, and Shore 00 hardness scale for gels and very soft elastomers.

Silicones or in other words polysiloxanes are synthetic polymers with an inorganic siloxane backbone and two organic groups such as methyl, ethyl, phenyl, or vinyl attached to each silicon atom. The organic groups are defining the chemical, mechanical and thermophysical properties of the silicone. For example, PDMS has the siloxane backbone with two methyl groups bonded to the silicon atoms. In addition to the side chains, length of the siloxane back bones, crosslinking of the polymer chains and possible filler content affect the properties of the silicone. Silicones are generally chemically inert and stable tolerating extreme environments and temperatures ranging from -50°C to 300°C. They can appear as liquids, gels, elastomers, or hard plastics depending on consistency. Cross-linked polymer chains of the elastomers are normally entangled and thus they have ability to stretch or compress under external loading returning to original shape after release of the loading. Silicone elastomers can tolerate large strains (even 1000% or more [18], [19]), have high deformability and low stiffness.

PDMS elastomers such as Sylgard 184 are one of the most common silicone elastomers used in soft devices and especially in microfluidics due to their valuable physical and chemical properties, inexpensiveness, and fabrication possibilities. The properties of Sylgard 184 are well-studied. Its optical transparency, chemical inertness, ability to cure at low temperatures, good thermal stability, nontoxicity, low autofluorescence and biocompatibility are beneficial especially for biological or chemical applications [2]. Gas permeability of the PDMS elastomers is an advantage in applications where for example gas separation is needed but can also cause problems for example in analytical microfluidic devices. The results of the analytical device can be distorted due to vapor loss or change in pH if carbon dioxide diffuses. [20] Strong hydrophobic nature and heterogenous sur-

face charge of the elastomer can also be complicate in biological applications since wetting of the surface with aqueous media is poor, and proteins, analytes, drugs, and other small molecules are non-specifically adsorbed to the surface. Thus, surface modification of PDMS elastomers is typically required to alter the surface to be hydrophilic and protein-resistant for example for microfluidic cell culture and immunoassay devices. [21], [22]

One of the main advantages of Sylgard 184 and other PDMS elastomers of Sylgard product family is that they can both reversibly or irreversibly seal to itself or other surfaces such as glass, silicon, or thermoplastics. This enables fabrication of microchannels, encapsulation and sealing other materials and structures. The reversible seal is based on van der Waals contact creating a waterproof bond. However, this seal can maintain pressures up to only 30 kPa. Irreversible bonding can tolerate over five times higher pressures and is achieved by altering the surface properties of Sylgard 184. [2] The PDMS elastomer and usually also the second surface of other material are exposed to oxygen plasma to oxidize the surfaces. After the oxidation the surfaces are brought to contact and irreversible bonding occurs when silanol (SiOH) groups form strong covalent bonds with appropriate functional groups of the other surface.

Deformability of the PDMS elastomers enables fabrication of different microfluidic components such as valves, pumps and switches for soft devices [2]. In addition, flexibility and stretchability of PDMS makes it one of the most commonly used polymer as support material in soft sensors [7]. Silicone elastomers are not naturally conductive, but the conductivity can be added to the elastomer matrix for example with a dispersed phase of solid particles such as carbon black, carbon nanotubes or silver nanoparticles and nanowires. [57] In addition, liquid metals and other conductive liquids are simple to embed into PDMS elastomer to produce flexible and stretchable electronics [13], [23], [24].

The mechanical properties of PDMS elastomers can be tailored to be more flexible and softer by altering for example the mixing ratio or curing conditions of the two-component elastomer. In general, increasing amount of cross-linking of the polymer network increases the stiffness of the elastomer similarly as the maximum elongation at break and durability decreases. The commercial Sylgard 184 among other PDMS kits is a two-component elastomer mixed from the curing agent and the base polymer in the ratio 1:10 of weight and cured in heat (e.g., 35 minutes at 100°C). It can tolerate repetitive bending but fractures already at 140% strains. Lower mixing ratio leads to lower modulus but decreases the ultimate tensile strength of the elastomer [25], [26]. For example, Wang et al. [26] obtained 0.56 MPa modulus with 1:33 mixing ratio compared to 2.61 MPa modulus with 1:10 mixing ratio. Similarly lower curing temperature makes Sylgard 184

able to tolerate higher strains and decreases the modulus: 1.32 MPa modulus when cured at 25°C and 2.97 MPa modulus when cured at 200°C [27]. However, there are limits in how much the curing temperature or the amount of curing agent can be reduced. Since higher tear resistance and ability to undergo high elongation at break is advantageous for materials of soft devices, usability of Sylgard 148 is limited [11].

There are also other commercial PDMS elastomer brands such as Dragon Skin and Ecoflex series (Smooth-On) that are available in several Shore hardness values. Thus, they are overcoming some physical limitations related to the flexibility, stretchability, and softness of Sylgard 184. Shore hardness values of the Dragon Skin (10A–30A) and Ecoflex (00-10–00-50) product series [18], [19] are in general lower than those of Sylgard 184 (Shore A hardness 50). Similarly, larger elongation at break (1000%) can be achieved with Dragon Skin and Ecoflex silicones. The cross-linking density in the elastomers of Dragon Skin and Ecoflex series is thus lower than with Sylgard 184. Higher elongation at break and softness makes the elastomers from Dragon Skin and Ecoflex series more suitable to components with larger deformations. Yet, according to the data sheets [18], [19] the maximum strain before fracturing is not increasing together with the Shore hardness and softness which must be considered when selecting PDMS elastomer form these product families.

Dragon Skin and Ecoflex elastomers are commonly used for fabrication of soft sensors and soft robots [7], [28]–[31] as they have high stretchability and durability. They cure in rather short time ranging from several minutes to few hours, depending on the temperature. Shrinking during curing of these two-component elastomers is negligible (~0.1%) and they have a low viscosity in precured form (3–23 Pa·s). In addition, the elastomers can tolerate stretching many times without tearing and return to initial shape after deformation. However, both Ecoflex and Dragon Skin elastomers are non-transparent which is limiting their usability in applications that require optical transparency. [18], [19]

The main disadvantage of these softer PDMS elastomers compared to Sylgard 184 is that they cannot be plasma bonded. That is due to the presence of low-molecular weight silicone oil species at the interface preventing adhesion and bonding. The silicone oils soften the polymer network making mechanical properties of the material desirable for soft devices. In other words, the elastomer is softened by applying non-crosslinked oligomers or cyclics into the formulation to decrease the cross-linking density. Those low-molecular weight polymer chains diffuse to the surface interfering the plasma bonding. [11] Similar effect is observed with oxidized Sylgard 184 as it recovers its hydrophobicity when uncross-linked low-molecular weight polymer chains migrate to the surface from the bulk substrate [21]. According to Park et al. [11] soft silicones must have Shore A

hardness higher than 15 to plasma bond properly. Therefore, other methods for sealing the elastomer substrates are required to fabricate soft devices from most softer elastomers.

2.2 Soft Microfluidic Devices

In microfluidic devices, small amounts (10^{-9} to 10^{-18} litres) of fluids are manipulated and processed in channels with dimensions of no more than hundreds of micrometres. Microfluidic devices typically contain a network of microchannels, together with microvalves, micropumps, micromixers, and other components, to process the fluid flowing in the device. Microanalytical methods such as gas-phase chromatography, high-pressure liquid chromatography and capillary electrophoresis are integrated into the system enabling high sensitivity and high resolution of microfluidic analytical devices. In addition, the advantages of microfluidic systems include short time for the analysis, relatively low costs, reduced and minimized size of the device, and need for only small quantities of samples and reagents. [1]

Initially, microfluidic systems were fabricated from silicon and glass with well-known micromachining processes adopted from microelectronics. However, their disadvantages including brittleness, rather high manufacturing expenses and incompatibility with biological samples in water and cells, have made polymeric materials such as elastomers more popular. [1] Choice of material depends on the intended application and sometimes the targeted applications demand stretchability. That is especially true in biomedical applications and in flexible and wearable electronics. Typically, stretchability and elasticity are both required since the fabricated components should return to their initial shape after the stress is released. Stretchability of the material leads to flexible microchannel which dimensions can change while fluid is flowing through it. [3] Deformations of soft microchannel caused by pressure-driven flow can be seen in Figure 2.

When microchannels are embedded in soft materials they can be called soft microchannels. Deformability of microchannels can be exploited for example in life sciences and organ-on-chip applications such as lung-on-a-chip [32] or gut-on-a-chip [33]. Cyclic suction inside side channels or chambers fabricated from soft elastomer mimic breathing motions or peristalsis. Deforming the wall between the side channel and cell-containing microchannels causes mechanical motion and stretching of the cultured cells similarly as *in vivo* microenvironment of the cell type. [32]–[34] Elastic and stretchable microchannels can also mimic human vascular systems and for example blood vessels and other tissues with tubular structures [35], [36]. With flexible channel walls and membranes

haemodynamic microenvironment containing fluid shear stress and cyclic stretching characteristic to blood vessels and vascular cells can be created. [12]

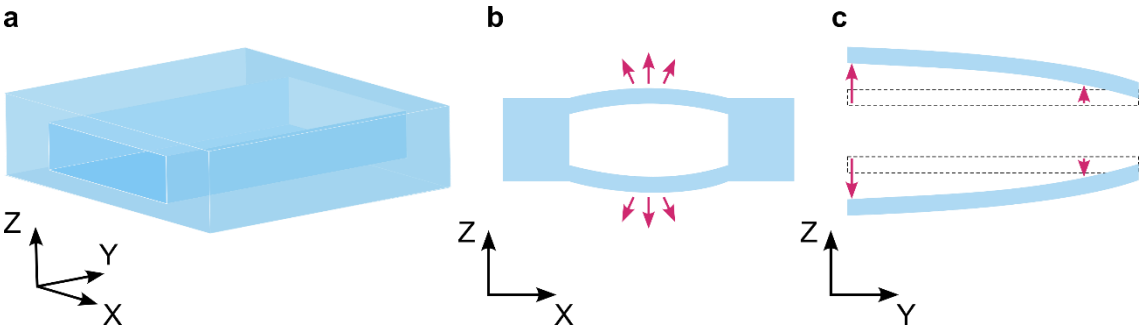

Figure 2. Schematic illustrations of a flexible microchannel. **a** Undeformed microchannel. **b** Cross-section of deformed microchannel perpendicularly to the flow. **c** Cross-section of deformed microchannel parallelly to the flow. All modified from [3].

In addition to life sciences, soft microfluidics are useful in several application areas such as chemistry, soft electronics, and biomedicine. As mentioned, compliance of soft materials have solved mechanical mismatch between conventional rigid materials and biological matter, which broadens the use of soft microfluidic devices [3]. The mechanical compliance for example enables integration of soft microfluidic systems to implantable devices intended for drug delivery or used as soft neural probes. For example, Minev et al. [37] have introduced a microfluidic channel fabricated from silicone elastomer for drug delivery and included soft electrodes to the same implantable device to provide and produce electrical excitation at site.

In soft electronics, microfluidic components can serve as sensing elements [9], stretchable interconnects [38], or radiofrequency identification system antennas [39]. Soft microchannels filled with conductive liquids such as liquid metals or ionic liquids, can tolerate extremely large deformations and stress, providing excellent bendability and stretchability when utilized as soft interconnects in flexible electrical circuits. They can be bent, twisted or stretched without affecting their electrical performance. [3], [38] Soft microchannels filled with conductive matter can also be used for detecting mechanical motion such as strain or compression, which is discussed later in sub-chapter 2.3. Similarly, soft microchannel can be used as a radiofrequency antenna, where the resonance frequency of the antenna can be tuned by deforming the channel containing conductive matter. Such an antenna, composed of Sylgard 184, Ecoflex 00-30 and liquid metal, can be stretched to over 100% strain, while it still maintains a high radiation efficiency. [39]

A biosensor with integrated microfluidics can be used to measure physiological state (e.g., temperature, electrolyte balance or hydration) by analysing biofluids such as blood, saliva or sweat. These biosensors contain a bioreceptor that selectively recognizes the

target analyte, and a transducer to translate the result of the biorecognition into a measurable output signal. [6] Koh et al. [40] developed a soft and wearable microfluidic sweat sensor, in which sweat samples are harvested directly from the skin and analysed in a microfluidic system. The device can be used for evaluating athletic performance or for continuous health monitoring. [40] Generally, wearable microfluidic devices provide new strategies for continuous health monitoring, diagnosis, and treatment.

One important application area for soft microfluidics, especially soft sensors, is soft robotics where they bring intelligence to the robotic system [8]. Soft robots are devices made from compliant materials such as soft polymers, fluids, gels, and other deformable materials that have moduli close to soft biological matter, including tissues. Compliancy and safety provided by soft robotics are valuable in applications that include interaction with soft materials and organisms, or mimic biological functionalities. Motion of soft actuators utilized in soft robotics is typically produced by the elastic deformation of the soft material as for example in fluidic actuators in which channels and cavities embedded in soft elastomer are inflated with fluids. The embedded channels and cavities expand under pressure causing the actuator to move due to its typically asymmetric design. [14] In addition to soft microfluidic sensors, networks of soft channels and components such as valves or pumps for flow control have recently obtain interest to include logic and control to soft robots for regulating the actuation of soft fluidic actuators of the system [41]–[45]. Integrated fluidic logic together with mechanical sensors fulfil soft robots as autonomous actor with perception [8].

In a soft channel, there is a strong interaction between the channel walls and the fluid inside. High pressure or high flow rate can cause deformation of the soft microchannel, changing its geometry and size. Usually, the deformation along the channel length is highest where the flow enters to the channel, decreasing until the exit (Figure 2c). [46] According to Hagen–Poiseuille law

$$\Delta p = \frac{8\pi\mu LQ}{A^2} \tag{1}$$

the pressure-drop (Δp) is dependent on the initial flow rate (Q) of the gas, and length (L) and cross-sectional area (A) of a microchannel when the fluid is incompressible Newtonian fluid in laminar flow. The pressure-drop of a soft microchannel also decreases if the cross-sectional area of the channel increases (Figure 2b). Deformability of the walls makes the hydraulic resistance of soft microchannels nonlinear when described as function of applied pressure or flow rate since the hydraulic resistance is partially defined by the dimensions of the channel. In addition, velocity of the flow, mixing, residence time,

dispersion and separation are all affected by the geometry and dimensions of the microchannel so deformations of flexible microchannels changes them. [3]

Soft microchannels can be used for improving mixing or microparticle separation. The flexible channel walls interact with the fluid flow, leading to instable flow which increases mixing. [3] Decrease of the cross-sectional area of the soft microchannel affects the flow rate enhancing separation. In inertial microfluidic separation, different forces and flow rate together sort microparticles based on their size [47]. Stretching of a microchannel in the longitudinal direction induces larger particles close to channel walls while guides smaller particles to the middle of the channel improving the separation. [48]

Microvalves are one of the basic mechanisms of microfluidic devices controlling timing and fluid flow in the system. Fabrication of the structures from soft materials enhances the valving function since better sealing is achieved and actuation requires less actuation power compared to silicon valves. An elastomeric sealing layer of diaphragm or flap microvalve ensures that there is no leakage with the conformality of the material. Soft passive valves can be embedded in the device and controlled internally, making them beneficial for flexible and stretchable microfluidic systems. [3] Valves can be integrated into flexible and stretchable microchannels as soft arches that open or close by bending or stretching the channel [49]. Another option is to restrict or prevent fluid flow in a soft microchannel with an adjacent pneumatic channel. When pressure is applied to the pneumatic channel, the thin wall between channels bulges, blocking the microchannel with the fluid. Such valves are called *Quake valves*. By using several adjacent pneumatic channels next to the flow channel, a peristaltic pump has been generated. [50] Pumps can also be made by integrating shape memory alloy actuators or piezoelectric actuators into the soft microfluidic devices to deform the soft microchannel. [3]

The soft microchannels can be fabricated from soft materials mainly with three methods: 1) casting channels into a mold, 2) 3D printing the structure from elastomeric material, and 3) subtractively etching out the microchannels from bulk for example with laser ablation. 3D printing is still limited with the properties of the material and geometry of the channels, since 3D printing microchannels from soft materials can easily lead to collapse of the channel. Etching the microchannel pattern to flat elastomer substrate increases the amount of fabrication steps as cleaning the structure after etching is crucial. In addition, etching can modify the surface of the elastomer preventing plasma bonding and sealing the channels. [51]

Fabrication of soft microchannels from castable soft silicones such as PDMS elastomers is typically executed with cast molding [2], [52] that is also adopted to the field of soft

robots [14], [31]. First, desired microchannel pattern is designed with conventional 3D computer-aided design software to be 3D printed as a mold. Since there typically are micro and even nanoscale features, the mold is often prepared with SU-8 photolithography. The liquid elastomer mixed from two components including the base polymer and curing agent is degassed in vacuum and poured to the mold to create a negative replica of the master. Low viscosity of the liquid elastomer enables thorough mixing and degassing together with easier pouring to the mold. Next, the silicone is let to cure either in room temperature or in an oven. Finally, the demolded substrate with open channels is sealed to another flat elastomer membrane to form closed microchannels. Schematic of the fabrication process is presented in Figure 3a.

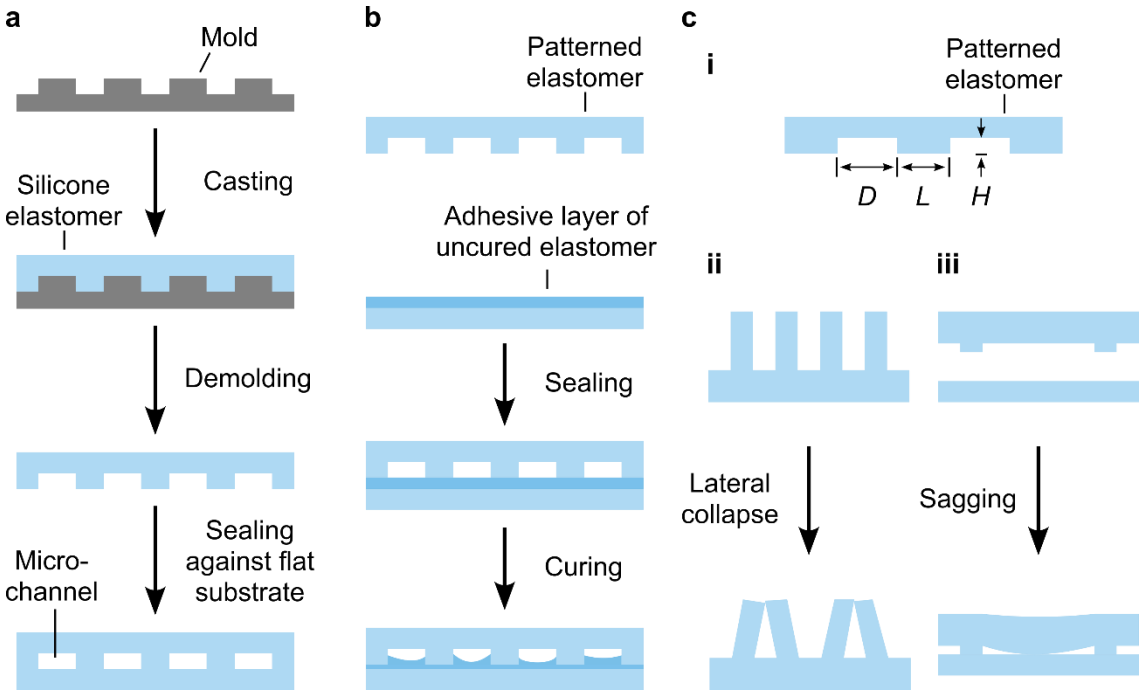

Figure 3. Schematic illustrations. **a** Fabrication process of microchannels with silicone casting. Modified from [2]. **b** Capillary action of uncured adhesive silicone layer. Modified from [53]. **c** Channel dimensions (i) and related problems: lateral collapse or "pairing" (ii) and sagging (iii). Modified from [12].

Sylgard 184 has ability to irreversible seal to itself or other materials which is beneficial in fabrication of soft microchannels. Since most softer PDMS elastomers do not have the same capability due to the low-molecular weight silicone oils interfering the adhesion, alternative approaches including corona discharge, ultraviolet (UV) ozone exposure, thermal bonding and partial curing have been proposed [11], [54]–[56]. Sealing the open channels is critical step in the fabrication process as the bond strength can determine the success of the device. High pressure applications require higher strength of the bond to prevent leaking and breakdown of the seal.

One common method for bonding soft elastomers is to use thin layer of uncured silicone as adhesive to seal the bond between two layers. The mixed and degassed uncured silicone is applied on flat elastomer substrate and spread evenly on the surface with spin coating, bar coating or doctor blade coating for instance. To prevent the silicone from flowing into the microchannels and blocking them, the adhesive layer can be partially cured before bonding. The elastomer substrate with open microchannels is placed on top of the adhesive layer with the patterned surface facing down. The monolithic structure is let to cure to obtain closed microchannels. However, the method is not yet reliable enough to be trivially used for fabrication of microchannels embedded in soft elastomers [11].

Drawback of bonding the elastomer substrates with a layer of elastomer as adhesive is blocking of the channels. Capillary forces dominate at microscale enabling the uncured liquid-like silicone to wet the walls of the microchannels and fill up the void space of the open channels. The phenomenon is utilized in soft lithography and more precisely in capillary force lithography to generate a negative replica of the elastomer stamp from polymeric material [53]. However, if the adhesive layer is thin and the interaction between the uncured silicone layer and cured silicone substrate is weak enough, the void space is not filled completely (Figure 3b). Hence thickness of the adhesive layer plays important role in the reliability of wet bonding process as thinner layer prevents filling up the void and blocking the channel. Similarly, partially curing the adhesive layer reduces the interaction between the layer and the silicone substrate but the pre-curing time cannot be too long so that high enough interfacial bonding is achieved [11].

In addition, it is stated that the softness of an elastomer restricts the aspect ratio (AR) of microstructures that can be fabricated from PDMS elastomers [41]. Too high or too low aspect ratio causes deformation and distortion of the elastomer substrate defecting the micropattern. The aspect ratio can be the ratio between the width of the channel (D) and thickness of the wall (L) between the channels or between the height (H) of the channel and the width or wall thickness (Figure 3c). The two possible problems caused by the softness of the elastomer are lateral collapse of relied structure and sagging of recessed structures as seen in Figure 3c. [12], [57]

With Sylgard 184, the lateral collapse (Figure 3c) occurs with channels that have aspect ratio (H/L) over 5. This phenomenon is also known as pairing. When the height of the channel increases and simultaneously thickness of the wall of the channel is decreased possibility for lateral collapse increases. Similarly, if height of the channel is much greater than the width pairing is expected. Sagging is caused by too low aspect ratio, $H/L < 0.5$ with Sylgard 184. Remarkable wide channel compared to the height of the channel leads

to sagging of the ceiling blocking the channel. [12] Thus, self-collapse of microchannels fabricated from soft elastomers must be carefully considered while designing geometry of microchannels for soft devices.

2.3 Soft Strain Sensors

Nowadays strain sensors are typically based on rigid metals making them inherently inflexible and deformable. In flexible electronics, the circuits, and electrical components such as sensors can be bent without damaging their functionality. Making rigid materials sufficiently thin renders them flexible up to certain point. However, thin structures based on rigid materials can be flexible but not stretchable. Stretchable materials can be elongated widening their application range compared to flexible ones. Stretchability enables comfortable contact to biological tissues such as skin which is important in medical applications. [9] Strategies for producing stretchable sensors include making wavy shapes or folds from rigid materials, but also using materials that are intrinsically soft [23]. Soft sensors can be used in electronic skins, wearable systems, implantable devices, and soft robots. [9]

Personalized and continuous health-monitoring, detection of human motion, human-machine interfaces and soft robotics benefit from sensors that are soft, compliant and stretchable [7]. Soft mechanical sensors can measure variables such as strain [7], [58], pressure and touch [59], [60]. In continuous health-monitoring, wearable technologies containing soft mechanical sensors can detect strains of skin caused by blood flow pulse or respiration and thus monitor heart or breath rates [7]. Skin-mountable sensors require compliancy from the material as the sensor must be able to adapt to the movements of the body without losing the contact. In addition, posture and activity can be sensed with soft tactile sensors included in wearable devices intended for the use of elderly, athletes or disabled. Prostheses need feedback about touch that can be achieved with integrated soft sensors. [61]

Soft sensors are needed to provide proprioception and exteroception for soft robots. Soft robots should be able to sense their surroundings, their own movement, and their posture. Since the body of soft robot is made from soft materials, soft sensors are the most suitable option for the application. Besides, conventional sensors are usually not capable of properly detecting large deformations produced by the soft actuators. There are five basic requirements for soft sensors intended to be integrated into soft robots. In addition to appropriate compliancy and ability to not alter the mechanical properties of the soft actuators, the soft sensors cannot restrict the robot and must allow it to move freely.

They should tolerate large strains and long periods of dynamic deformation without failure in different environments and applications. Finally, the fabrication methods and materials should be selected to be same or similar as in the body of the soft robot to simplify the integration. [8] Hence, for integrating the sensors into soft robots, mechanical properties of the sensor, such as the modulus, should be similar to the mechanical properties of the robot body and the actuators. The fabrication can also be simplified if the robot body, actuators, and sensors are all based on the same materials. Currently, the soft sensors usually detect strain or position of the soft robot. [62] Curvature sensors are required for proprioception since the actuation in soft robots is usually based on bending. For effective control, monitoring of environment and comfortable interaction with humans, soft robots need tactile sensing. That also enables the robot to have ability for performing skilled tasks such as dexterous manipulations or separating objects based on their morphology or shape. [8]

Sensing technologies, such as resistive, piezoresistive, piezoelectric, capacitive, and optical, varies depending on the demands of the application. Optical strain sensors detect the deformations in light transmission medium produced by applied strain or pressure as changes in intensity of the light. They typically contain a light source, a photodetector, and the light transmission medium such as optical fiber or elastic wave guide. [8] Similarly, magnetic sensors contain a miniature magnet, magnetic field sensor such as Hall-effect sensor, and a soft medium that can be stretched, compressed or twisted, causing change in the output of the sensor [63]. Thus, integration of magnetic sensors to soft devices is limited by the need of the miniature magnet and the semiconductor-based Hall element, which are not inherently soft or flexible components [64]. Same problems are also related to the optical sensors: some of the components are rigid and cannot be located in the parts of the soft device that stretch. [63]

Pneumatic air chamber fabricated from soft elastomers can be used as a soft sensing element for measuring contact force and deformation. Deformation of the air chamber changes its volume, causing pressure inside the chamber to change, which then can be detected with a pressure sensor. The air chamber can be integrated to a pneumatic actuator to measure its curvature [65], to a soft robotic finger for measuring its position or touch [66], or to human-machine interfaces [67]. Forces from different directions can be sensed with several air chambers in one structure [68]. However, when fluids and air are sealed inside closed silicone chambers, any leaking alters the output of the sensor, especially in long term measurements.

In resistive and piezoresistive sensors, the resistance changes due to change in the dimensions of the sensor, intrinsic resistive response of the material, disconnection mechanism, crack generation or tunnelling effect [13]. Typically, soft resistive sensors are fabricated from electrically conductive materials: conductive liquids, conductive polymers or conductive fillers embedded in non-conductive elastomer matrix. Same conductive materials are utilized in capacitive sensors as stretchable electrodes for measuring the changes of capacitance while the elastic body is deforming [8]. Fabrication techniques of soft resistive and capacitive soft sensors from soft elastomers and conductive additives include for example chemical synthesis, coating and sputtering, liquid-phase blending, laser micromachining, and printing [13].

When the highly stretchable elastomers are loaded with conductive additives, compromises related to the conductivity and softness of the structure are made. Larger amount of conductive particles increase the conductivity but simultaneously stiffens the material. [62] Metals provide higher electrical conductivity than carbon but form insulating surface oxide layers easily affecting the performance of the sensor. They can be either deposited as a thin film on the soft substrate with different techniques such as screen printing and sputtering or added as nanoparticles to the elastomer by which better stretchability is maintained. Carbon in different forms including carbon black and grease nanotubes is mechanically more appropriate for soft strain sensors but its electrical conductivity is rather low and limits its suitability especially for measuring larger strains. [24]

Intrinsically conductive polymers such as polyacetylene, polypyrrole and polyaniline are a recent alternative for the fabrication of soft resistive sensors that are used for detecting strain and pressure. Conductivity of the polymers is based on π-conjugation, and varying single and double covalent bonds, which conduct electrons. In addition, ionic dopants can be used to improve the electronic conductivity. [69] However, conductive polymers are typically much stiffer than silicone elastomers with modulus around a few gigapascals. The conductive polymer can be combined into inherently soft polymer matrix as conductive fillers to produce flexible and soft conductive polymer composites. [70] As an example, Wang et al. [71] have developed a conductive polymer composite from polyaniline, polyacrylic acid and phytic acid that can withstand even 500% strain. From this composite, a strain sensor could be fabricated. Compared to metallic or carbon additives in soft polymers, polymer chain-level intrinsic conductivity provided by the conductive polymer fillers enables significant improvement to flexibility and compliancy of the construct [69]. Yet, these composites are also more rigid when the amount of conductive polymer fillers is increased.

Currently microfluidic sensors with liquid metals inside microchannels are popular as soft sensors since they have good conductivity and high compliance. When encased in elastomers, liquid metals are intrinsically stretchable meaning that they can maintain conductivity under dynamic elongation and elastic deformation. [9] Such soft microfluidic sensors are fabricated by first producing the microchannels embedded in soft elastomer, and then injecting the conductive liquid inside the channels. Compared to adding rigid materials or fillers in a polymer matrix, utilizing liquid metals does not increase internal stresses or decrease stretchability of the construct [72]. Furthermore, better conductivity at higher maximum strains is achieved with liquid metals regardless whether the conductivity is obtained with metallic nanowires or nanoparticles, carbon based solutions, conductive polymers, or ionogels [9], [73], [74]. However, the melting point of liquid metals constrains their applicability in low temperatures and density is often higher than the surrounding elastomeric matrix. Eutectic Gallium-Indium (EGaIn) is one of the most used liquid metals in microfluidic sensors with a melting point of only 15°C, making it suitable for room temperature applications. Moreover, the fabrication process of soft microfluidic sensors based on liquid metals is rather complex since the liquid metal must be patterned to the soft material. The liquid metal can be injected to fabricated soft microchannels, or, for example, applied with direct-writing, stencil printing, inkjet printing, or spray coating on surface of the soft polymer matrix. The construct is finalized by sealing the patterned liquid metal inside the elastomer. [8], [9], [24]

When the geometry of the patterned liquid metal inside the elastomer changes due to external force, the resistance of the liquid metal changes. [9] For example, as the liquid metal is filling a microchannel, it has ability to flow during the deformation of the channel sustaining electrical continuity [75]. Thus, strain, touch and pressure can be detected with soft sensors based on liquid metals. Strain in the axial direction of the channel increases the length of the channel simultaneously as the cross-sectional area of it decreases. This causes growth of the overall electrical resistance of the channel filled with liquid conductor. Similarly, applied pressure or compressive force on the channel decreases the cross-sectional area of the channel while the length is stable leading to increase of the resistance. [76]

An alternative approach to microchannels filled with conductive fluid is a novel pneumatic strain sensor that our research group has recently proposed [10]. The pneumatic strain gauge consists of a meandering microchannel, embedded in soft elastomer. The pressure drop of the channel can be measured to derive the fluidic resistance of the channel. Change in the dimensions such as length or cross-sectional area of the channel under

mechanical loading changes the fluidic resistance. Thus, the meandering pneumatic microchannel in soft elastomer filled with pressurized air or fluid and vented to air pressure is analogous to electrical resistive strain gauges. The pneumatic microchannel in soft elastomer can be used for measuring strain, curvature or compression. [10] The sensor is fabricated from soft elastomer without a need for any additional materials such as conductive fillers making the sensor inherently soft. For measuring larger strains that can be achieved with Sylgard 184, softer PDMS elastomers from Dragon Skin and Ecoflex series are used for the highly stretchable strain sensor.

3. AIMS OF THE STUDY

This work aims to enhance the reliability and reproducibility of microchannel fabrication from commercial PDMS elastomers (Dragon Skin 30, Ecoflex 00-50 and Ecoflex 00-20) which are all softer than Sylgard 184. The fabrication is conducted by using a thin adhesive layer of the PDMS elastomer to seal open microchannels to a flat elastomer substrate. As discussed, wet bonding is rather unreliable fabrication technique since the channels and other features are easily ruined by the adhesive layer. However, capillary action and flowing of the uncured elastomer can be restrained with the thickness of the adhesive layer and by partially curing the elastomer. The hypothesis is that smaller layer thickness would be favourable for minimizing the capillary action and successfully fabricating the channels. Similarly, partially curing the adhesive layer is expected to prevent blocking the microchannels. In addition, the optimal aspect ratios reported by Whitesides Research Group [12] for Sylgard 184 are expected to be invalid for the selected softer PDMS elastomers as the softness of the elastomer causes problems such as pairing or sagging.

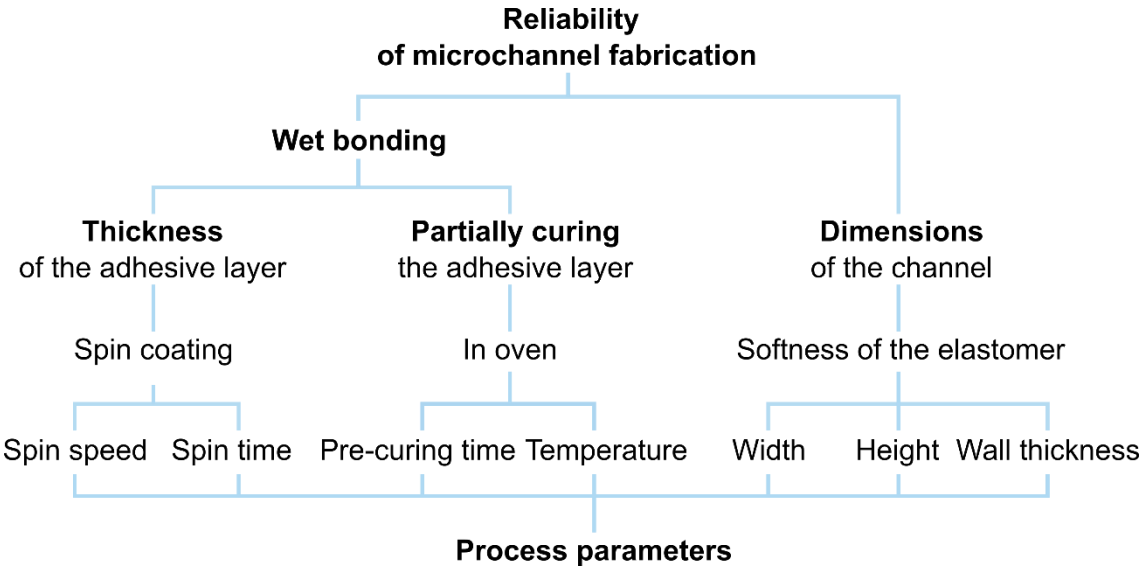

Figure 4. Parameters affecting the reliability of microchannel fabrication with wet bonding process.

In this work, spin coater is used to spread the adhesive layer evenly on the surface of a flat elastomer substrate, so the layer thickness is defined by the spin coating parameters including spin speed and spin time. Partially curing the layer is done in an oven so curing time and temperature of the oven are affecting the curing rate. Thus, suitable values for parameters including spin speed, spin time, temperature of the oven and pre-curing time,

as presented in Figure 4, are searched in this work to discover suitable parameters for reliable and reproducible fabrication with the studied method. All the tested PDMS elastomers have different properties such as viscosity, curing time and softness, so the suitable parameters are expected to differ. As the softness of the elastomer has also an effect on the feasible size of the channels, different channel dimensions are also tested.

In addition, the studied microchannel fabrication technique is used to fabricate a novel pneumatic strain sensor to demonstrate a practical application for the technique. The response of the fabricated pneumatic sensor to varying strain is measured and its sensitivity is determined. The measurements and characterizations were conducted together with A. Koivikko, and we have also reported the design and characterization of the novel pneumatic sensor in a scientific journal [10].

4. MATERIALS AND METHODS

4.1 Soft Silicone Elastomers and Mold Design

Commercial soft elastomers Dragon Skin 30, Ecoflex 00-50 and Ecoflex 00-20 from Smooth-On are selected for the fabrication of the microchannels in this work. All these elastomers are softer than Sylgard 184 and thus more suitable for manufacturing of soft devices. Dragon Skin 30 is the most rigid elastomer in Dragon Skin series as well as Ecoflex 00-50 in Ecoflex series, both remarkably softer than Sylgard 184. As seen in Table 1, Dragon Skin 30 can tolerate over twice the strain before break compared to Sylgard 184. Softer Ecoflex 00-50 has the highest elongation at break (980%) from the elastomers used in this study. Ecoflex 00-20 is softest with the lowest Shore hardness, but it cannot withstand as high of a strain as Ecoflex 00-50.

Table 1. Properties of Sylgard 184 and softer PDMS elastomers used in this work based on their datasheets.

	Sylgard 184	Dragon Skin 30	Ecoflex 00-50	Ecoflex 00-20
Shore hardness A	50	30	11*	-
Shore hardness 00	85*	69*	50	20
100 % modulus (kPa)	-	593	83	55
Tensile strength (MPa)	7.1	3.4	2.2	1.1
Elongation at break (%)	140	364	980	845
Color	Transparent	Translucent	Translucent	Translucent
Viscosity (Pa·s)	4	20	8	3
Cure time at 25°C	48 h	16 h	3 h	4 h
Plasma bond	Yes	No	No	No

*Estimated by using Table I in Qi et al. [17]

Uncured Sylgard 184 has low viscosity (Table 1), so it easily flows into molds even with small micro or nanoscale features. Softer PMDS elastomers Dragon Skin 30 and Ecoflex 00-50 used in this study are more viscous in uncured form which can limit the size of structures that can be fabricated with them. Ecoflex 00-20 has viscosity of 3 Pa·s which is close to the value of Sylgard 184. Viscosity of the elastomers has also an effect on the wet bonding process as the layer thickness achieved with spin coating is dependent on the viscosity of the liquid. Due to this, the spin speeds used in this study to produce the bonding layer is changing from elastomer to elastomer and achieved layer thicknesses are studied.

In addition to viscosity, curing time of the elastomer must be considered when planning the fabrication process as the adhesive layer is partially cured. All PDMS elastomers from Dragon Skin and Ecoflex series cure in room temperature from several minutes to couple hours. Dragon Skin 30 has the longest curing time of 16 hours (Table 1). However, the curing time can be decreased by increasing the temperature. In this work, all elastomers are pre-cured in an oven, at 60°C, to decrease the curing time.

To test fabricable channel geometries and dimensions for soft elastomers, a channel pattern containing rectangular channels with varying widths and wall thicknesses was created with Solidworks CAD software. The design contained four channel networks next to each other. Pattern of the channel networks used in this study is expressed in Figure 5.

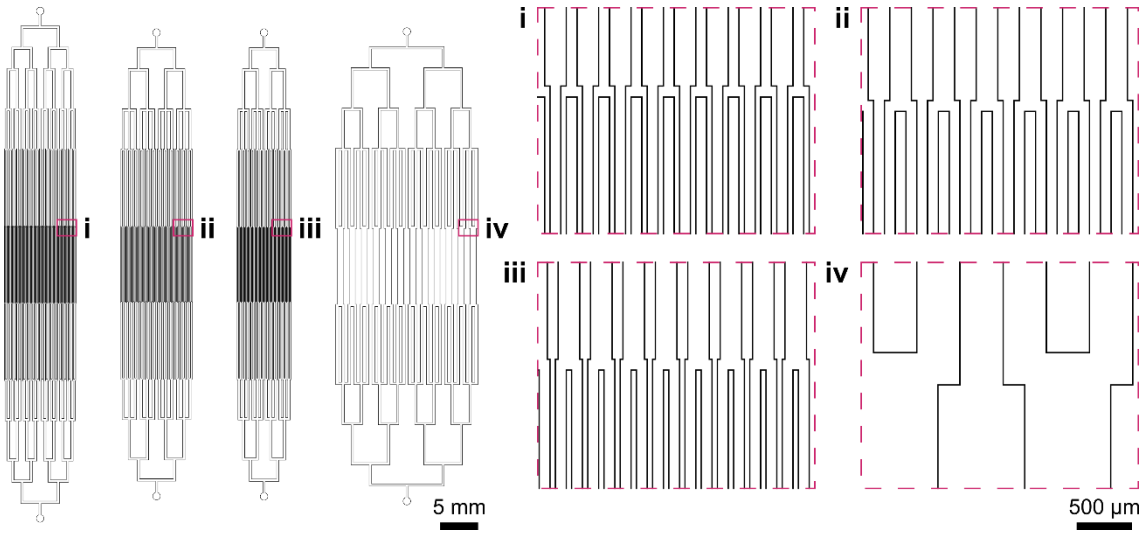

Figure 5. Pattern of channel networks used in this study: (i) 100 µm wide channels with 200 µm wall thickness and 50 µm wide channels with 100 µm wall thickness, (ii) 200 µm wide channels with 200 µm wall thickness and 100 µm wide channels with 100 µm wall thickness, (iii) 200 µm wide channels with 100 µm wall thickness and 100 µm wide channels with 50 µm wall thickness, and (iv) 400 µm wide channels with 400 µm wall thickness and 800 µm wide channels with 800 µm wall thickness.

Dividing and reuniting geometry of the channel network enables observing whether the channels are open by pumping dyed liquid through the network. Three of the channel networks started with a 300 µm wide inlet channel dividing gradually into thinner channels that later reunite to form again wider channels and eventually a 300 µm wide outlet channel. The fourth channel network also contained a 300 µm wide inlet channel dividing into wider 400 µm and 800 µm channels before reuniting to a 300 µm wide outlet channel. Dimensions and aspect ratios (AR) of microchannels studied in this work are given in Table 2.

Table 2. Channel aspect ratios (AR) and corresponding channel dimensions used in the study.

AR (D/L)	AR (H/L)	AR (H/D)	Width (D)	Wall thickness (L)	Height (H)
0.5	2	4	50 µm	100 µm	200 µm
2	4	2	100 µm	50 µm	200 µm
1	2	2	100 µm	100 µm	200 µm
0.5	1	2	100 µm	200 µm	200 µm
2	2	1	200 µm	100 µm	200 µm
1	1	1	200 µm	200 µm	200 µm
1	0.5	0.5	400 µm	400 µm	200 µm
1	0.25	0.25	800 µm	800 µm	200 µm

For testing how small channels can be done with softer PDMS elastomers than Sylgard 184, the widths of the thinner channels were 200, 100 and 50 µm. To see how densely the channels can be packed the wall thicknesses varied as 200, 100 and 50 µm. Thus, the thinnest channel type was 50 µm with 100 µm wall thickness and smallest wall thickness was in combination of 100 µm wide channel with 50 µm wall thickness. Aspect ratios (D/L) of the channels were 2, 1 and 0.5. For studying sagging of the microchannels fabricated from soft elastomers the fourth channel network contained 400 µm and 800 µm wide channels with aspect ratios (H/L) as 0.5 and 0.25 respectively. The length of all the tested channels was one centimetre and height of the channels was 200 µm.

4.2 Mold Fabrication with Photolithography

Based on the design in Figure 5, a mask was created from a commercial chrome-on-glass mask blank, coated with a positive photoresist. The resist was exposed with a direct writing device (µpg501, Heidelberg Instruments Mikrotechnik GmbH, 390 nm 10 W UV light source). Next, the exposed mask was immersed into developer (AZ351B Developer, MicroChemicals) solution for one minute to remove the areas of the photoresist treated with UV light. Chrome was etched from the exposed areas with a chrome etchant (CHROME ETCH 16, OSC GmbH) to reveal the design as a transparent pattern on the mask. Next, the mask was exposed to UV light for one minute to make the residual photoresists soluble to the developer. Finalizing was done by developing the mask in the developer solution for one minute, and then rinsing the mask with DI-water and drying it.

The molds were fabricated with a photolithography process. First, silicon wafers were cleaned and treated with oxygen plasma in a reactive ion etcher (Vision 320 Mk II RIE, Advanced Vacuum) for two minutes, to enhance the adhesion of photoresist onto the wafer. Negative SU-8 3050 photoresist (micro resist technology GmbH) was spin coated

with a three-step program (500 RPM for 15 s, 700 RPM for 40 s and 100 RPM for 15 s) on the silicon wafers to form a 200 µm thick layer. The photoresist layer was prebaked on a hot plate (5 min at 65°C and 120 min at 95°C) before being exposed to UV light for one minute through the fabricated mask with a mask aligner J500 VIS (OAI) device. After post-baking on the hot plate (5 min at 65°C and 10 min at 95°C), a chemical developer (mr-Dev 600, micro resist technology GmbH) was used to remove the resist from areas that were not exposed to UV light. Finally, the photoresist was hard baked for 15 minutes at 150°C.

The prepared SU-8 molds were adhered to a glass wafer with double-sided tape to provide a rigid base for the fragile silicon wafer and to prevent it from breaking. Next, the double-sided tape was used to fix the glass wafer with the SU-8 mold to the bottom of a Petri plate to finalize the replica molds for silicone casting. For the substrates without channels, molds were prepared by adhering glass wafers to the bottom of Petri plate with the double-sided tape. All the molds were treated with trichloro(1H,1H,2H,2H-perfluorooctyl)silane to make it easier to demold the cured elastomer.

4.3 Fabrication of Soft Elastomeric Microchannels

Fabrication process of the microchannels with wet bonding is illustrated in Figure 6 and process parameters used for the study in Table 2 and in Table 3. All elastomers used in this work are two-component polymers, containing of base part (part A) and curing agent (part B). At the beginning of the casting process, the parts were properly mixed using 1:1 ratio by weight and then the mixture was degassed in a vacuum chamber. The liquid elastomer was poured into the molds with and without the pattern of the channels, degassed and let to fully cure in the oven at 60°C for at least one hour. Later, the cured elastomer substrates containing the open channels were demolded (Figure 6a).

Table 3. Parameters used in this study to fabricate the adhesive layer.

Spin speed (RPM)	Spin time (s)	Pre-curing time (s)	Pre-curing temperature
1500[1]	90	0	60°C
2000[1,2]		20	
2500[2]		30	
		40	

[1] Ecoflex 00-20
[2] Dragon Skin 30, Ecoflex 00-50

To form closed channels, a thin layer of uncured elastomer was applied on a flat elastomer substrate to act as glue. Approximately 1.5 g of uncured elastomer was spin coated

(WS-400 spin coater, Laurell technologies Corp) with a two-step program to fabricate the layer (Figure 6b). The first step is to spin 10 seconds at 300 RPM, followed by 90 seconds at 1500, 2000, or 2500 RPM, depending on the elastomer. For partially curing the adhesive layer, the flat silicone substrate with the adhesive layer was placed into the oven at 60°C for 20, 40 or 60 seconds (Figure 6c, Table 3). Channels were also fabricated without partially curing the adhesive layer (Table 3). Different combinations of parameters expressed in Table 3 were tested for the fabrication. Elastomer substrate with open channels was placed on top right after (Figure 6d) to create closed channels and the construct was let to fully cure before demolding. Inlets and outlets were created by cutting the ready-made structures so that the ends of the channels were uncovered (Figure 6e).

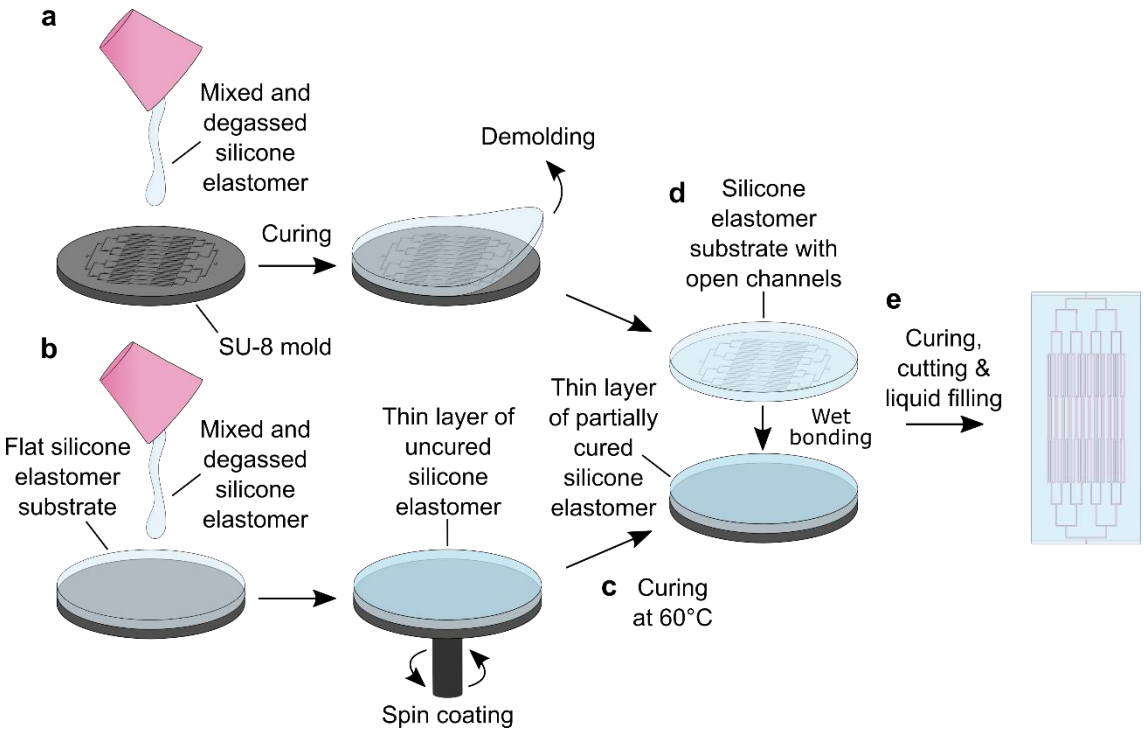

Figure 6. Microchannel fabrication with wet bonding process. **a** Fabrication of open microchannels with replica molding, curing and demolding. **b** Spin coating thin layer of uncured elastomer on top of fabricated flat elastomer substrate. **c** Partially curing the adhesive elastomer layer in the oven. **d** Placing the elastomer substrate with open channels on top of the adhesive layer. **e** After curing, cutting the microchannel network with open inlet and outlet from the substrate and filling with colorful liquid for visualiazation.

To study the thickness of the spin coated silicone layer, different spin speeds ranging from 1500 RPM to 4000 RPM were used for the second step of the spin program. To make sure that the spin coated layer can be distinguished from the elastomer substrate, the flat substrate under the spin coated layer was dyed green (Silc Pig™ Electric Green, Smooth-On, mixed to the part A of the elastomer). When the undyed elastomer was spin coated and cured on the dyed elastomer substrate, the thickness of the spin coated layer

could be clearly observed. A cross-sectional sample was cut from the middle of the elastomer substrate and the thickness of the spin coated layer was observed with an inverted optical microscope (Zeiss Axio Observer.Z1, Carl Zeiss Microscopy).

4.4 Evaluation of Fabricated Microchannels and Statistical Analysis

The yield of the fabricated channels was studied by injecting dyed deionized water into the channels, to see if the channels are open or closed and if the geometry is as designed. Even though silicones from Dragon Skin and Ecoflex series are translucent and not transparent as Sylgard 184, blocked microchannels are visible and flow of colorful fluid can easily be seen by eye. However, as the distance between adjacent microchannels is 50 µm at smallest, distinguishing channels from each other can be eased with microscopy. Hence, the number of open channels was counted manually while observing them with a digital microscope (HAYEAR 34MP 2K Digital Microscope Camera 180X Lens, Figure 10b).

Different groups or classes were formed from the results based on unifying factor such as the elastomer, spin speed, curing time or geometry of the channel. The results were also divided into populations based on the elastomer and again grouping or classing was done with the other parameters including spinning speed, curing time and channel geometry to study effect of the material. Yields for the channels with different grouping were calculated by dividing the number of successful channels with the total number of fabricated channels of that channel group.

Statistical analysis for the results was done with Chi-square test to investigate the dependence of success of the channel fabrication, varying fabrication parameters and elastomers. The chi-square test evaluates the independence of variables by studying if there is a statistical difference between observed and expected values. The null hypothesis of the test is that the observations are independent of the variables. In this work, testing for independency was done by using the chi-square distribution via contingency tables. The chi-square test statistic was calculated with equation

$$\chi_c{}^2 = \sum \frac{(O_i - E_i)^2}{E_i} \tag{2}$$

where O_i is the observed value in a given cell of a 2 x *n* contingency table, and E_i is the theoretical or expected count in a given cell of if the null hypothesis were true. With the degree of freedom as number of variables minus one, the p-value is obtained from the

chi-square test. If the probability or p-value is close to zero (< 0.0001), the null hypothesis can be rejected, and it is assumed that there is dependency between the variables.

4.5 Fabrication and Characterization of Soft Pneumatic Strain Sensor

The soft pneumatic strain gauge was fabricated from Ecoflex 00-50 with the process described in previous chapters. Open microchannels, cast using SU-8 molds, were bonded to a flat elastomer substrate using the wet bonding method studied in this thesis. The sensor design was the same as in [10], containing a 200 µm wide and 200 µm high meandering microchannel, with five turns and a total length of 183 mm. The overall sensing area was 30 mm × 3.84 mm. The adhesive layer was spin coated for 90 seconds at 2500 RPM, and the layer was partially cured for 40 seconds in the 60°C oven before bonding. After curing and demolding the substrate with embedded channel was cut to shape of the sensor, and a needle was used to open the inlet and outlet. Metallic connections were sealed to the inlet and outlet with a silicon glue (Sil-Poxy, Smooth-On). Schematic illustration of the soft pneumatic strain sensor is shown in Figure 7a.

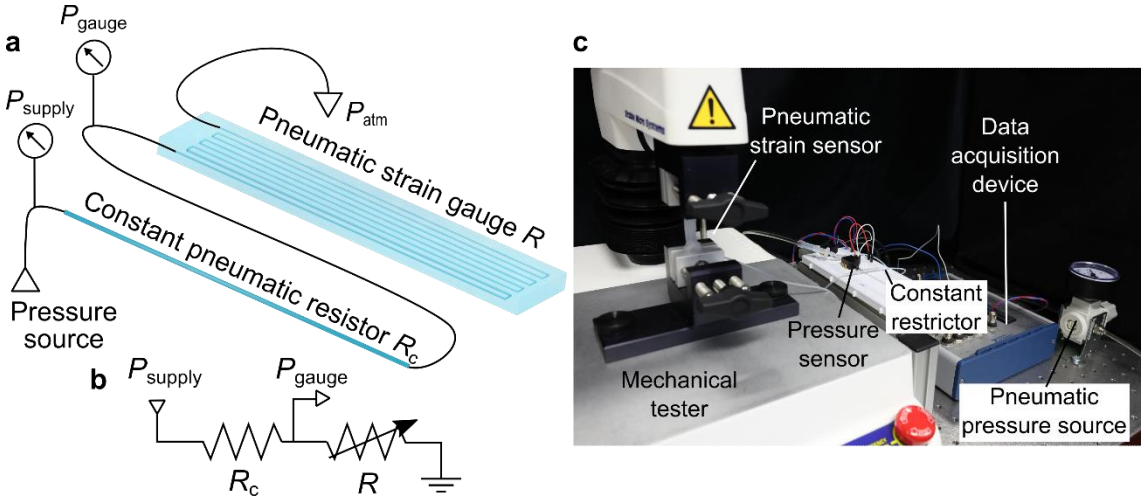

Figure 7. Soft pneumatic strain sensor. **a** Schematic of the strain sensor and its pneumatic circuit containing pneumatic resistor R_c and the strain sensor R in series as the sensor is vented to atmospheric pressure P_{atm}. A pressure sensor measures the pressure P_{gauge} between the resistor and the strain sensor. **b** Electrical circuit corresponding to the pneumatic circuit. **c** Measurement setup for the strain sensor. All reported also in [10].

To demonstrate that soft microchannel embedded in elastomer can be used to measure strains, the fabricated sensor was connected in series to pneumatic circuit with a constant pneumatic resistor R_c (Teflon tube, inner diameter = 0.2 mm) and two pressure sensors (015PDAA5, Honeywell, 15 PSI Differential 5 V) similarly as in [10]. The pressure sensors measured the supply pressure P_{supply} and pressure inside the pneumatic

strain sensor P_{gauge} (Figure 7b). A data acquisition device (USB-6356, National Instruments) was used to record the data from the pressure sensors. A mechanical tester (TA.XT Plus, Stable Micro Systems) was used stretch the pneumatic sensor during tensile measurements. The measurement setup, pneumatic circuit and its electrical equivalence are shown in Figure 7a–c.

Using electrofluidic analogy, the measured pressures can be converted to pneumatic resistance by calculating the ratio of pneumatic resistance of the strain gauge (R) and the constant pneumatic resistor (R_c) with equation

$$\frac{R}{R_c} = \frac{\Delta P_{gauge}}{\Delta P_{gauge} - \Delta P_{supply}} \tag{3}$$

where $\Delta P_{gauge,supply}$ are small pressures relative to the atmospheric pressure. The derivation of the equation and related assumptions are reported by Koivikko et al. [10]. External strain on the strain gauge either increases or decreases the pneumatic resistance of the gauge ($R = R_0 + \Delta R$) depending on whether it is elongated or shortened. There was variation in R_0 across the samples as they are not identical even though the design is the same due to variation caused by the fabrication process and the adhesive layer. The ratio $\Delta R/R_c$ is used instead of R/R_c because it was noted that ΔR had less variation than R_0 from sample to sample.

To study the sensitivity of a strain gauge, its gauge factor (GF) can be calculated with equation

$$GF = \frac{dR/R}{dL/L} \tag{4}$$

as the ratio of relative change in the output signal ($\Delta R/R$) to applied strain ($\Delta L/L$). The measurement setup for the pneumatic strain gauge that was introduced above cannot record the R, only R/R_c. In addition, to study the GF as response to engineering strain ε that is defined as the ratio of the amount of deformation in the direction of the applied force to the initial length, Equation (4) was derived to form

$$GF = \frac{d(R/R_c)}{d\varepsilon} \cdot \frac{1+\varepsilon}{R/Rc} \tag{5}$$

as reported by Koivikko et al. [10].

5. RESULTS AND DISCUSSION

5.1 Fabrication of Soft Elastomeric Microchannels with Wet Bonding

To achieve reliable fabrication process of microchannels embedded in soft elastomer with wet bonding, different parameters including spin speed, pre-curing time, and geometry of the channel were tested for elastomers Dragon Skin 30, Ecoflex 00-50 and Ecoflex 00-20. Over 9000 microchannels were fabricated from each PDMS elastomer. The yield was calculated by counting the amount of successful open channels magnified with the digital microscope (Figure 10b) and dividing it with the number of fabricated channels. Spin speed determines the thickness of the adhesive layer and thus affects to possible blocking of the channel. Figure 8 shows the thickness of the spin coated layers of the elastomers on a flat elastomer substrate at various spin speeds with constant 90 s spin time.

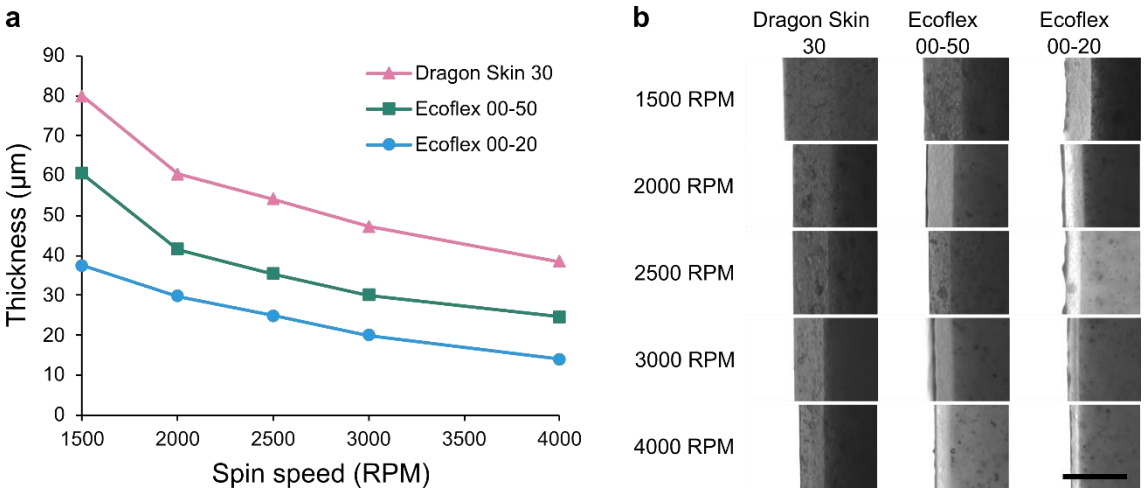

Figure 8. Thickness of spin coated layer. **a** Thickness of the spin coated layer as function of spin speed for the soft silicone elastomers. **b** Cross-sectional micrographs of the spin coated layers with different spin speeds. Scale bar: 100 µm.

As viscosity of the spin coated material determines how thin membrane can be achieved with certain spin speed, different speeds were used for each PDMS elastomer. Figure 8 shows thickness of spin coated layers of Dragon Skin 30, Ecoflex 00-50 and Ecoflex 00-20 elastomers on flat substrate of same material at various spin speeds with constant 90 s spin time. As expected, the layer thickness decreased as function of spin speed. Since viscosity of Ecoflex 00-50 is lower, the achieved layer thickness with same spin speed was smaller (Figure 8) than with Dragon Skin 30. Same effect can be seen with Ecoflex 00-50 and Ecoflex 00-20.

Based on the results of the tests in Figure 8, spin speeds 2000 RPM and 2500 RPM were selected to be tested for wet bonding with Dragon Skin 30 (Table 3). The surface of the membrane fabricated from Dragon Skin 30 with higher speeds contained some roughness that could be seen by eye and could lead to leaking of the channels. Also, due to the higher viscosity of Dragon Skin 30 compared to other elastomers of the study (Table 1) capillary action was expected to be smaller and thus, a thicker bonding layer was assumed to be suitable for reliable fabrication. Time for the elastomer to capillary spread into the cavity is limited by curing of the elastomer and viscous forces are retarding the spreading.

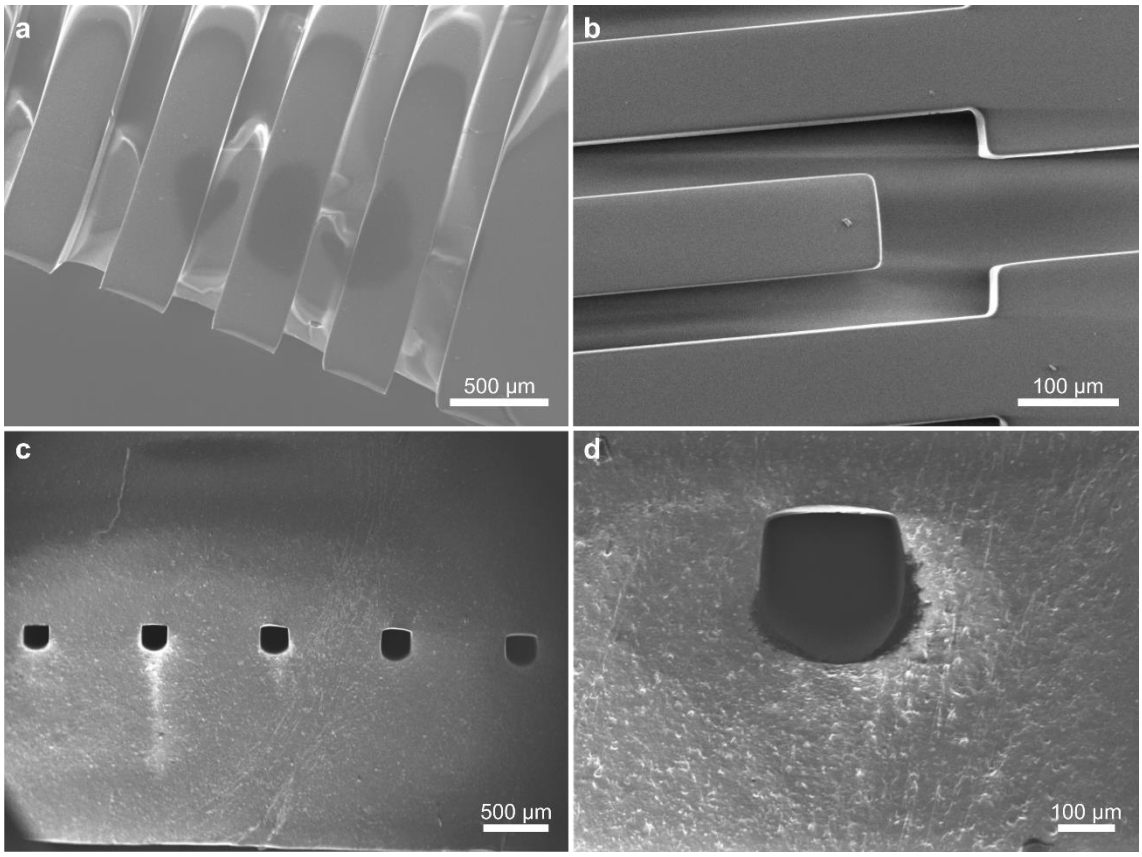

Figure 9. Scanning electron micrographs of fabricated microchannels. **a** Open 200 µm wide channels from Ecoflex 00-50 with 300 µm wall thickness. **b** Open 50 µm and 100 µm wide channels from Dragon Skin 30 with 100 µm and 200 µm wall thickness respectively. **c & d** Cross-sectional micrographs of 200 µm high and 200 µm wide microchannels fabricated from Ecoflex 00-50 by wet bonding with 2500 RPM spin speed and 40 s pre-curing time at 60°C.

It was also qualitatively discovered that with thinner bonding layer the bond between the layers was not as strong. However, the adhesion strength between the layers was not measured or observed in this study. The same spin coating parameters were used with Ecoflex 00-50 as with Dragon Skin 30 for simplicity (Table 3). Spin speeds 1500 RPM

and 2000 RPM were selected for Ecoflex 00-20 (Table 3) since the layer thickness achieved with 1500 RPM is close to the value with Ecoflex 00-50 at 2500 RPM.

It was expected that by increasing the pre-curing rate of the adhesive layer, wetting of the channel walls and blocking of the channels caused by capillary action could be decreased and prevented. However, if the adhesive layer is let to partially cure for too long, the adhesion between the layers is weak. Thus, one minute was used as maximum curing time in this study. Since there still must be interaction between the adhesive layer and the substrate with open channels to create the bonding, wetting of the channel walls and capillary action could not be avoided completely as seen in Figure 9c&d. The geometry of the fabricated closed channels is not perfectly rectangular as the other end is rounded (Figure 9c&d). In Figure 9a&b it can be noted that the open channels were rectangular before bonding and therefore the rounded end is due to wetting and the capillary action caused by the adhesive layer.

To test whether the thickness and pre-curing of the adhesive layer affects the channel yields, the adhesive layers were spin coated with spin speeds 1500 RPM, 2000 RPM and 2500 RPM, and partially cured for varying times from 0 to 60 seconds. The results of channel fabrication are presented in Figure 10 and in Appendix (Table A1 & Table A2). As seen in Figure 10a, the greatest yield (97%) was achieved with Dragon Skin 30. For softer Ecoflex 00-50 and Ecoflex 00-20 the yields were 77% and 67% respectively. The p-value from chi-square test (degrees of freedom (df) = 2) was close to zero so the null hypothesis of independence between whether the channel is open or closed and the elastomer type can be rejected. Thus, there is dependency between the elastomer and how many channels are open.

As for the spin speed of the adhesive layer it can be seen (Figure 10c) that increasing speed and decreasing layer thickness has better yields. Spin speed 1500 RPM was used in fabrication of only Ecoflex 00-20 with 63% yield. The yields for speeds 2000 RPM (all elastomers) and 2500 RPM (only Dragon Skin 30 and Ecoflex 00-50) were 81% and 87% respectively. The chi-square test of independence indicates that there is dependency between the spin speed and the yield ($df = 2$, $p < 0.0001$).

When grouping the results based on the time that was used when partially curing the adhesive layer (Figure 10d), the yields were close to each other varying in the range from 81% to 84%. The gain of unblocked open microchannels without partially curing the layer was lowest (73%) as expected. The chi-square test of independence indicates that there is dependency between the curing time and yield ($df = 3$, $p < 0.0001$). However, as the variation between the yields for pre-curing times from 20–40 seconds is minor, these

results could be taken to suggest that some pre-curing is beneficial to achieve higher yields, but the effect is not very remarkable.

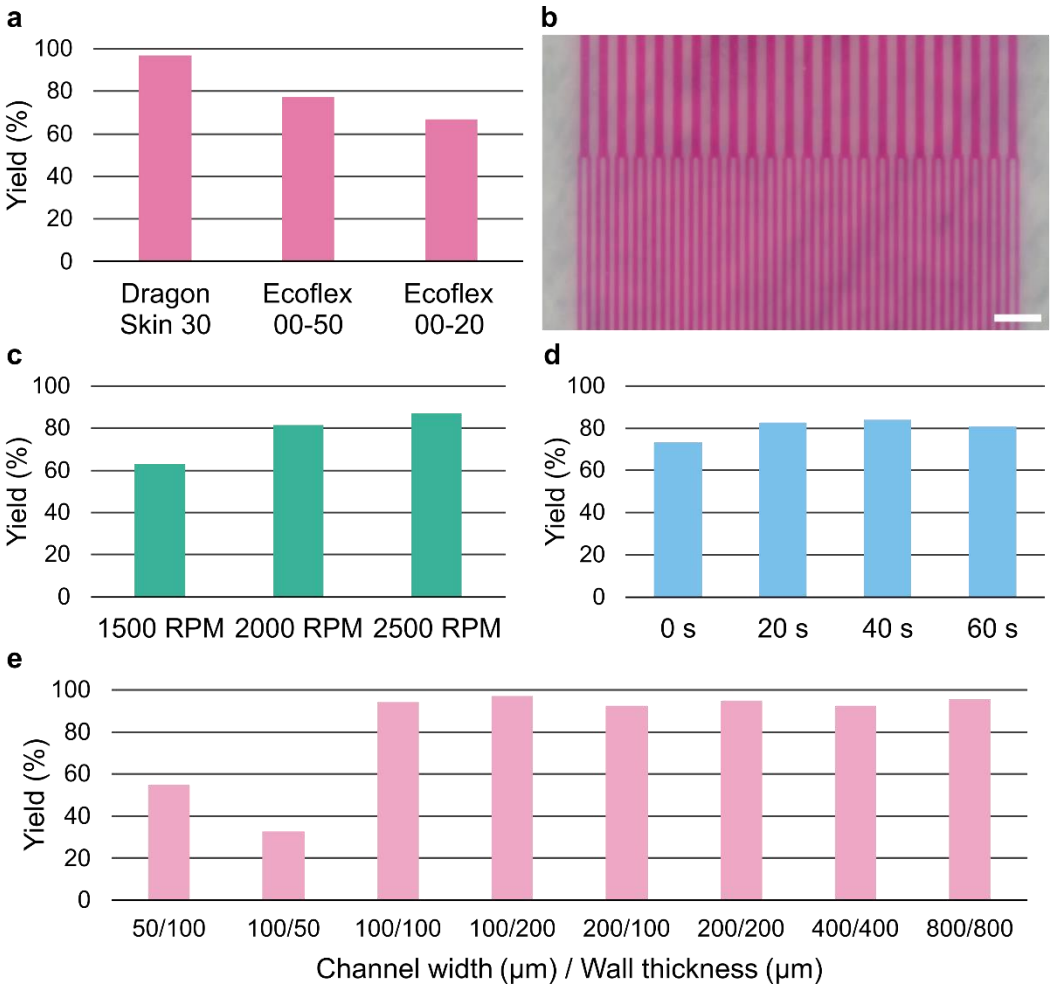

Figure 10. Overview of the channel fabrication results. **a** Yields of channels grouped by material ($p < 0.0001$). **b** Micrograph of 200 µm and 100 µm wide channels with AR (D/L) as 1 fabricated from Dragon Skin 30 with 2500 RPM spin speed and 40 s pre-curing time at 60°C. Channels are filled with pink liquid to visualize them. Scale bar: 500 µm. **c** Yields of channels grouped based on spin speed ($p < 0.0001$). **d** Yields of channels grouped by pre-curing time ($p < 0.0001$). **e** Yields of channels grouped based on the geometry of the channel ($p < 0.0001$).

The results grouped by the channel geometry is presented in Figure 10e. The yield for narrowest channel 50 µm with 100 µm wall thickness was 55%. Densest tested channel geometry with dimensions of 100 µm width and 50 µm wall thickness had the lowest yield of 33%. With the tested 100 µm and wider channels and aspect ratios (D/L) 0.5, 1 and 2, the yields were above 90% varying from 93% to 97%. The chi-square test of independence ($df = 7$, $p < 0.0001$) indicates that there is dependency between the channel geometry and the yield. Overall, the yields for smallest and densest channels significantly low, but the variation within others channel types was small. Thus, the dependency of geometry and the yield is not so clear.

The results of fabrication of microchannels in soft PDMS elastomers were also grouped based on the used elastomer to investigate the reliable fabrication process for each specific PDMS elastomer. Since they have different properties such as viscosity, curing time and softness, it was expected that there would be difference in suitable values of the fabrication process. Yields of varying fabrication parameters with elastomers Dragon Skin 30, Ecoflex 00-50 and Ecoflex 00-20 are expressed in Figure 11.

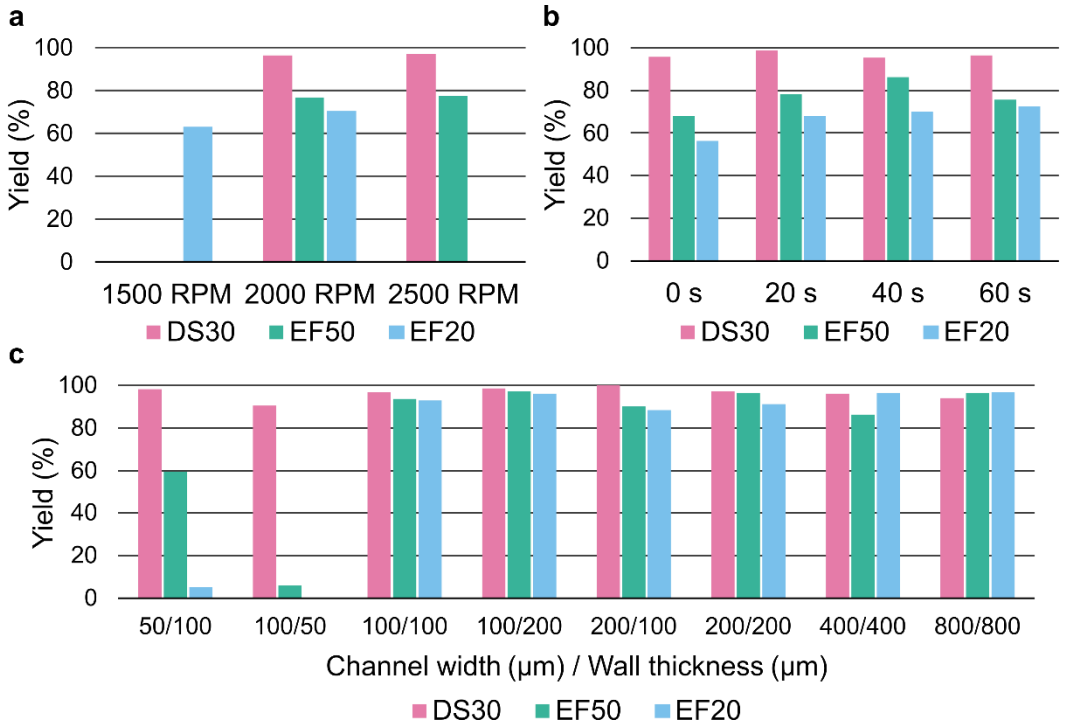

Figure 11. Yields of microchannels per soft silicone elastomers Dragon Skin 30 (DS30), Ecoflex 00-50 (EF50) and Ecoflex 00-20 (EF20). **a** Yields for spin speeds grouped by material. **b** Yields for pre-curing times grouped by material. **c** Yields for channel geometries grouped by material.

Yields for Dragon Skin 30. For microchannels embedded in Dragon Skin 30, the effect of the thickness or spin speed to the yield can be seen in Figure 11a. The yield achieved with 2000 RPM spin speed corresponding to around 60 µm layer thickness (Figure 8) was 96%. The yield with 2500 RPM and 5 µm thinner layer was increased with the value of 97%. According to the chi-square test of independence, the tested spin speeds, and reliability of the fabrication process with Dragon Skin 30 are not dependent ($df = 1$, $p = 0.033$). As for partially curing the adhesive layer, yields for 0, 20, 40 and 60 seconds (Figure 11b) were 96%, 99%, 96% and 97% respectively. In addition, the yield for different channel types were varying in range from 91% to approximately 100% (Figure 11c). The chi-square test for independence indicates that the yield is dependent of the curing time of the fabrication process ($df = 3$, $p < 0.0001$) as well as the geometry of the channel ($df = 7$, $p < 0.0001$).

Yields for Ecoflex 00-50. As the result 77% of the microchannels embedded in Ecoflex 00-50 with layer thickness around 40 µm obtained with 2000 RPM spin speed (Figure 8 & Figure 11a) were open. The yield was also the same with value of 78% when 2500 RPM was used as spin speed. The chi-square test for independence (df = 1, p = 0.27) indicates that the yield is independent of the spin speed used in the fabrication process. There was greater variation in the yields achieved with different pre-curing times (Figure 11b). The smallest yield of 68.0% was obtained without partially curing the layer. For 20– and 40–second pre-curing, the yield was increasing as 78% and 86% respectively. However, the gain obtained with 60 s curing time was 76%. According to the chi-square test of independence (df = 3, p < 0.0001) there is dependency between the pre-curing time and yield of the fabricated microchannels with Ecoflex 00-50. As seen in Figure 11c, the yield for 50 µm wide channels fabricated from Ecoflex 00-50 was 59%. The wider channels with aspect ratios (D/L) 0.5, 1 and 2 got higher values ranging from around 86% to 97%. However, the densest channel type with 100 µm width and 50 µm wall thickness could not be fabricated reliably from Ecoflex 00-50 as the yield was only 5.8%. The p-value of the chi-square test of independence (df = 7) was close to zero, so the null hypothesis can be rejected and there is dependency between the channel geometry and the yields.

Yields for Ecoflex 00-20. The difference in yields with different spin speeds was greater with Ecoflex 00-20 than with Dragon Skin 30 and Ecoflex 00-50 (Figure 11a). Approximately 40 µm thick adhesive layer fabricated with 1500 RPM spin speed (Figure 8a) led to 63% yield. With 2000 RPM spin speed, 70% of the channels were fully open. The chi-square test for independence (df = 1, p < 0.0001) indicates that the yield is dependent of the spin speed used in the fabrication process. As for partially curing the adhesive layer, there was clear increase in the reliability of the fabrication when the curing time was longer (Figure 11b). Without partially curing the layer, 56% of the channels were successful. Even 20 second curing in 60°C oven increased the yield up to 68% whereas 40 seconds lead to 70% and 60 seconds to 72% yields. The p-value of the chi square test of independence (df = 3) was close to zero, so the null hypothesis can be rejected and there is dependency between the curing time and the yields. As for the effect to geometry of the channels (Figure 11c), the thinnest and densest channels could not be fabricated from Ecoflex 00-20 since the yields were only 5.3% and 0% respectively. The yield for the other wider channels with aspect ratios (D/L) 0.5, 1 and 2 varied in the range from 88% to 97%. The chi-square test for independence (df = 1, p < 0.0001) shows that the yield is dependent of the geometry of the channel embedded in Ecoflex 00-20.

The densest channel type with 100 µm width and 50 µm wall thickness was almost impossible to fabricate with the tested wet bonding parameters using softer elastomers Ecoflex 00-50 and Ecoflex 00-20 (Figure 11c). Similarly, the fabrication of the smallest channel type with 50 µm width and 100 µm wall thickness was not reliable especially for Ecoflex 00-20 (5.3% yield) and also for Ecoflex 00-50 with gain under 60%. This is mainly because the channels were deformed already after demolding as seen in Figure 12. With Ecoflex 00-50 and densest channel type with 50 um wall thickness, there was undulation on the surface of the demolded open microchannels. Thus, most of the fabricated channels were blocked and deformed giving a yield that was only 5.8%.

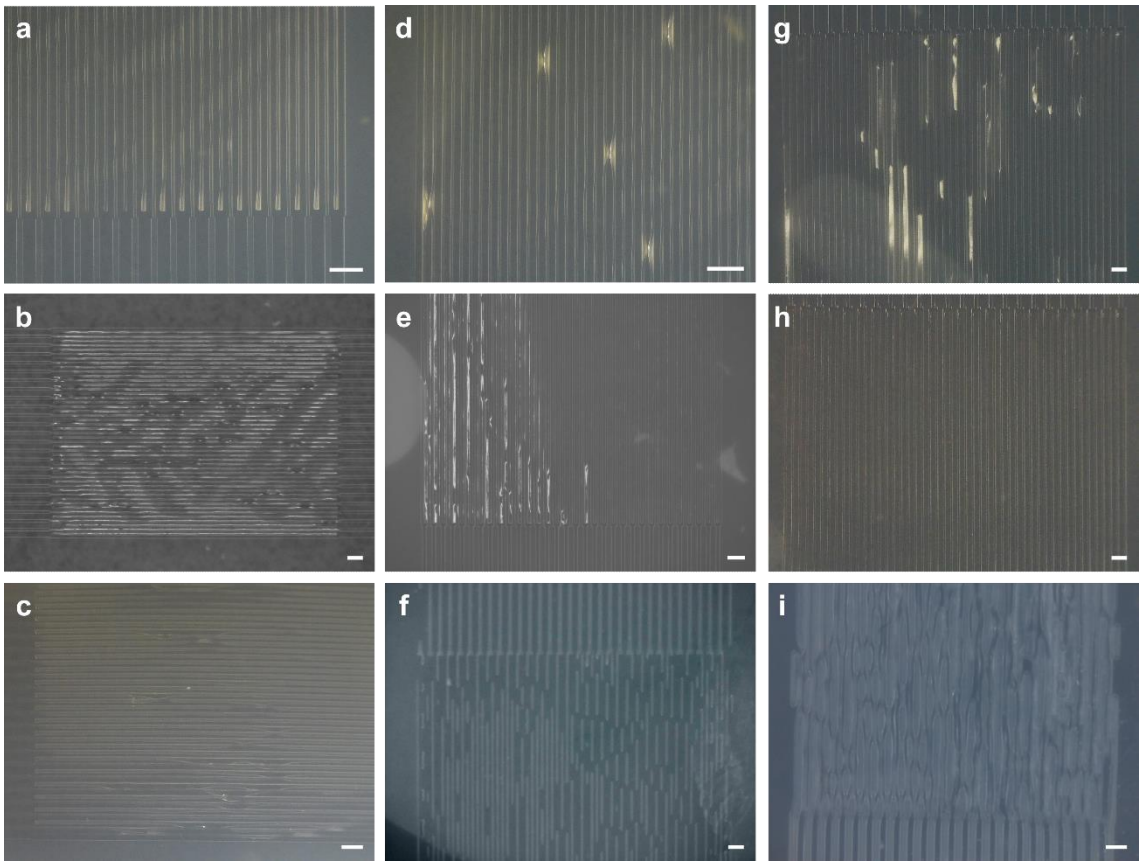

Figure 12. Micrographs of fabricated microchannels. **a** Undulation, **b** deformation, and **c** lateral collapse and undulation of 100 µm wide open channels with 50 µm wall thickness fabricated from Ecoflex 00-50. **e**, **d** Lateral collapse of 50 µm wide open channels with 100 µm wall thickness fabricated from Ecoflex 00-50 and Ecoflex 00-20 respectively. **f** Blocked 50 µm wide closed channels with 100 µm wall thickness fabricated from Ecoflex 00-20 without partially curing the adhesive layer applied with 1500 RPM spin speed. **g** Lateral collapse of 50 µm wide open channels with 200 µm wall thickness before and **h** after stretching (Ecoflex 00-20). **i** Unsuccessful 100 µm wide closed channels with 50 µm wall thickness fabricated from Ecoflex 00-20 with pre-curing the adhesive layer (1500 RPM spin speed) for 20 s. All scale bars: 500 µm.

Pairing of the neighboring channel walls could be seen with digital microscope with open channels with dimensions of 50 µm width and 100 µm wall thickness fabricated from both

Ecoflex 00-50 and Ecoflex 00-20. Micrographs of the lateral collapse or pairing is presented in Figure 12c-e&g. Thus, by stretching the open channels manually in opposite direction as the channels were running, pairing was corrected (Figure 12g&h), and the number of successfully fabricated channels could be increased. However, the impact of stretching the channels to correct pairing was notable only with Ecoflex 00-50. The channels fabricated from Ecoflex 00-20 were still deformed even with the pre-stretching (Figure 12i) and also blocking with capillary action was notable (Figure 12f).

As the yield of 50 µm wide microchannel embedded in Ecoflex 00-20 was poor, new mold was created to test if greater wall thickness would improve the yield. The new mold contained 50 µm wide channels with 200 µm and 300 µm thick walls. To test whether channels thinner than 100 µm could even be fabricated from Ecoflex 00-20 with the wet bonding process and studied parameters, the new mold also contained 80 µm wide channels with 140 µm wall thickness so that the aspect ratio (D/L) was 0.57 which is a little higher than with the 50 µm wide channels that gave only 5.3% yield. The height of the channels was 200 µm and length of one centimetre as in the other mold as well. Thus, the aspect ratio (H/D) was now decreased to 2.5 with the 80 µm wide channels compared to 50 µm width and aspect ratio (H/D) as 4.

Results of the follow-up test are expressed in Figure 13 and in Appendix (Table A3 & Table A4). As seen in Figure 13a, the yields of the follow-up study were improved compared to previous one with Ecoflex 00-20 (Figure 11). The yield for 50 µm wide channel with 200 µm wall thickness was 55% while increased wall thickness of 300 µm gave only the yield of 25%. The fabrication of 80 µm wide channel was 49% which is greater than with the 50 µm and the same aspect ratio (D/L) as 0.5 (5.3% yield). However, deformation of the channels after sealing (Figure 13a) was probable to occur with most of the channels. Similar pairing effect of the open channels could be noticed with the 50 µm wide channels (Figure 12g). Now, the pre-stretching before bonding improved the yield of channels embedded in Ecoflex 00-20. The capillary action related to the adhesive layer was also blocking the smallest 50 µm channels regardless of the density of the channels (Figure 11c&d). Thus, the yields are not high enough to note that fabrication of thinner microchannels than 100 µm embedded in Ecoflex 00-20 would be reliable with wet bonding process and parameters used in this study.

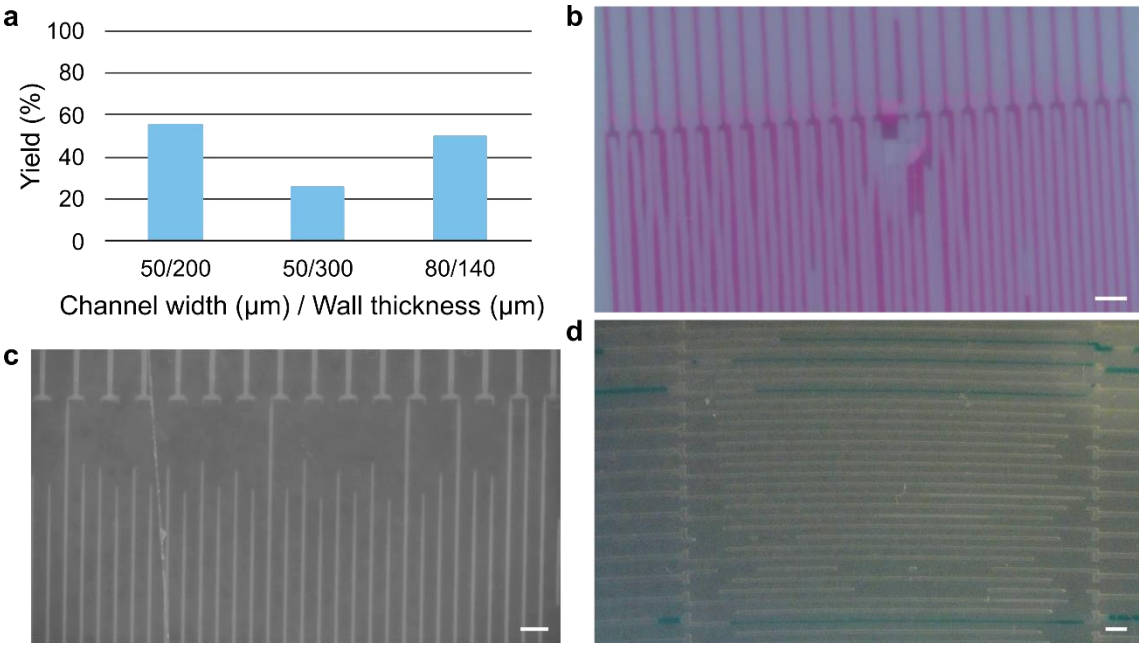

Figure 13. Follow-up study for Ecoflex 00-20. **a** Yields for different channel geometries fabricated from Ecoflex 00-20. **b** Micrograph of 80 µm wide embedded channels with 140 µm wall thickness fabricated from Ecoflex 00-20 with wet bonding process (2000 RPM, 20 s at 60°C). **c** Micrograph of 50 µm wide embedded channels with 300 µm wall thickness fabricated from Ecoflex 00-20 by spin coating the adhesive layer with 2000 RPM and without partially curing it. **d** Micrograph of 50 µm wide closed channels with 200 µm wall thickness fabricated from Ecoflex 00-20 with wet bonding process (2000 RPM, 40 s at 60°C). Channels filled with colorful liquid to visualize them. All scale bars: 500 µm.

As mentioned, the adhesion strength of the seal was not studied in this work, but it was observed that with too thin layer thickness the bond was weak. Therefore, from the parameters used in this study, lower spin speed (2000 RPM) leading to slightly thicker adhesive layer (Figure 8) would be advisable for the wet bonding process with Dragon Skin 30 and Ecoflex 00-50. With Ecoflex 00-20 the increase in yield with faster spin speed (2000 RPM > 1500 RPM) was notable. Thus, it should be used for the fabrication process. The difference in the result for the effect of spin speeds to the yield based on elastomer is due to the difference in slopes seen in Figure 8. As seen in Figure 11a, the change caused by increasement of the spin speed was notable only with Ecoflex 00-20. For Dragon Skin 30 and Ecoflex 00-50 the decrease in thickness is lower when increasing the spin speed from 2000 RPM to 2500 RPM compared to Ecoflex 00-20 with increasement from 1500 RPM to 2000 RPM.

Without partially curing the adhesive layer before bonding, the yield of the fabricated channels was smaller as expected (Figure 10d). However, with Dragon Skin 30 the fabrication process was remarkably high (96%) even without partially curing the layer. Dragon Skin 30 is the most viscous in liquid form of the tested PDMS elastomers (Table 1), which suggests that the viscosity of the elastomer prevents the uncured elastomer

from wetting and blocking the channels before it has time to fully cure as expected. Partially curing the adhesive layer and longer curing times increased the reliability of the process for Ecoflex 00-50 and Ecoflex 00-20. Together with previously mentioned pairing and need for pre-stretching the substrate with open channels, some air bubbles were created between the elastomer substrates while layering, ruining the channels. Similar variation caused probably by human errors can be seen with the results of channel fabrication from Dragon Skin 30, as the yield with different pre-curing times were varying in the range of 96–99%.

In general, it was stated that too long curing time causes weak bonding or can even prevent it totally. Hence, based on the result of this study, optimal curing time for the bonding layer would be in the range of 20–40 seconds for Ecoflex 00-50 and 00-20 when curing in the oven at 60°C temperature. Then there would still be clearance before the layer is fully cured. Curing times of the elastomers from Dragon Skin and Ecoflex series are several hours in room temperature, but the required time can be reduced by heating. In addition, with tens of micrometres thick layers, too cured state for effective bonding is reached even in shorter times. As the variation of the yield for Dragon Skin 30 was minor regardless of the curing time, it would be beneficial to use an uncured adhesive layer and not partially cure it in the oven, but only when the layer is thin enough. In this way one step can be erased from the bonding process simplifying the fabrication.

Figure 9c&d revealed that the capillary action of the adhesive layer cannot be totally prevented. Two corners of the rectangular cross-section are rounded and thus the geometry of the fabricated channels is not exactly as intended. This must be taken into account if the cross-sectional geometry of the channels has an effect to the performance and output of the desired application. For example, with soft sensors the issue can be overcome with calibration.

Proposed parameters for fabrication of microchannels embedded in selected PDMS elastomers with wet bonding process in which the adhesive layer is applied with spin coating are collected in Table 4. Parameters are valid when the diameter of the flat substrate is around 110 mm and the amount of applied uncured elastomer is approximately 1.5 g. In general, the wet bonding process contains four main steps including fabrication of the sealing layer and the layer with open channels, applying the adhesive layer, partially curing the adhesive layer and bonding after pre-stretching if it is needed. As discussed, the third step can be skipped when using Dragon Skin 30 for the fabrication. Contrary to expectations, the proposed values do not differ notably from elastomer to elastomer.

Table 4. Proposed parameters for reliable wet bonding process based on this study for the fabrication of microchannels embedded in selected commercial soft elastomers by applying the adhesive layer with spin coating and partially curing the layer in oven.

Elastomer	Spin speed	Spin time	Curing time	Temperature
Dragon Skin 30	2000 RPM	90 s	-	-
Ecoflex 00-50	2000 RPM	90 s	20–40 s	60°C
Ecoflex 00-20	2000 RPM	90 s	20–40 s	60°C

The wet bonding process with proposed parameters can possibly be applied also to other elastomers from Dragon Skin and Ecoflex series produced by Smooth-On. For example, elastomers Dragon Skin 20 (Shore A hardness 20) and Dragon Skin 15 (Shore A hardness 15) have 21 Pa·s mixed viscosity according to their data sheets which is almost the same as with Dragon Skin 30 (20 Pa·s). Thus, the same spin speed 2000 RPM as proposed for Dragon Skin 30 could produce as high rate of reliability for the fabrication process as with Dragon Skin 20 and Dragon Skin 15. Softer Dragon Skin 10 Medium (Shore A hardness 10) has higher viscosity (23 Pa·s) so slightly thicker layer is expected with 2000 RPM spin speed, but still the same parameters may be suitable for fabricating microchannels with the studied method. Curing times of other silicones than Dragon Skin 30 of Dragon Skin series are less than 16 hours in room temperature as opposed to Dragon Skin 30. However, as partially curing the layer was not essential for reliable wet bonding process with Dragon Skin 30, it can be expected that it is also valid for the other elastomers of the series as they have approximately the same viscosity.

Some silicones from Ecoflex series have similar viscosity and curing times as Ecoflex 00-50 or 00-20 studied in this work. For example, Ecoflex 00-30 (Shore 00 hardness 30) and Ecoflex 00-45 Near Clear (Shore 00 hardness 45) have the same viscosity and cure times than Ecoflex 00-20 with the values of 3 Pa·s and 4 hours respectively. Thus, proposed process parameters are also appropriate for those PDMS elastomers. For applications that require even softer elastomer, Ecoflex 00-10 (Shore 00 hardness 10) has higher viscosity (14 Pa·s) than Ecoflex 00-50 (8 Pa·s). However, it can be beneficial to try the proposed parameters first when using it for fabrication of microchannels with the studied method. Cure time of Ecoflex 00-10 is also four hours as with Ecoflex 00-20 so partially curing for 20–40 seconds in 60°C oven can be enough for reliable fabrication process.

In this work, the adhesive layer was spread with spin coating, but also other methods can be used in wet bonding process. For example, bar coating is another rather straightforward technique to spread the uncured elastomer evenly on the surface of flat elastomer substrate. Currently spin coating is effective only for coating small substrates. Bar

coating can be more suitable for larger components needed for example in soft robotic applications. The thickness of the obtained layer is determined by the applicator and typically a spiral film applicator is used in bar coating. The spiral film applicator consists of a cylindrical bar with a wire wrapped around it. The gaps between the wire and the flat elastomer substrate determines the thickness of the spread layer. According to Figure 8 the layer thicknesses with the proposed 2000 RPM spin speed are approximately 60 µm, 40 µm and 30 µm for Dragon Skin 30, Ecoflex 00-50 and Ecoflex 00-20 respectively. Thus, spiral film applicators that can produce those layer thicknesses can be used for spreading the adhesive layer in wet bonding process to maintain the reliability of the process achieved with spin coating. Doctor blading technique that is very much alike to bar coating is another option for spreading the elastomer. A blade is moved over the substrate, or the substrate is moved underneath the blade. The gap between the substrate and the blade determines the thickness of the fabricated layer. There are also other well-known methods for thin-film fabrication such as dip coating and slot-die coating. However, results of this study are not directly useful for adopting those techniques to the wet bonding process as their operation principles and parameters are different.

The PDMS elastomers studied in this work are softer than Sylgard 184 and thus, the optimal aspect ratios reported by Whitesides Research Group [12] for Sylgard 184 (optimal: $0.5 < H/L < 5$ and $H/D > 0.05$) were expected to be invalid. The channels tested in this work had ARs in range of 0.25 to 4 for both H/L and H/D. With Sylgard 184 sagging occurs when the AR calculated by dividing height (H) of the channel with the width (D) of the channel is under 0.5 [12]. In this study the smallest H/D value was 0.25 µm with 800 µm wide and 200 high channels with 800 µm wall thickness. That channel type was reliably fabricated from all elastomers used in the study with 94% or higher yield. Thus, sagging of the fabricated channels was not observed in this study even though the H/L value was smaller than the limit value for Sylgard 184. One possible reason is that the thickness of the fabricated elastomer substrates with and without the open channels were varying from 1.0 mm to 2.4 mm. As the height of all channels was 200 µm, the ceiling was still quite bulky and perhaps prevented the sagging. With thinner ceilings and elastomer substrates sagging can be expected and must be considered. In addition, the pressure caused by injecting the dyed water inside the channels may have raised the sagged ceiling.

The difference between Dragon Skin 30 and Sylgard 184 according to pairing could not be made either. Channels with H/L as high as 5 were not tested in this study as the highest values was 4. The yield for the tested channel types fabricated from Dragon Skin 30 was higher than 90%. Thus, it can be stated that the proposed process parameters

are reliable for the channel sizes listed in Table 2. As the softness of Dragon Skin 30 is close to Sylgard 184, it can be expected that it has almost the same threshold values for optimal aspect ratios. Therefore, the maximum H/L value is probably placed between 4 and 5.

As expressed in Figure 12c, open channels fabricated from Ecoflex 00-50 paired when the 200 µm height channels were 50 µm wide and had 100 µm thick walls. The H/L aspect ratios of such channel type is 2. However, as the 200 µm wide and 200 µm high channels with 100 µm wall thickness had the yield of over 93%, even though the H/L aspect ratio was the same. Similarly, the 100 µm wide and 200 µm high channels with 100 µm thick walls and 2 as H/L aspect ratio had the yield of over 90% but 100 µm wide and 200 µm high channels with 50 µm wall thickness and 4 as H/L aspect ratio were already ruined after demolding or paired before bonding. Undulation of open microchannels was reported in Figure 12a. This observation arises a question whether the dimensions of the channels were too small that the soft elastomer seizes into such tiny features and demolding deforms it. Thus, this can be another problem caused by the softness of the elastomer in addition to lateral collapse and sagging.

However, based on this study, 50 µm thick walls or wide channels cannot be reliably fabricated from Ecoflex 00-50 with wet bonding regardless of the aspect ratios. Similar limits were observed with Ecoflex 00-20 as the 100 µm wide and 100 µm high channels with 100 µm thick walls were the smallest type that could be fabricated reliably (92% yield). The follow-up test studied whether smaller than 100 µm wide channels with wider walls than 100 µm could be fabricated from Ecoflex 00-20, but as seen in Figure 13, results indicated that 100 µm is the limit for both wall thickness and width. Pre-stretching helped with pairing especially with Ecoflex 00-50, probably because softer walls fabricated from Ecoflex 00-20 recollapse more easily and faster. However, such manual work complicates the fabrication process and decreases the reliability and reproducibility as influence of the person performing the work increases. Thus, it is beneficial to avoid the pre-stretching by making larger channels if the application allows.

5.2 Soft Pneumatic Strain Sensor

To prove that soft pneumatic strain sensor with meandering microchannels proposed by Koivikko et al. [10] can be fabricated with the method studied in this work, a soft pneumatic strain gauge was fabricated from Ecoflex 00-50. Since Ecoflex 00-50 is extremely soft elastomer, the fabricated soft sensor can be stretched, twisted or bent without damaging it (Figure 14d). The elongation at break of Ecoflex 00-50 is 980% (Table 1) so the soft strain sensor is highly stretchable and can be used for measuring large strains. The

sensor did not rupture or fail before close to 500% strains, but 300% strain was used as maximum in the measurements. For demonstrating that the fabricated pneumatic strain gauge can be used to detect strain the sensor was elongated with varying strain up to 300% while recording the relative change in pneumatic resistance (Figure 14). The results of the demonstrations are reported also in [10].

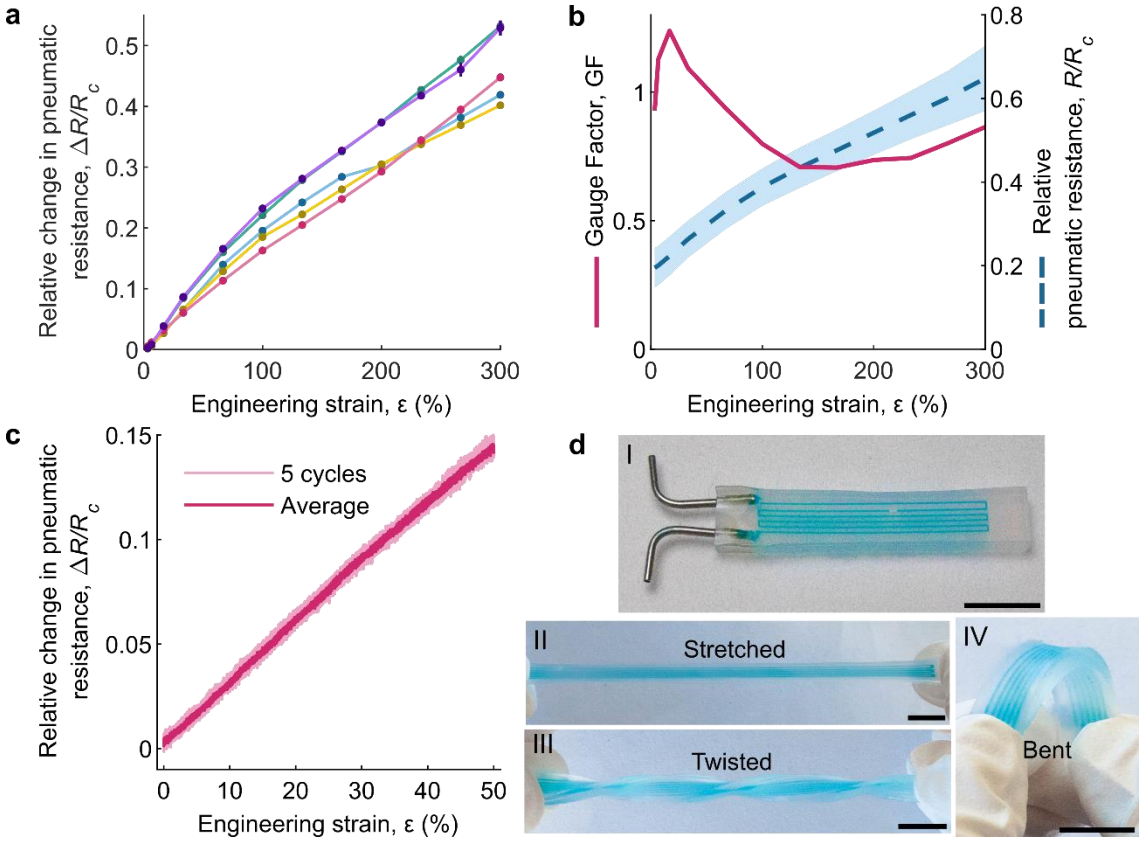

Figure 14. Soft pneumatic strain gauge. **a** Relative change in pneumatic resistance as function of engineering strain for five strain sensor samples. Each curve is an average of five measurements with one sample. Error bars represent standard deviation (n = 5). **b** Gauge factor (average of five strain gauges) calculated from the data of the measurement expressed in **a** with Equation 5. Shaded blue area represent standard deviation (n = 5). **c** Hysteric behavior of the strain sensor while stretching the sensor five times up to 50% engineering strain with 0.01 mm/s strain rate. **d** Pictures of the pneumatic strain sensor as relaxed (I), stretched (II), twisted (III) and bent (IV). Blue liquid is used to fill the microchannel for visualization. All scale bars: 1 cm. All reported also in [10].

The results for five strain sensor samples are expressed in Figure 14a. As seen in the graph, the relative change in the pneumatic resistance increased as a function of the engineering strain with all five samples. Each curve represents one strain sensor sample and is an average of five measurements with that sensor. The behavior of the samples is rather consistent even though there is some variation across the samples. Also, the variation between the five measurements from each sample was minor as the error bars representing standard deviation are mostly too small to be seen.

To study the sensitivity of the soft pneumatic strain sensor, the gauge factor was calculated with Equation (5) from the average of the data of five strain gauges used in Figure 14a. The GF and average of the relative pneumatic resistance (R/R_c) as function of applied engineering strain is presented in Figure 14b. With smaller strains under 50% the GF increased to 1.2 but made a parabolic slope with minimum of 0.71 when the strain increased. However, the value was small and close to 1 for the entire range of strains tested.

The rate-independent hysteric behavior of the soft strain sensor was studied by applying 50% engineering strain with a 0.01 mm/s strain rate for five times while recording the relative change in pneumatic resistance. Slow strain rate was used to avoid rate-dependent effects such as dynamic viscoelastic effects. The result of the experiment is presented in Figure 14c. As seen in the graph, the hysteresis of the sensor was negligible and cannot be distinguished from the noise level of the sensor which was 5% within the tested strain range. Even the average of the five experiments does not reveal any hysteresis.

Table 5. Summary of recently reported stretchable microfluidic strain sensors and their characteristics. N.R. = not reported.

Materials	Fabrication method	Sensor type	Max. strain tested (%)	Hysteresis (%)	Gauge factor	Reference
Sylgard 184, Galinstan	Casting, channel filling	Resistive	105	0.07	2.33	[77]
Ecoflex. EGaIn	Casting, channel filling	Resistive	550	N.R.	4.95	[56]
Ecoflex 00-30, ionic solution, EGaIn	Casting, channel filling	Resistive	100	N.R.	~3	[29]
Ecoflex 00-30, EGaIn	Casting, channel filling	Resistive	100	~0	3.7	[76]
Ecoflex, ionic solution	Casting, channel filling	Resistive	400	N.R.	31.6	[78]
Ecoflex 00-50	**Casting**	**Pneumatic**	**300**	**~0***	**~1**	**This work****

*Measured in 50% with 0.01 mm/s strain rate
**Reported also in [10]

Comparison of the fabricated pneumatic strain sensor to other microfluidic strain sensors based on deformation of the microchannels and reported in the literature is expressed in Table 5. Compared terms are materials, fabrication method, type of the sensor, maximum strain, hysteresis, and gauge factor. The soft pneumatic strain gauge of this work is highly stretchable tolerating at least 500% straining without rupturing. Even though the

elongation at break of Ecoflex 00-50 is 980%, as high strains cannot be measured with the sensor since the elongation at break value is for bulk. The meandering microchannel inside the elastomer substrate reduces the capability of the elastomer to resist the deformation without cracking. Fabricating sensor with the same design from softer elastomer such as Ecoflex 00-20 would not make the sensor more stretchable as the elongation at break of Ecoflex 00-20 is slightly smaller with the value of 845%. Compared to other fluidic strain sensors listed in Table 5, stretchability of the sensor is competitive.

The GF of the pneumatic strain gauge varied around 1 revealing that the sensor is more sensitive to large strains. Low GF value indicates that the change of the output of the sensor with small strains can be too minor to be detected limiting the usability of the sensor. Compared to selected strain sensors with microchannels filled with liquid metal, ionic liquid, or both (Table 5), the sensitivity of the pneumatic strain sensor is weakest with smaller strains. However, the sensor is suitable to detect larger strains as intended.

Rate-independent hysteresis of the soft pneumatic strain sensor was so negligible that it could not be distinguished from the noise level as seen in Figure 14c. Hysteric behavior of stretchable strain sensors typically occurs due to the viscoelastic nature of the supporting elastomer [7] which is not studied in this work as the measurement was executed with low strain rate to avoid the rate-dependent effects. Typically, capacitive sensors have lower hysteretic behavior compared to resistive sensors due to combined effect of the viscoelasticity of the polymer and conductive fillers [7]. As seen in Table 5, microfluidic resistive strain sensors also have negligible hysteresis as well as the pneumatic strain sensor since the contribution of fluids to the hysteric behavior is smaller compared to other conductive matter.

Fabrication of the pneumatic strain sensor was performed with wet bonding process using 2500 RPM spin speed, 90 second spin time and 40 second pre-curing time in the oven at 60°C. This differs from the suggested parameters for the reliable fabrication process (Table 4) for the spin speed because the pneumatic sensors were fabricated before the thorough exploration and optimization of all the bonding parameters was completed. The initial pneumatic resistance of the strain gauge at rest (R_0) varies from sample to sample and thus the ratio $\Delta R/R_c$ was used instead of R/R_c. The variation can be caused by the fabrication process as the capillary action related to the adhesive layer could not be fully avoided (Figure 9c&d). Thus, the cross-sectional area of the meandering microchannel varies between the samples but also within the length of one channel. The pressure inside the microchannel is dependent on the cross-sectional area leading to variation of the pneumatic resistance as well. Even though the reliability of the wet bonding process and fabrication of microchannels was increased in this work, sample to sample

variation related to the cross-sectional area of the channels cannot be completely prevented.

Main difference of the soft strain sensor in this work, compared to others reported in the literature, is that the strain detection is based on change in pneumatic resistance and not electrical resistance (Table 5). Application areas of the pneumatic strain sensor is for example in soft robotics, where it can be used to detect deformations and movement of the soft actuators as reported in [10]. In addition, the pneumatic sensor could be used to measure physical contact as a tactile sensor since transverse compression also decreases the cross-sectional area of the microchannel which leads to increase in the pneumatic resistance.

Since the sensor can be fabricated monolithically and from the same elastomer as the rest of the robot with commonly used silicone casting [35], integration of it to the body of the soft robot is rather straight forward as proven by Bilodeau et al. [79] and also reported in [10]. Channels of the strain sensor can be applied to the same mold as the robot and its actuators. Thus, there is no need to build the sensors and actuators separately and integrate them afterwards. The wet bonding can be utilized in the fabrication if the robot is constructed in the way that spreading the adhesive layer is possible.

When the sensor type is pneumatic instead of electrically resistive, one step of the fabrication process can be left out as the channels of the sensors do not have to be filled with liquid metal or ionic liquid for example. Soft actuators used in soft robotics are generally fluidic and especially pneumatically driven. The actuation is produced by filling channels and cavities embedded in soft elastomers as they expand due to the applied pressure. [14], [62] Thus, benefit of pneumatic sensors compared to electrical in soft robotics is that the complexity of the system decreases. When the sensors are pneumatic as well as the soft actuators, there is no need for separate control or power systems for sensing and actuation. Similarly, signals do not have to be transduced from one energy domain to another if the actuation is controlled with observations of the sensors.

6. CONCLUSIONS AND FUTURE WORK

The aim of this thesis was to enhance the reliability and repeatability of wet bonding process for bonding microchannels from soft silicone elastomers. The problem related to wet bonding is the blocking of the microchannels with the uncured elastomer used as adhesive between the layers. Three different commercial elastomers (Dragon Skin 30, Ecoflex 00-50 and Ecoflex 00-20) were used for the study. The adhesive layer was spread on the flat elastomer substrate with a spin coater and pre-cured in the oven at 60°C temperature. Different spin speeds and pre-curing times were tested to obtain as high yield as possible for the fabricated channels. In addition, channels with different dimensions were bonded, to discover the range of channel sizes that can be fabricated with the process. Finally, a practical application of the wet bonding method was demonstrated using it to bond a soft pneumatic strain sensor.

The result was that spin coating the adhesive layer with 2000 RPM for 90 s produces thin enough layer to decrease the capillary action with all studied elastomers when the diameter of the flat elastomer substrate is around 110 mm and approximately 1.5 g of the uncured elastomer is applied. Suitable pre-curing time in the oven at 60°C is 20 to 40 seconds for Ecoflex 00-50 and Ecoflex 00-20. Partially curing is not mandatory with Dragon Skin 30 if the layer is thin enough. The yields for 100 µm wide channels were over 90% with 200 µm height and at least as wide channel walls with all the elastomers. However, 50 µm for both width and channel wall thickness were producible only with Dragon Skin 30.

It is assumed, that the results of this work can also be applied to other elastomers from Dragon Skin and Ecoflex series when utilizing the studied microchannel fabrication technique. As a future work, this hypothesis should be tested. Similarly, the assumption that different methods for spreading the layer are applicable, and proposed thickness of the adhesive layer (60 µm, 40 µm and 30 µm for Dragon Skin 30, Ecoflex 00-50 and Ecoflex 00-20 respectively) are suitable for reliable fabrication process, follow-up studies are needed.

Clear optimal aspect ratios as reported for Sylgard 184 [12] were not found in this study. It can be assumed based on the results that Dragon Skin 30 has limits close to Sylgard 184. The limitations for Ecoflex 00-50 and 00-20 are somewhere close to 100 µm thick walls and 100 µm wide channels, but precise optimal range for dimensions or ARs cannot be directed from the results of this study. Therefore, more research is needed to discover

how small and dense channels or features can be fabricated from such soft elastomers. In addition, the microchannels fabricated in this work were all 200 µm high. It would be beneficial to study the wet bonding process also for lower channels since the thickness of the adhesive layer may limit the height of the channels. Capillary action cannot be totally prevented and low channels especially with height close to the thickness of the adhesive layer can get blocked more easily than higher channels.

Placement of the elastomer substrate with open channels on the surface of the adhesive layer is conducted manually in this work. This increases the possibility of human errors during the fabrication. To step up precision, the placing should be done with an automated system similar as for example a micro stamping device (i.e., Fineplacer pico-MA, Finetech). The device stacks the layer with a constant force and pressing the substrate with open channels into the adhesive layer would be avoided.

It was qualitatively observed in this study that when the adhesive layer was too thin the strength of the seal is weak, and the layers can be separated easily. However, the bond strength was not quantitively measured as a part of this thesis work. As a future work, the bond strength as a function of layer thickness should be quantified. A suitable test method could be a kind of a 180° peeling experiment, where a mechanical tester is used to separate the two layers while measuring peel strength.

Another aspect that needs more attention is the fabrication of microchannels meandering in 3D and embedded in elastomers. Microfluidic channels fabricated from Sylgard 184 can be running in several layers. Such structures are fabricated with layer-by-layer method by stacking several Sylgard 184 substrates with open channels on top of each other with plasma bonding. The connections are created before the bonding by punching a hole where the vias are intended to be. Same technique is not suitable for softer PDMS elastomers that cannot be plasma bonded since the punched holes will be blocked by the adhesive layer when the microchannel fabrication method studied in this work is used. Another problem related to 3D channels is aligning the channels on top of each other as designed. With Sylgard 184 optical methods such as microscopes and alignment markers included in the Sylgard 184 substrate can be used because the material is transparent. Silicones from Dragon Skin and Ecoflex series are translucent but not transparent, so development of enhanced or other alignment methods are needed.

A practical application for the studied fabrication technique was demonstrated as the soft pneumatic strain sensor proposed by Koivikko et al. [10] was fabricated and characterized. The highly stretchable strain gauge fabricated from Ecoflex 00-50 with the method can tolerate at least up to 300% strains, has negligible hysteresis and GF close to 1

revealing its suitability to measure large strains. The capillary action of the adhesive layer in the bonding technique causes sample to sample variation to the response of the pneumatic sensor as the cross-sectional area of the pneumatic microchannel embedded in elastomer slightly varies.

Integration of pneumatic logic and control to soft robotics and development of electronics free soft robots has recently obtained increased interest. Current solutions involve external piping acting as interconnections between the components of the pneumatic circuits. [41]–[44] Combining soft microfluidic components and microchannels to soft robotics can be beneficial for further development of the soft devices. Microfluidics can help to miniaturize the soft robotic systems and actuators making them more practical and aesthetically pleasing [80] as the pipes used as interconnections are replaced with microchannels integrated into the body of the robot. Similarly, pneumatic logic circuits and sensors could be integrated to the robot.

REFERENCES

[1] G. M. Whitesides, “The origins and the future of microfluidics,” *Nature*, vol. 442, no. 7101, pp. 368–373, Jul. 2006.

[2] J. C. McDonald and G. M. Whitesides, “Poly(dimethylsiloxane) as a material for fabricating microfluidic devices,” *Acc. Chem. Res.*, vol. 35, no. 7, pp. 491–499, 2002.

[3] H. Fallahi, J. Zhang, H. P. Phan, and N. T. Nguyen, “Flexible microfluidics: Fundamentals, recent developments, and applications,” *Micromachines*, vol. 10, no. 12, p. 830, 2019.

[4] S. Krpovic, K. Dam-Johansen, and A. L. Skov, “Importance of Mullins effect in commercial silicone elastomer formulations for soft robotics,” *J. Appl. Polym. Sci.*, vol. 138, no. 19, p. 50380, May 2021.

[5] E. Luis *et al.*, “3D Printed Silicone Meniscus Implants: Influence of the 3D Printing Process on Properties of Silicone Implants,” *Polym. 2020, Vol. 12, Page 2136*, vol. 12, no. 9, p. 2136, Sep. 2020.

[6] J. Kim, A. S. Campbell, B. E. F. de Ávila, and J. Wang, “Wearable biosensors for healthcare monitoring,” *Nat. Biotechnol.*, vol. 37, no. 4, pp. 389–406, Feb. 2019.

[7] M. Amjadi *et al.*, “Stretchable, Skin-Mountable, and Wearable Strain Sensors and Their Potential Applications: A Review,” *Adv. Funct. Mater.*, vol. 26, no. 11, pp. 1678–1698, Mar. 2016.

[8] H. Wang, M. Totaro, and L. Beccai, “Toward Perceptive Soft Robots: Progress and Challenges,” *Adv. Sci.*, vol. 5, no. 9, p. 1800541, Sep. 2018.

[9] M. D. Dickey, “Stretchable and Soft Electronics using Liquid Metals,” *Adv. Mater.*, vol. 29, no. 27, p. 1606425, Jul. 2017.

[10] A. Koivikko, V. Lampinen, M. Pihlajamäki, K. Yiannacou, V. Sharma, and V. Sariola, “Integrated stretchable pneumatic strain gauges for electronics-free soft robots,” *Commun. Eng.*, vol. 1, no. 1, pp. 1–10, Jun. 2022.

[11] S. Park *et al.*, “Silicones for Stretchable and Durable Soft Devices: Beyond Sylgard-184,” *ACS Appl. Mater. Interfaces*, vol. 10, no. 13, pp. 11261–11268, 2018.

[12] D. Qin, Y. Xia, and G. M. Whitesides, “Soft lithography for micro- and nanoscale patterning,” *Nat. Protoc.*, vol. 5, no. 3, p. 491, 2010.

[13] H. Souri *et al.*, “Wearable and Stretchable Strain Sensors: Materials, Sensing Mechanisms, and Applications,” *Adv. Intell. Syst.*, vol. 2, no. 8, p. 2000039, Aug. 2020.

[14] D. Rus and M. T. Tolley, “Design, fabrication and control of soft robots,” *Nature*, vol. 521, no. 7553, pp. 467–475, May 2015.

[15] K. Larson, “Can You Estimate Modulus From Durometer Hardness for Silicones?,”

Dow White Pap., 2017.

[16] A. N. Gent, “On the Relation between Indentation Hardness and Young’s Modulus,” *Rubber Chem. Technol.*, vol. 31, no. 4, pp. 896–906, 1958.

[17] H. J. Qi, K. Joyce, and M. C. Boyce, “Durometer hardness and the sress-strain behavior of elastomeric materials,” *Rubber Chem. Technol.*, vol. 76, no. 2, pp. 419–435, 2003.

[18] “Dragon Skin™ Series.” https://www.smooth-on.com/tb/files/DRAGON_SKIN_SERIES_TB.pdf (accessed Sep. 27, 2022).

[19] “Ecoflex™ Series.” https://www.smooth-on.com/tb/files/ECOFLEX_SERIES_TB.pdf (accessed Sep. 27, 2022).

[20] J. Kuncová-Kallio and P. J. Kallio, “PDMS and its suitability for analytical microfluidic devices,” *Annu. Int. Conf. IEEE Eng. Med. Biol. - Proc.*, pp. 2486–2489, 2006.

[21] I. Wong and C. M. Ho, “Surface molecular property modifications for poly(dimethylsiloxane) (PDMS) based microfluidic devices,” *Microfluid. Nanofluidics 2009 73*, vol. 7, no. 3, pp. 291–306, Apr. 2009.

[22] B. J. van Meer *et al.*, “Small molecule absorption by PDMS in the context of drug response bioassays,” *Biochem. Biophys. Res. Commun.*, vol. 482, no. 2, pp. 323–328, Jan. 2017.

[23] J. A. Rogers, T. Someya, and Y. Huang, “Materials and mechanics for stretchable electronics,” *Science (80-.).*, vol. 327, no. 5973, pp. 1603–1607, Mar. 2010.

[24] D. McCoul, W. Hu, M. Gao, V. Mehta, and Q. Pei, “Recent Advances in Stretchable and Transparent Electronic Materials,” *Advanced Electronic Materials*, vol. 2, no. 5. Blackwell Publishing Ltd, p. 1500407, May 01, 2016.

[25] A. Mata, A. J. Fleischman, and S. Roy, “Characterization of Polydimethylsiloxane (PDMS) Properties for Biomedical Micro/Nanosystems,” *Biomed. Microdevices 2005 74*, vol. 7, no. 4, pp. 281–293, Dec. 2005.

[26] Z. Wang, A. A. Volinsky, and N. D. Gallant, “Crosslinking effect on polydimethylsiloxane elastic modulus measured by custom-built compression instrument,” *J. Appl. Polym. Sci.*, vol. 131, no. 22, p. 41050, Nov. 2014.

[27] E. Delplanque *et al.*, “Mechanical characterization of bulk Sylgard 184 for microfluidics and microengineering,” *J. Micromechanics Microengineering*, vol. 24, no. 3, p. 035017, Feb. 2014.

[28] R. F. Shepherd *et al.*, “Multigait soft robot,” *Proc. Natl. Acad. Sci.*, vol. 108, no. 51, pp. 20400–20403, Dec. 2011.

[29] J. B. Chossat, Y. L. Park, R. J. Wood, and V. Duchaine, “A soft strain sensor based on ionic and metal liquids,” *IEEE Sens. J.*, vol. 13, no. 9, pp. 3405–3414, 2013, doi: 10.1109/JSEN.2013.2263797.

[30] M. Wehner *et al.*, “An integrated design and fabrication strategy for entirely soft, autonomous robots,” *Nature*, vol. 536, no. 7617, pp. 451–455, Aug. 2016.

[31] F. Ilievski, A. D. Mazzeo, R. F. Shepherd, X. Chen, and G. M. Whitesides, “Soft robotics for chemists,” *Angew. Chemie - Int. Ed.*, vol. 50, no. 8, pp. 1890–1895, Feb. 2011.

[32] D. Huh, B. D. Matthews, A. Mammoto, M. Montoya-Zavala, H. Yuan Hsin, and D. E. Ingber, “Reconstituting organ-level lung functions on a chip,” *Science (80-.).*, vol. 328, no. 5986, pp. 1662–1668, Jun. 2010.

[33] H. J. Kim, D. Huh, G. Hamilton, and D. E. Ingber, “Human gut-on-a-chip inhabited by microbial flora that experiences intestinal peristalsis-like motions and flow,” *Lab Chip*, vol. 12, no. 12, pp. 2165–2174, May 2012.

[34] D. Huh, Y. S. Torisawa, G. A. Hamilton, H. J. Kim, and D. E. Ingber, “Microengineered physiological biomimicry: Organs-on-Chips,” *Lab Chip*, vol. 12, no. 12, pp. 2156–2164, May 2012.

[35] B. Yuan *et al.*, “A Strategy for Depositing Different Types of Cells in Three Dimensions to Mimic Tubular Structures in Tissues,” *Adv. Mater.*, vol. 24, no. 7, pp. 890–896, Feb. 2012.

[36] W. Zheng, B. Jiang, D. Wang, W. Zhang, Z. Wang, and X. Jiang, “A microfluidic flow-stretch chip for investigating blood vessel biomechanics,” *Lab Chip*, vol. 12, no. 18, pp. 3441–3450, Aug. 2012.

[37] I. R. Minev *et al.*, “Electronic dura mater for long-term multimodal neural interfaces,” *Science (80-.).*, vol. 347, no. 6218, pp. 159–163, Jan. 2015.

[38] H. J. Kim, C. Son, and B. Ziaie, “A multiaxial stretchable interconnect using liquid-alloy-filled elastomeric microchannels,” *Appl. Phys. Lett.*, vol. 92, no. 1, p. 011904, Jan. 2008.

[39] M. Kubo *et al.*, “Stretchable microfluidic radiofrequency antennas,” *Adv. Mater.*, vol. 22, no. 25, pp. 2749–2752, Jul. 2010.

[40] A. Koh *et al.*, “A soft, wearable microfluidic device for the capture, storage, and colorimetric sensing of sweat,” *Sci. Transl. Med.*, vol. 8, no. 366, p. 366ra16, Nov. 2016.

[41] S. V. Kendre *et al.*, “The Soft Compiler: A Web-Based Tool for the Design of Modular Pneumatic Circuits for Soft Robots,” *IEEE Robot. Autom. Lett.*, vol. 7, no. 3, pp. 6060–6066, Jul. 2022.

[42] D. J. Preston *et al.*, “Digital logic for soft devices,” *Proc. Natl. Acad. Sci. U. S. A.*, vol. 116, no. 16, pp. 7750–7759, Apr. 2019.

[43] D. Drotman, S. Jadhav, D. Sharp, C. Chan, and M. T. Tolley, “Electronics-free pneumatic circuits for controlling soft-legged robots,” *Sci. Robot.*, vol. 6, no. 51, p. eaay2627, Feb. 2021.

[44] W. K. Lee *et al.*, “A buckling-sheet ring oscillator for electronics-free, multimodal locomotion,” *Sci. Robot.*, vol. 7, no. 63, p. eabg5812, Feb. 2022.

[45] C. J. Decker *et al.*, “Programmable soft valves for digital and analog control,” *Proc. Natl. Acad. Sci. U. S. A.*, vol. 119, no. 40, p. e2205922119, Oct. 2022.

[46] A. Raj, P. P. A. Suthanthiraraj, and A. K. Sen, “Pressure-driven flow through

PDMS-based flexible microchannels and their applications in microfluidics," *Microfluid. Nanofluidics*, vol. 22, no. 11, pp. 1–25, Nov. 2018.

[47] D. Di Carlo, "Inertial microfluidics," *Lab Chip*, vol. 9, no. 21, pp. 3038–3046, Nov. 2009.

[48] H. Fallahi, J. Zhang, J. Nicholls, H. P. Phan, and N. T. Nguyen, "Stretchable Inertial Microfluidic Device for Tunable Particle Separation," *Anal. Chem.*, vol. 92, no. 18, pp. 12473–12480, Sep. 2020.

[49] D. P. Holmes, B. Tavakol, G. Froehlicher, and H. A. Stone, "Control and manipulation of microfluidic flow via elastic deformations," *Soft Matter*, vol. 9, no. 29, pp. 7049–7053, Jul. 2013.

[50] M. A. Unger, H. P. Chou, T. Thorsen, A. Scherer, and S. R. Quake, "Monolithic microfabricated valves and pumps by multilayer soft lithography," *Science (80-.).*, vol. 288, no. 5463, pp. 113–116, Apr. 2000.

[51] M. C. Yuen and R. K. Kramer, "Fabricating Microchannels in Elastomer Substrates for Stretchable Electronics," *ASME 2016 11th Int. Manuf. Sci. Eng. Conf. MSEC 2016*, p. V002T01A014; 1–9, Sep. 2016.

[52] D. C. Duffy, J. C. McDonald, O. J. A. Schueller, and G. M. Whitesides, "Rapid prototyping of microfluidic systems in poly(dimethylsiloxane)," *Anal. Chem.*, vol. 70, no. 23, pp. 4974–4984, Dec. 1998.

[53] J. Kong, M. G. Chapline, and H. Dai, "Capillary force lithography," *Adv. Mater.*, vol. 13, no. 18, pp. 1386–1389, 2001.

[54] M. A. Eddings, M. A. Johnson, and B. K. Gale, "Determining the optimal PDMS-PDMS bonding technique for microfluidic devices," *J. Micromechanics Microengineering*, vol. 18, no. 6, p. 067001, 2008.

[55] Kenry, J. C. Yeo, J. Yu, M. Shang, K. P. Loh, and C. T. Lim, "Highly Flexible Graphene Oxide Nanosuspension Liquid-Based Microfluidic Tactile Sensor," *Small*, vol. 12, no. 12, pp. 1593–1604, 2016.

[56] Q. Gao, H. Li, J. Zhang, Z. Xie, J. Zhang, and L. Wang, "Microchannel Structural Design For a Room-Temperature Liquid Metal Based Super-stretchable Sensor," *Sci. Rep.*, vol. 9, no. 1, pp. 1–8, 2019.

[57] Y. Xia and G. M. Whitesides, "SOFT LITHOGRAPHY," *Annu. Rev. Mater. Sci*, vol. 28, pp. 153–84, 1998.

[58] N. Lu, C. Lu, S. Yang, and J. Rogers, "Highly Sensitive Skin-Mountable Strain Gauges Based Entirely on Elastomers," *Adv. Funct. Mater.*, vol. 22, no. 19, pp. 4044–4050, 2012.

[59] F. L. H. Iii, R. K. Kramer, Q. Wan, R. D. Howe, and R. J. Wood, "Soft Tactile Sensor Arrays for Force Feedback in Micromanipulation," *IEEE Sens. J.*, vol. 14, no. 5, pp. 1443–1452, 2014.

[60] R. D. Ponce Wong, J. D. Posner, and V. J. Santos, "Flexible microfluidic normal force sensor skin for tactile feedback," *Sensors Actuators A Phys.*, vol. 179, pp. 62–69, Jun. 2012.

[61] T. Yang, D. Xie, Z. Li, and H. Zhu, “Recent advances in wearable tactile sensors: Materials, sensing mechanisms, and device performance,” *Mater. Sci. Eng. R Reports*, vol. 115, pp. 1–37, May 2017.

[62] P. Polygerinos *et al.*, “Soft Robotics: Review of Fluid-Driven Intrinsically Soft Devices; Manufacturing, Sensing, Control, and Applications in Human-Robot Interaction,” *Adv. Eng. Mater.*, vol. 19, no. 12, p. 1700016, Dec. 2017.

[63] S. Li, H. Zhao, and R. F. Shepherd, “Flexible and stretchable sensors for fluidic elastomer actuated soft robots,” *MRS Bull.*, vol. 42, no. 2, pp. 138–142, Feb. 2017.

[64] M. Luo *et al.*, “Toward modular soft robotics: Proprioceptive curvature sensing and sliding-mode control of soft bidirectional bending modules,” *Soft Robot.*, vol. 4, no. 2, pp. 117–125, Jun. 2017.

[65] H. Yang, Y. Chen, Y. Sun, and L. Hao, “A novel pneumatic soft sensor for measuring contact force and curvature of a soft gripper,” *Sensors Actuators A Phys.*, vol. 266, pp. 318–327, Oct. 2017.

[66] C. Tawk, H. Zhou, E. Sariyildiz, M. In Het Panhuis, G. M. Spinks, and G. Alici, “Design, Modeling, and Control of a 3D Printed Monolithic Soft Robotic Finger with Embedded Pneumatic Sensing Chambers,” *IEEE/ASME Trans. Mechatronics*, vol. 26, no. 2, pp. 876–887, Apr. 2021.

[67] C. Tawk, M. in het Panhuis, G. M. Spinks, and G. Alici, “Soft Pneumatic Sensing Chambers for Generic and Interactive Human–Machine Interfaces,” *Adv. Intell. Syst.*, vol. 1, no. 1, p. 1900002, May 2019.

[68] H. Choi and K. Kong, “A Soft Three-Axis Force Sensor Based on Radially Symmetric Pneumatic Chambers,” *IEEE Sens. J.*, vol. 19, no. 13, pp. 5229–5238, 2019.

[69] H. Yuk, B. Lu, and X. Zhao, “Hydrogel bioelectronics,” *Chem. Soc. Rev.*, vol. 48, no. 6, pp. 1642–1667, Mar. 2019.

[70] K. Zhou, K. Dai, C. Liu, and C. Shen, “Flexible conductive polymer composites for smart wearable strain sensors,” *SmartMat*, vol. 1, no. 1, p. e1010, Dec. 2020.

[71] T. Wang *et al.*, “A Self-Healable, Highly Stretchable, and Solution Processable Conductive Polymer Composite for Ultrasensitive Strain and Pressure Sensing,” *Adv. Funct. Mater.*, vol. 28, no. 7, p. 1705551, 2017.

[72] S. I. Rich, R. J. Wood, and C. Majidi, “Untethered soft robotics,” *Nat. Electron.*, vol. 1, no. 2, pp. 102–112, 2018.

[73] S. Zhu *et al.*, “Ultrastretchable Fibers with Metallic Conductivity Using a Liquid Metal Alloy Core,” *Adv. Funct. Mater.*, vol. 23, no. 18, pp. 2308–2314, May 2013.

[74] N. Matsuhisa *et al.*, “Printable elastic conductors with a high conductivity for electronic textile applications,” *Nat. Commun. 2015 61*, vol. 6, no. 1, pp. 1–11, Jun. 2015.

[75] Y. Huang, Y. Wang, L. Xiao, H. Liu, W. Dong, and Z. Yin, “Microfluidic serpentine antennas with designed mechanical tunability,” *Lab Chip*, vol. 14, no. 21, pp. 4205–4212, 2014.

[76] Y. L. Park, B. R. Chen, and R. J. Wood, “Design and fabrication of soft artificial skin using embedded microchannels and liquid conductors,” *IEEE Sens. J.*, vol. 12, no. 8, pp. 2711–2718, 2012.

[77] Y. Wu *et al.*, “Liquid Metal-Based Strain Sensor with Ultralow Detection Limit for Human–Machine Interface Applications,” *Adv. Intell. Syst.*, vol. 3, no. 10, p. 2000235, Oct. 2021.

[78] M. Xu, J. Qi, F. Li, and Y. Zhang, “Highly stretchable strain sensors with reduced graphene oxide sensing liquids for wearable electronics,” *Nanoscale*, vol. 10, no. 11, pp. 5264–5271, Mar. 2018.

[79] R. Adam Bilodeau, E. L. White, and R. K. Kramer, “Monolithic fabrication of sensors and actuators in a soft robotic gripper,” in *IEEE International Conference on Intelligent Robots and Systems*, Dec. 2015, pp. 2324–2329.

[80] R. Z. Gao and C. L. Ren, “Synergizing microfluidics with soft robotics: A perspective on miniaturization and future directions,” *Biomicrofluidics*, vol. 15, no. 1, p. 011302, Feb. 2021.

APPENDIX: RESULTS OF THE MICROCHANNEL FABRICATION

Table A1. Fabricated channel networks from one SU-8 mold (disk) with the wet bonding process from Dragon Skin 30, Ecoflex 00-50 and Ecoflex 00-20.

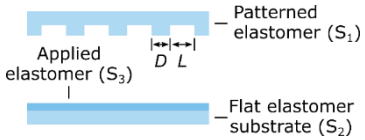

Disk	Date	Elastomer	S_1 (g)	Weight of S_2 (g)	S_3 (g)	Spin speed (RPM)	Pre-curing time (s)	Comments
1/3 EF50	1.3.2021	EF50	13.67	12.85	1,01	2000	40–60	
2/3 EF50	2.3.2021	EF50	19.4	15	0,87	2500	40–60	
10/3 EF20	10.3.2021	EF20	-	17.68	1,05	2500	40–60	
18/6 EF50 2	18.6.2021	EF50	10.29	12.55	1,28	2500	40	
18/6 EF50 1	18.6.2021	EF50	10.17	16.48	1,46	2500	60	C1&C3 channels destroyed before bonding
24/6 EF50 1	24.6.2021	EF50	10.66	15.78	1.45	2000	60	C1&C3 channels destroyed before bonding
24/6 EF50 2	24.6.2021	EF50	10.32	16.09	1.44	2000	40	
2/7 EF50 1	2.7.2021	EF50	10.7	13.1	1.18	2500	20	on the table for couple minutes before pre-curing
2/7 EF50 2	2.7.2021	EF50	10.49	15.77	1.42	2000	20	
23/8 EF50	23.8.2021	EF50	12.92	20.93	2.59	2500	20	
25/8 EF50	25.8.2021	EF50	13.02	15.8	1.95	2500	20	
14/9 EF50 3	14.9.2021	EF50	16.18	20.21	2	2000	60	
14/9 EF50 1	14.9.2021	EF50	16.19	20.23	2.84	2500	60	
14/9 EF50 2	14.9.2021	EF50	16.69	23.38	2.31	2500	40	
15/9 EF50 2	15.9.2021	EF50	16.4	18.04	1.28	2000	40	
15/9 EF50 1	15.9.2021	EF50	15.2	24.68	1.58	2000	20	on the table for one minute after pre-curing
30/9 DS30 2	30.9.2021	DS30	17.56	12.6	1.7	2500	40	
30/9 DS30 1	30.9.2021	DS30	15.82	20.4	2.41	2500	60	
8/10 DS30	8.10.2021	DS30	15.79	-	1.47	2500	20	
5/1 DS30 2	5.1.2022	DS30	16.5	10.21	1.53	2500	20	
5/1 DS30 1	5.1.2022	DS30	17.29	10.53	1.24	2500	20	
10/1 DS30 1	10.1.2022	DS30	8.96	10.93	1.26	2500	40	air bubbles around channels
10/1 DS30 2	10.1.2022	DS30	10.1	12.22	1.18	2500	40	
13/1 DS30 1	13.1.2022	DS30	9.5	12.35	1.7	2500	60	
13/1 DS30 2	13.1.2022	DS30	9.92	12.74	1.77	2500	60	air bubble in C2
19/1 DS30 1	19.1.2022	DS30	10.24	11.13	1.88	2000	20	
19/1 DS30 2	19.1.2022	DS30	11.11	11.65	1.21	2000	20	
20/1 DS30	20.1.2022	DS30	6.6	15.02	1.15	2000	20	
31/1 DS30	31.1.2022	DS30	10.63	12.1	1.38	2000	20	
7/2 DS30 2	7.2.2022	DS30	16.86	9.71	1.35	2000	40	
7/2 DS30 1	7.2.2022	DS30	16.18	10.22	1.72	2000	40	
9/3 DS30 1	9.3.2022	DS30	11.56	13.32	1.21	2000	40	
9/3 DS30 2	9.3.2022	DS30	8.44	13.57	1.2	2000	60	
10/3 DS30 2	10.3.2022	DS30	8.9	11.41	1.51	2000	60	
10/3 DS30 1	10.3.2022	DS30	10.91	11.67	1.48	2000	60	
31/3 EF50 1	31.3.2022	EF50	-	15.17	2.03	2500	40	2 x C3&C4
31/3 EF50 2	31.3.2022	EF50	12.99	15.65	2.99	2500	60	
1/4 EF50 1	1.4.2022	EF50	10.34	13.33	2.94	2000	60	
1/4 EF50 2	1.4.2022	EF50	10.68	14.36	2.65	2000	60	
5/4 EF50	5.4.2022	EF50	10.63	14.49	2.35	2000	20	
7/4 EF50	7.4.2022	EF50	-	14.35	1.39	2500	20	3xC3
11/4 EF50	11.4.2022	EF50	12.41	14.76	1.92	2000	40	
13/4 DS30 2	13.4.2022	DS30	8.53	15.6	1.63	2500	-	
13/4 DS30 1	13.4.2022	DS30	10.21	17.16	1.59	2000	-	
14/4 EF50	14.4.2022	EF50	10.81	13.71	1.61	2500	-	
19/4 EF50 1	19.4.2022	EF50	12.07	11.94	1.66	2500	-	
19/4 EF50 2	19.4.2022	EF50	11.66	12.65	1.74	2500	-	
21/4 EF50 1	21.4.2022	EF50	12.6	10.33	1.82	2000	-	
21/4 EF50 2	21.4.2022	EF50	13.14	11.93	1.84	2000	-	
26/4 EF50	26.4.2022	EF50	14.31	14.04	1.61	2000	-	
27/4 EF20 2	27.4.2022	EF20	11.44	12.08	1.74	1500	-	
28/4 EF20 3	28.4.2022	EF20	7.33	12.35	1.9	1500	-	
2/5 EF20	2.5.2022	EF20	13.33	13.85	2.02	1500	-	
3/5 EF20 2	3.5.2022	EF20	11.58	11.59	1.8	1500	20	
3/5 EF20 4	3.5.2022	EF20	10.22	11.74	1.87	1500	40	
3/5 EF20 1	3.5.2022	EF20	11.82	11.9	2.06	1500	20	
3/5 EF20 3	3.5.2022	EF20	13.6	12.18	2.08	1500	20	
4/5 EF20 3	4.5.2022	EF20	13.01	11.7	1.66	1500	60	
4/5 EF20 2	4.5.2022	EF20	10.65	12.7	1.61	1500	40	
4/5 EF20 4	4.5.2022	EF20	11.7	13.83	1.55	1500	60	
4/5 EF20 1	4.5.2022	EF20	11.74	16.36	1.54	1500	40	
5/5 EF20 2	5.5.2022	EF20	10.03	12.95	1.66	2000	60	
5/5 EF20 1	5.5.2022	EF20	11.49	13.3	1.9	1500	60	
5/5 EF20 3	5.5.2022	EF20	11.2	13.73	1.65	2000	-	
6/5 EF20	6.5.2022	EF20	13.37	13.24	1.7	2000	60	
9/5 EF20 2	9.5.2022	EF20	12.6	10.57	1.5	2000	20	
9/5 EF20 1	9.5.2022	EF20	10.11	12.06	1.64	2000	60	
10/5 EF20 1	10.5.2022	EF20	12.08	9.88	1.6	2000	20	
10/5 EF20 2	10.5.2022	EF20	11.24	12.3	1.92	2000	20	
10/5 EF20 3	10.5.2022	EF20	10.92	12.62	1.83	2000	40	
11/5 EF20 2	11.5.2022	EF20	10.3	9.08	1.5	2000	40	
11/5 EF20 3	11.5.2022	EF20	10.89	12.22	2.13	2000	-	
11/5 EF20 4	11.5.2022	EF20	12.1	12.25	1.93	2000	-	
11/5 EF20 1	11.5.2022	EF20	11.13	13.63	1.56	2000	40	

11/7 DS30 1	11.7.2022	DS30	11.71	12.95	1.53	2000	-
11/7 DS30 2	11.7.2022	DS30	10.26	15.01	1.65	2000	-
12/7 DS30 2	12.7.2022	DS30	9.56	12.57	1.58	2500	-
12/7 DS30 1	12.7.2022	DS30	10.28	13.35	1.61	2500	-

Table A2. Fabricated microchannels with the wet bonding process from Dragon Skin 30, Ecoflex 00-50 and Ecoflex 00-20.

Chip*	Disk	D (µm) / L (µm)	Open channels / Total	Observation date	Pre-curing time (s)	Comments
C1	2/3 EF50	50/100 & 100/200	64/64 & 64/64	18.6.2021	40	
C2	2/3 EF50	100/100 & 200/200	48/48 & 48/48	18.6.2021	40	
C3	2/3 EF50	200/100	41/48	18.6.2021	60	
C4	2/3 EF50	800/800 & 400/400	12/12 & 48/48	18.6.2021	60	
C1	18/6 EF50 1	50/100 & 100/200	0/0 & 62/64	18.6.2021	60	smallest channels ruined before bonding
C2	18/6 EF50 1	100/100 & 200/200	48/48 & 48/48	18.6.2021	60	
C3	18/6 EF50 1	200/100	48/48	18.6.2021	60	
C4	18/6 EF50 1	800/800 & 400/400	12/12 & 48/48	18.6.2021	60	
C1	18/6 EF50 2	50/100 & 100/200	64/64 & 64/64	18.6.2021	40	
C2	18/6 EF50 2	100/100 & 200/200	48/48 & 48/48	18.6.2021	40	
C3	18/6 EF50 2	200/100	48/48	18.6.2021	40	
C4	18/6 EF50 2	800/800 & 400/400	12/12 & 48/48	18.6.2021	40	
C1	24/6 EF50 1	50/100 & 100/200	0/48 & 64/64	24.6.2021	60	smallest channels ruined before bonding
C2	24/6 EF50 1	100/100 & 200/200	48/48 & 48/48	24.6.2021	60	
C3	24/6 EF50 1	100/50 & 200/100	0/48 & 32/48	24.6.2021	60	smallest channels ruined before bonding
C4	24/6 EF50 1	800/800 & 400/400	12/12 & 30/48	24.6.2021	60	
C1	24/6 EF50 2	50/100 & 100/200	62/64 & 63/64	24.6.2021	40	
C2	24/6 EF50 2	100/100 & 200/200	48/48 & 48/48	24.6.2021	40	
C3	24/6 EF50 2	200/100	46/48	24.6.2021	40	
C4	24/6 EF50 2	800/800 & 400/400	7/12 & 24/48	24.6.2021	40	
C1	1/3 EF50	50/100 & 100/200	48/64 & 50/64	28.6.2021	40	
C2	1/3 EF50	100/100 & 200/200	46/48 & 32/48	28.6.2021	40	
C3	1/3 EF50	100/50 & 200/100	0/48 & 14/48	28.6.2021	60	smallest channels ruined before bonding
C4	1/3 EF50	800/800 & 400/400	12/12 & 29/48	28.6.2021	60	
C1	10/3 EF20	50/100 & 100/200	0/64 & 16/64	9.6.2021	40	
C2	10/3 EF20	100/100 & 200/200	0/48 & 11/48	9.6.2021	40	
C1	2/7 EF50 1	50/100 & 100/200	58/64 & 60/64	2.7.2021	20	
C2	2/7 EF50 1	100/100 & 200/200	0/48 & 24/48	2.7.2021	20	channels ruined by pressing with finger
C3	2/7 EF50 1	200/100	4/48	2.7.2021	20	channels ruined by pressing with finger
C4	2/7 EF50 1	800/800 & 400/400	12/12 & 38/48	2.7.2021	20	
C1	2/7 EF50 2	50/100 & 100/200	50/64 & 54/64	2.7.2021	20	
C2	2/7 EF50 2	100/100 & 200/200	48/48 & 48/48	2.7.2021	20	
C3	2/7 EF50 2	200/100	35/48	2.7.2021	20	
C4	2/7 EF50 2	800/800 & 400/400	12/12 & 32/48	2.7.2021	20	
C1	23/8 EF50	50/100 & 100/200	63/64 & 61/64	24.8.2021	20	
C2	23/8 EF50	100/100 & 200/200	47/48 & 48/48	24.8.2021	20	
C3	23/8 EF50	200/100	48/48	24.8.2021	20	
C4	23/8 EF50	800/800 & 400/400	12/12 & 32/48	24.8.2021	20	
C1	25/8 EF50	50/100 & 100/200	63/64 & 64/64	3.9.2021	20	
C2	25/8 EF50	100/100 & 200/200	38/48 & 48/48	3.9.2021	20	
C3	25/8 EF50	100/50 & 200/100	0/0 & 43/48	3.9.2021	20	
C4	25/8 EF50	800/800 & 400/400	12/12 & 48/48	3.9.2021	20	
C1	14/9 EF50 1	50/100 & 100/200	61/64 & 64/64	15.9.2021	60	
C2	14/9 EF50 1	100/100 & 200/200	47/48 & 48/48	15.9.2021	60	
C3	14/9 EF50 1	100/50 & 200/100	0/48 & 48/48	15.9.2021	60	
C4	14/9 EF50 1	800/800 & 400/400	12/12 & 47/48	15.9.2021	60	
C1	14/9 EF50 2	50/100 & 100/200	56/64 & 61/64	15.9.2021	40	
C2	14/9 EF50 2	100/100 & 200/200	46/48 & 47/48	15.9.2021	40	
C3	14/9 EF50 2	100/50 & 200/100	0/48 & 44/48	15.9.2021	40	
C4	14/9 EF50 2	800/800 & 400/400	12/12 & 44/48	15.9.2021	40	
C1	14/9 EF50 3	50/100 & 100/200	60/64 & 64/64	16.9.2021	60	
C2	14/9 EF50 3	100/100 & 200/200	47/48 & 48/48	16.9.2021	60	
C3	14/9 EF50 3	100/50 & 200/100	3/48 & 46/48	16.9.2021	60	
C4	14/9 EF50 3	800/800 & 400/400	12/12 & 46/48	16.9.2021	60	
C1	15/9 EF50 1	50/100 & 100/200	48/64 & 57/64	15.9.2021	20	
C2	15/9 EF50 1	100/100 & 200/200	42/48 & 45/48	15.9.2021	20	
C3	15/9 EF50 1	100/50 & 200/100	34/48 & 43/48	15.9.2021	20	!!! ?
C4	15/9 EF50 1	800/800 & 400/400	12/12 & 33/48	15.9.2021	20	air bubble
C1	15/9 EF50 2	50/100 & 100/200	58/64 & 61/64	16.9.2021	40	
C2	15/9 EF50 2	100/100 & 200/200	47/48 & 48/48	16.9.2021	40	
C3	15/9 EF50 2	100/50 & 200/100	0/48 & 45/48	16.9.2021	40	
C4	15/9 EF50 2	800/800 & 400/400	12/12 & 46/48	16.9.2021	40	
C1	30/9 DS30 1	50/100 & 100/200	61/64 & 62/64	1.10.2021	60	
C2	30/9 DS30 1	100/100 & 200/200	46/48 & 48/48	1.10.2021	60	
C3	30/9 DS30 1	100/50 & 200/100	48/48 & 48/48	1.10.2021	60	
C4	30/9 DS30 1	800/800 & 400/400	12/12 & 48/48	1.10.2021	60	
C1	30/9 DS30 2	50/100 & 100/200	61/64 & 63/64	1.10.2021	40	
C2	30/9 DS30 2	100/100 & 200/200	46/48 & 48/48	1.10.2021	40	
C3	30/9 DS30 2	100/50 & 200/100	41/48 & 47/48	1.10.2021	40	
C4	30/9 DS30 2	800/800 & 400/400	12/12 & 48/48	1.10.2021	40	
C1	8/10 DS30	50/100 & 100/200	64/64 & 64/64	14.10.2021	20	
C2	8/10 DS30	100/100 & 200/200	45/48 & 48/48	14.10.2021	20	
C3	8/10 DS30	100/50 & 200/100	46/48 & 47/48	14.10.2021	20	
C4	8/10 DS30	800/800 & 400/400	12/12 & 48/48	14.10.2021	20	
C1	5/1 DS30 1	50/100 & 100/200	62/64 & 64/64	10.1.2022	20	
C2	5/1 DS30 1	100/100 & 200/200	48/48 & 47/48	10.1.2022	20	
C3	5/1 DS30 1	100/50 & 200/100	48/48 & 48/48	10.1.2022	20	
C4	5/1 DS30 1	800/800 & 400/400	12/12 & 48/48	10.1.2022	20	
C1	5/1 DS30 2	50/100 & 100/200	64/64 & 64/64	10.1.2022	20	
C2	5/1 DS30 2	100/100 & 200/200	48/48 & 48/48	10.1.2022	20	
C3	5/1 DS30 2	100/50 & 200/100	48/48 & 48/48	10.1.2022	20	
C4	5/1 DS30 2	800/800 & 400/400	12/12 & 48/48	10.1.2022	20	
C1	10/1 DS30 1	50/100 & 100/200	64/64 & 64/64	12.1.2022	40	
C2	10/1 DS30 1	100/100 & 200/200	48/48 & 48/48	12.1.2022	40	
C3	10/1 DS30 1	100/50 & 200/100	48/48 & 48/48	12.1.2022	40	
C4	10/1 DS30 1	800/800 & 400/400	3/12 & 26/48	12.1.2022	40	air bubble in the middle
C1	10/1 DS30 2	50/100 & 100/200	64/64 & 64/64	12.1.2022	40	

C2	10/1 DS30 2	100/100 & 200/200	47/48 & 48/48	12.1.2022	40	
C3	10/1 DS30 2	100/50 & 200/100	48/48 & 48/48	12.1.2022	40	
C4	10/1 DS30 2	800/800 & 400/400	12/12 & 48/48	12.1.2022	40	
C1	13/1 DS30 1	50/100 & 100/200	64/64 & 64/64	13.1.2022	60	
C2	13/1 DS30 1	100/100 & 200/200	48/48 & 48/48	13.1.2022	60	
C3	13/1 DS30 1	100/50 & 200/100	47/48 & 48/48	13.1.2022	60	
C4	13/1 DS30 1	800/800 & 400/400	12/12 & 48/48	13.1.2022	60	
C1	13/1 DS30 2	50/100 & 100/200	64/64 & 64/64	13.1.2022	60	
C2	13/1 DS30 2	100/100 & 200/200	26/48 & 14/48	13.1.2022	60	air bubble in the middle
C3	13/1 DS30 2	100/50 & 200/100	47/48 & 48/48	13.1.2022	60	
C4	13/1 DS30 2	800/800 & 400/400	12/12 & 48/48	13.1.2022	60	
C1	19/1 DS30 1	50/100 & 100/200	63/64 & 64/64	19.1.2022	20	
C2	19/1 DS30 1	100/100 & 200/200	46/48 & 48/48	19.1.2022	20	
C3	19/1 DS30 1	100/50 & 200/100	46/48 & 48/48	19.1.2022	20	
C4	19/1 DS30 1	800/800 & 400/400	12/12 & 38/48	19.1.2022	20	
C1	19/1 DS30 2	50/100 & 100/200	64/64 & 64/64	19.1.2022	20	
C2	19/1 DS30 2	100/100 & 200/200	47/48 & 48/48	19.1.2022	20	
C3	19/1 DS30 2	100/50 & 200/100	46/48 & 48/48	19.1.2022	20	
C4	19/1 DS30 2	800/800 & 400/400	12/12 & 48/48	19.1.2022	20	
C1	7/2 DS30 2	50/100 & 100/200	64/64 & 64/64	9.3.2022	40	
C2	7/2 DS30 2	100/100 & 200/200	48/48 & 48/48	9.3.2022	40	
C3	7/2 DS30 2	100/50 & 200/100	34/48 & 48/48	9.3.2022	40	
C4	7/2 DS30 2	800/800 & 400/400	12/12 & 48/48	9.3.2022	40	
C1	7/2 DS30 1	50/100 & 100/200	64/64 & 64/64	9.3.2022	40	
C2	7/2 DS30 1	100/100 & 200/200	48/48 & 48/48	9.3.2022	40	
C3	7/2 DS30 1	100/50 & 200/100	48/48 & 48/48	9.3.2022	40	
C4	7/2 DS30 1	800/800 & 400/400	12/12 & 48/48	9.3.2022	40	
C1	31/1 DS30	50/100 & 100/200	63/64 & 64/64	9.3.2022	20	
C2	31/1 DS30	100/100 & 200/200	47/48 & 48/48	9.3.2022	20	
C3	31/1 DS30	100/50 & 200/100	46/48 & 48/48	9.3.2022	20	
C4	31/1 DS30	800/800 & 400/400	12/12 & 48/48	9.3.2022	20	
C1	20/1 DS30	50/100 & 100/200	64/64 & 64/64	9.3.2022	20	
C2	20/1 DS30	100/100 & 200/200	47/48 & 48/48	9.3.2022	20	
C3	20/1 DS30	100/50 & 200/100	48/48 & 48/48	9.3.2022	20	
C4	20/1 DS30	800/800 & 400/400	12/12 & 48/48	9.3.2022	20	
C1	9/3 DS30 1	50/100 & 100/200	58/64 & 64/64	10.3.2022	40	
C2	9/3 DS30 1	100/100 & 200/200	48/48 & 48/48	10.3.2022	40	
C3	9/3 DS30 1	100/50 & 200/100	12/48 & 48/48	10.3.2022	40	
C4	9/3 DS30 1	800/800 & 400/400	12/12 & 48/48	10.3.2022	40	
C1	9/3 DS30 2	50/100 & 100/200	64/64 & 64/64	10.3.2022	60	
C2	9/3 DS30 2	100/100 & 200/200	48/48 & 48/48	10.3.2022	60	
C3	9/3 DS30 2	100/50 & 200/100	36/48 & 48/48	10.3.2022	60	
C4	9/3 DS30 2	800/800 & 400/400	12/12 & 48/48	10.3.2022	60	
C1	10/3 DS30 1	50/100 & 100/200	63/64 & 64/64	10.3.2022	60	
C2	10/3 DS30 1	100/100 & 200/200	48/48 & 48/48	10.3.2022	60	
C3	10/3 DS30 1	100/50 & 200/100	48/48 & 48/48	10.3.2022	60	
C4	10/3 DS30 1	800/800 & 400/400	12/12 & 48/48	10.3.2022	60	
C1	10/3 DS30 2	50/100 & 100/200	64/64 & 64/64	10.3.2022	60	
C2	10/3 DS30 2	100/100 & 200/200	48/48 & 48/48	10.3.2022	60	
C3	10/3 DS30 2	100/50 & 200/100	48/48 & 48/48	10.3.2022	60	
C4	10/3 DS30 2	800/800 & 400/400	12/12 & 48/48	10.3.2022	60	
C3	31/3 EF50 1	100/50 & 200/100	2/48 & 48/48	11.4.2022	40	
C4	31/3 EF50 1	800/800 & 400/400	12/12 & 48/48	11.4.2022	40	
C3	31/3 EF50 1	100/50 & 200/100	1/48 & 48/48	11.4.2022	40	
C4	31/3 EF50 1	800/800 & 400/400	12/12 & 48/48	11.4.2022	40	
C1	31/3 EF50 2	50/100 & 100/200	15/64 & 64/64	11.4.2022	60	
C2	31/3 EF50 2	100/100 & 200/200	48/48 & 48/48	11.4.2022	60	
C3	31/3 EF50 2	100/50 & 200/100	0/48 & 48/48	11.4.2022	60	
C4	31/3 EF50 2	800/800 & 400/400	8/12 & 48/48	11.4.2022	60	
C1	5/4 EF50	50/100 & 100/200	46/64 & 64/64	11.4.2022	20	
C2	5/4 EF50	100/100 & 200/200	48/48 & 48/48	11.4.2022	20	
C3	5/4 EF50	100/50 & 200/100	4/48 & 48/48	11.4.2022	20	
C4	5/4 EF50	800/800 & 400/400	12/12 & 48/48	11.4.2022	20	air bubble
C1	1/4 EF50 1	50/100 & 100/200	56/64 & 64/64	11.4.2022	60	
C2	1/4 EF50 1	100/100 & 200/200	48/48 & 48/48	11.4.2022	60	
C3	1/4 EF50 1	100/50 & 200/100	0/48 & 48/48	11.4.2022	60	
C4	1/4 EF50 1	800/800 & 400/400	12/12 & 48/48	11.4.2022	60	
C1	1/4 EF50 2	50/100 & 100/200	52/64 & 64/64	11.4.2022	60	
C2	1/4 EF50 2	100/100 & 200/200	48/48 & 48/48	11.4.2022	60	
C3	1/4 EF50 2	100/50 & 200/100	0/48 & 48/48	11.4.2022	60	
C4	1/4 EF50 2	800/800 & 400/400	12/12 & 48/48	11.4.2022	60	
C3	7/4 EF50	100/50 & 200/100	8/48 & 48/48	11.4.2022	20	
C3	7/4 EF50	100/50 & 200/100	10/48 & 48/48	11.4.2022	20	
C3	7/4 EF50	100/50 & 200/100	2/48 & 48/48	11.4.2022	20	
C1	11/4 EF50	50/100 & 100/200	64/64 & 64/64	12.4.2022	40	
C2	11/4 EF50	100/100 & 200/200	48/48 & /4848	12.4.2022	40	
C3	11/4 EF50	100/50 & 200/100	0/48 & 48/48	12.4.2022	40	
C4	11/4 EF50	800/800 & 400/400	12/12 & 48/48	12.4.2022	40	
C1	13/4 DS30 1	50/100 & 100/200	63/64 & 64/64	13.4.2022	-	
C2	13/4 DS30 1	100/100 & 200/200	47/48 & 48/48	13.4.2022	-	
C3	13/4 DS30 1	100/50 & 200/100	40/48 & 48/48	13.4.2022	-	
C4	13/4 DS30 1	800/800 & 400/400	3/12 & 32/48	13.4.2022	-	
C1	13/4 DS30 2	50/100 & 100/200	64/64 & 64/64	13.4.2022	-	
C2	13/4 DS30 2	100/100 & 200/200	48/48 & 48/48	13.4.2022	-	
C3	13/4 DS30 2	100/50 & 200/100	48/48 & 48/48	13.4.2022	-	
C4	13/4 DS30 2	800/800 & 400/400	12/12 & 48/48	13.4.2022	-	
C1	14/4 EF50	50/100 & 100/200	0/64 & 64/64	20.4.2022	-	
C2	14/4 EF50	100/100 & 200/200	47/48 & 48/48	20.4.2022	-	
C3	14/4 EF50	100/50 & 200/100	0/48 & 48/48	20.4.2022	-	
C4	14/4 EF50	800/800 & 400/400	12/12 & 48/48	20.4.2022	-	
C1	19/4 EF50 1	50/100 & 100/200	0/64 & 64/64	20.4.2022	-	
C2	19/4 EF50 1	100/100 & 200/200	46/48 & 48/48	20.4.2022	-	
C3	19/4 EF50 1	100/50 & 200/100	0/48 & 44/48	20.4.2022	-	
C4	19/4 EF50 1	800/800 & 400/400	12/12 & 48/48	20.4.2022	-	
C1	19/4 EF50 2	50/100 & 100/200	0/64 & 64/64	20.4.2022	-	
C2	19/4 EF50 2	100/100 & 200/200	48/48 & 48/48	20.4.2022	-	
C3	19/4 EF50 2	100/50 & 200/100	0/48 & 48/48	20.4.2022	-	
C4	19/4 EF50 2	800/800 & 400/400	12/12 & 48/48	20.4.2022	-	
C1	21/4 EF50 1	50/100 & 100/200	0/64 & 62/64	26.4.2022	-	
C2	21/4 EF50 1	100/100 & 200/200	46/48 & 48/48	26.4.2022	-	
C3	21/4 EF50 1	100/50 & 200/100	0/48 & 44/48	26.4.2022	-	

C4	21/4 EF50 1	800/800 & 400/400	12/12 & 48/48	26.4.2022	-	
C1	21/4 EF50 2	50/100 & 100/200	0/64 & 62/64	26.4.2022	-	
C2	21/4 EF50 2	100/100 & 200/200	46/48 & 48/48	26.4.2022	-	
C3	21/4 EF50 2	100/50 & 200/100	0/48 & 44/48	26.4.2022	-	
C4	21/4 EF50 2	800/800 & 400/400	9/12 & 12/48	26.4.2022	-	
C1	26/4 EF50	50/100 & 100/200	0/64 & 64/64	26.4.2022	-	
C2	26/4 EF50	100/100 & 200/200	46/48 & 48/48	26.4.2022	-	
C3	26/4 EF50	100/50 & 200/100	6/48 & 48/48	26.4.2022	-	
C4	26/4 EF50	800/800 & 400/400	12/12 & 48/48	26.4.2022	-	
C1	27/4 EF20 2	50/100 & 100/200	0/64 & 40/64	28.4.2022	-	
C2	27/4 EF20 2	100/100 & 200/200	28/48 & 10/48	28.4.2022	-	
C3	27/4 EF20 2	100/50 & 200/100	0/48 & 8/48	28.4.2022	-	
C4	27/4 EF20 2	800/800 & 400/400	12/12 & 26/48	28.4.2022	-	
C1	28/4 EF20 3	50/100 & 100/200	0/64 & 56/64	4.5.2022	-	
C2	28/4 EF20 3	100/100 & 200/200	35/48 & 3/48	4.5.2022	-	
C3	28/4 EF20 3	100/50 & 200/100	0/48 & 20/48	4.5.2022	-	
C4	28/4 EF20 3	800/800 & 400/400	12/12 & 34/48	4.5.2022	-	
C1	2/5 EF20	50/100 & 100/200	0/64 & 57/64	4.5.2022	-	
C2	2/5 EF20	100/100 & 200/200	44/48 & 33/48	4.5.2022	-	
C3	2/5 EF20	100/50 & 200/100	0/48 & 30/48	4.5.2022	-	
C4	2/5 EF20	800/800 & 400/400	12/12 & 48/48	4.5.2022	-	
C1	3/5 EF20 1	50/100 & 100/200	0/64 & 61/64	4.5.2022	20	
C2	3/5 EF20 1	100/100 & 200/200	40/48 & 45/48	4.5.2022	20	
C3	3/5 EF20 1	100/50 & 200/100	0/48 & 42/48	4.5.2022	20	
C4	3/5 EF20 1	800/800 & 400/400	6/12 & 48/48	4.5.2022	20	curly
C1	3/5 EF20 2	50/100 & 100/200	0/64 & 64/64	4.5.2022	20	
C2	3/5 EF20 2	100/100 & 200/200	36/48 & 48/48	4.5.2022	20	
C3	3/5 EF20 2	100/50 & 200/100	0/48 & 46/48	4.5.2022	20	
C4	3/5 EF20 2	800/800 & 400/400	12/12 & 48/48	4.5.2022	20	
C1	3/5 EF20 3	50/100 & 100/200	0/64 & 64/64	4.5.2022	20	
C2	3/5 EF20 3	100/100 & 200/200	38/48 & 48/48	4.5.2022	20	
C3	3/5 EF20 3	100/50 & 200/100	0/48 & 46/48	4.5.2022	20	
C4	3/5 EF20 3	800/800 & 400/400	12/12 & 48/48	4.5.2022	20	
C1	3/5 EF20 4	50/100 & 100/200	0/64 & 64/64	4.5.2022	40	
C2	3/5 EF20 4	100/100 & 200/200	34/48 & 48/48	4.5.2022	40	
C3	3/5 EF20 4	100/50 & 200/100	0/48 & 48/48	4.5.2022	40	
C4	3/5 EF20 4	800/800 & 400/400	12/12 & 48/48	4.5.2022	40	
C1	4/5 EF20 1	50/100 & 100/200	7/64 & 64/64	4.5.2022	40	
C2	4/5 EF20 1	100/100 & 200/200	36/48 & 48/48	4.5.2022	40	
C3	4/5 EF20 1	100/50 & 200/100	0/48 & 48/48	4.5.2022	40	
C4	4/5 EF20 1	800/800 & 400/400	12/12 & 48/48	4.5.2022	40	
C1	4/5 EF20 2	50/100 & 100/200	11/64 & 64/64	10.5.2022	40	
C2	4/5 EF20 2	100/100 & 200/200	48/48 & 48/48	10.5.2022	40	
C3	4/5 EF20 2	100/50 & 200/100	0/48 & 48/48	10.5.2022	40	
C4	4/5 EF20 2	800/800 & 400/400	12/12 & 47/48	10.5.2022	40	
C1	4/5 EF20 3	50/100 & 100/200	0/64 & 64/64	10.5.2022	60	
C2	4/5 EF20 3	100/100 & 200/200	46/48 & 48/48	10.5.2022	60	
C3	4/5 EF20 3	100/50 & 200/100	0/48 & 48/48	10.5.2022	60	
C4	4/5 EF20 3	800/800 & 400/400	12/12 & 48/48	10.5.2022	60	
C1	4/5 EF20 4	50/100 & 100/200	4/64 & 64/64	10.5.2022	60	
C2	4/5 EF20 4	100/100 & 200/200	47/48 & 48/48	10.5.2022	60	
C3	4/5 EF20 4	100/50 & 200/100	0/48 & 47/48	10.5.2022	60	
C4	4/5 EF20 4	800/800 & 400/400	12/12 & 48/48	10.5.2022	60	
C1	5/5 EF20 1	50/100 & 100/200	16/64 & 64/64	10.5.2022	60	
C2	5/5 EF20 1	100/100 & 200/200	48/48 & 48/48	10.5.2022	60	
C3	5/5 EF20 1	100/50 & 200/100	0/48 & 48/48	10.5.2022	60	
C4	5/5 EF20 1	800/800 & 400/400	12/12 & 48/48	10.5.2022	60	
C1	5/5 EF20 2	50/100 & 100/200	0/64 & 64/64	10.5.2022	60	
C2	5/5 EF20 2	100/100 & 200/200	48/48 & 48/48	10.5.2022	60	
C3	5/5 EF20 2	100/50 & 200/100	0/48 & 48/48	10.5.2022	60	
C4	5/5 EF20 2	800/800 & 400/400	12/12 & 48/48	10.5.2022	60	
C1	5/5 EF20 3	50/100 & 100/200	10/64 & 47/64	10.5.2022	-	
C2	5/5 EF20 3	100/100 & 200/200	48/48 & 47/48	10.5.2022	-	
C3	5/5 EF20 3	100/50 & 200/100	0/48 & 43/48	10.5.2022	-	
C4	5/5 EF20 3	800/800 & 400/400	12/12 & 48/48	10.5.2022	-	
C1	6/5 EF20	50/100 & 100/200	29/64 & 64/64	10.5.2022	60	
C2	6/5 EF20	100/100 & 200/200	47/48 & 48/48	10.5.2022	60	
C3	6/5 EF20	100/50 & 200/100	0/48 & 48/48	10.5.2022	60	
C4	6/5 EF20	800/800 & 400/400	12/12 & 48/48	10.5.2022	60	
C1	9/5 EF20 1	50/100 & 100/200	0/64 & 64/64	10.5.2022	60	
C2	9/5 EF20 1	100/100 & 200/200	48/48 & 48/48	10.5.2022	60	
C3	9/5 EF20 1	100/50 & 200/100	0/48 & 48/48	10.5.2022	60	
C4	9/5 EF20 1	800/800 & 400/400	10/12 & 48/48	10.5.2022	60	
C1	9/5 EF20 2	50/100 & 100/200	4/64 & 63/64	12.5.2022	20	
C2	9/5 EF20 2	100/100 & 200/200	46/48 & 48/48	12.5.2022	20	
C3	9/5 EF20 2	100/50 & 200/100	0/48 & 47/48	12.5.2022	20	
C4	9/5 EF20 2	800/800 & 400/400	12/12 & 44/48	12.5.2022	20	air bubble
C1	10/5 EF20 1	50/100 & 100/200	0/64 & 64/64	12.5.2022	20	
C2	10/5 EF20 1	100/100 & 200/200	48/48 & 48/48	12.5.2022	20	
C3	10/5 EF20 1	100/50 & 200/100	0/48 & 46/48	12.5.2022	20	
C4	10/5 EF20 1	800/800 & 400/400	12/12 & 48/48	12.5.2022	20	
C1	10/5 EF20 2	50/100 & 100/200	1/64 & 64/64	12.5.2022	20	
C2	10/5 EF20 2	100/100 & 200/200	48/48 & 48/48	12.5.2022	20	
C3	10/5 EF20 2	100/50 & 200/100	0/48 & 48/48	12.5.2022	20	
C4	10/5 EF20 2	800/800 & 400/400	12/12 & 48/48	12.5.2022	20	
C1	10/5 EF20 3	50/100 & 100/200	0/64 & 64/64	12.5.2022	40	
C2	10/5 EF20 3	100/100 & 200/200	48/48 & 48/48	12.5.2022	40	
C3	10/5 EF20 3	100/50 & 200/100	0/48 & 48/48	12.5.2022	40	
C4	10/5 EF20 3	800/800 & 400/400	12/12 & 48/48	12.5.2022	40	
C1	11/5 EF20 1	50/100 & 100/200	0/64 & 64/64	12.5.2022	40	
C2	11/5 EF20 1	100/100 & 200/200	48/48 & 48/48	12.5.2022	40	
C3	11/5 EF20 1	100/50 & 200/100	0/48 & 48/48	12.5.2022	40	
C4	11/5 EF20 1	800/800 & 400/400	12/12 & 48/48	12.5.2022	40	
C1	11/5 EF20 2	50/100 & 100/200	0/64 & 64/64	12.5.2022	40	
C2	11/5 EF20 2	100/100 & 200/200	48/48 & 48/48	12.5.2022	40	
C3	11/5 EF20 2	100/50 & 200/100	0/48 & 47/48	12.5.2022	40	
C4	11/5 EF20 2	800/800 & 400/400	12/12 & 48/48	12.5.2022	40	
C1	11/5 EF20 3	50/100 & 100/200	0/64 & 64/64	12.5.2022	-	
C2	11/5 EF20 3	100/100 & 200/200	47/48 & 48/48	12.5.2022	-	
C3	11/5 EF20 3	100/50 & 200/100	0/48 & 44/48	12.5.2022	-	
C4	11/5 EF20 3	800/800 & 400/400	11/12 & 47/48	12.5.2022	-	

C1	11/5 EF20 4	50/100 & 100/200	0/64 & 64/64	12.5.2022	-
C2	11/5 EF20 4	100/100 & 200/200	47/48 & 48/48	12.5.2022	-
C3	11/5 EF20 4	100/50 & 200/100	0/48 & 44/48	12.5.2022	-
C4	11/5 EF20 4	800/800 & 400/400	12/12 & 48/48	12.5.2022	-
C1	11/7 DS30 1	50/100 & 100/200	62/64 & 48/64	13.7.2022	-
C2	11/7 DS30 1	100/100 & 200/200	46/48 & 48/48	13.7.2022	-
C3	11/7 DS30 1	100/50 & 200/100	28/48 & 48/48	13.7.2022	-
C4	11/7 DS30 1	800/800 & 400/400	12/12 & 48/48	13.7.2022	-
C1	11/7 DS30 2	50/100 & 100/200	61/64 & 59/64	13.7.2022	-
C2	11/7 DS30 2	100/100 & 200/200	47/48 & 48/48	13.7.2022	-
C3	11/7 DS30 2	100/50 & 200/100	46/48 & 48/48	13.7.2022	-
C4	11/7 DS30 2	800/800 & 400/400	12/12 & 48/48	13.7.2022	-
C1	12/7 DS30 1	50/100 & 100/200	61/64 & 64/64	13.7.2022	-
C2	12/7 DS30 1	100/100 & 200/200	48/48 & 48/48	13.7.2022	-
C3	12/7 DS30 1	100/50 & 200/100	46/48 & 48/48	13.7.2022	-
C4	12/7 DS30 1	800/800 & 400/400	12/12 & 48/48	13.7.2022	-
C1	12/7 DS30 2	50/100 & 100/200	62/64 & 64/64	13.7.2022	-
C2	12/7 DS30 2	100/100 & 200/200	48/48 & 48/48	13.7.2022	-
C3	12/7 DS30 2	100/50 & 200/100	46/48 & 48/48	13.7.2022	-
C4	12/7 DS30 2	800/800 & 400/400	12/12 & 48/48	13.7.2022	-

*Chips:

C1: Channel network in Figure 5i
C2: Channel network in Figure 5ii
C3: Channel network in Figure 5iii
C4: Channel network in Figure 5iv

Table A3. Fabricated channel networks from one SU-8 mold (disk) for the follow-up study with Ecoflex 00-20.

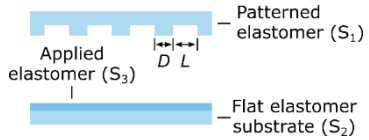

Disk	Date	S_1 (g)	Weight of S_2 (g)	S_3 (g)	Spin speed (RPM)	Partially curing time (s)	Comments
2/7 EF20 1	2.7.2021	26.85	16.15	1.78	1500	60	only C1
2/7 EF20 2	2.7.2021	23.26	20.13	2.52	1500	20–40	
5/7 EF20	5.7.2021	10.76	15.58	1.52	1500	40–60	
7/7 EF20 1	7.7.2021	12.48	15.21	1.23	2000	40–60	
7/7 EF20 2	7.7.2021	13.81	18.58	1.27	1500	60	Flat substrate uneven (2 mm vs. 0.2 mm)
13/7 EF20 1	13.7.2021	11.77	14.15	1.78	1500	60	pre-stretched, flat substrate uneven, smallest channels blocked
13/7 EF20 2	13.7.2021	13.99	14.46	1.17	2000	60	pre-stretched, flat substrate uneven
14/7 EF20 1	14.7.2021	12.73	15.64	1.16	2000	40	C1 did not fit to the flat substrate (alignment error)
14/7 EF20 2	14.7.2021	13.2	17.52	1.61	2000	60	
19/8 EF20 2	19.8.2021	12.46	20.35	1.72	1500	60	pre-stretched
19/8 EF20 1	19.8.2021	13.25	26.76	1.84	1500	40	pre-stretched
25/8 EF20	25.8.2021	11.28	21.48	1.86	2000	40	air bubbles
13/10 EF20 1	13.10.2021	15.98	11.73	1.19	1500	40	
13/10 EF20 2	13.10.2021	15.64	17.92	1.3	2000	40	
13/10 EF20 3	13.10.2021	15.98	19.31	1.28	2000	60	
14/10 EF20 2	14.10.2021	18.16	16.93	1.98	2000	20	
14/10 EF20 1	14.10.2021	16.82	17.61	1.86	2000	20	
14/10 EF20 3	14.10.2021	15.76	18.71	1.92	2000	20	
3/1 EF20 2	3.1.2022	15.86	12.08	1.01	1500	20	
3/1 EF20 1	3.1.2022	15.57	13.81	1.16	1500	20	
5/4 EF20	5.4.2022	14.42	13.81	1.97	1500	20	
26/4 EF20 3	26.4.2022	11.63	13.2	1.7	1500	-	
26/4 EF20 2	26.4.2022	13.81	13.99	1.96	1500	-	
26/4 EF20 1	26.4.2022	11.44	16.4	2.4	2000	-	
27/4 EF20 1	27.4.2022	13.36	13.32	1.87	1500	-	
28/4 EF20 2	28.4.2022	14.16	12.59	1.68	2000	-	
28/4 EF20 1	28.4.2022	10.59	13.32	1.68	2000	-	

Table A4. Fabricated microchannels from Ecoflex 00-20 for the follow-up study.

Chip*	Disk	D (µm) / L (µm)	Open channels (total = 48)	Observation date	Pre-curing time (s)	Comments
C1	2/7 EF20 1	50/200	34	2.7.2021	60	
C1	2/7 EF20 2	50/200	34	2.7.2021	20	
C3	2/7 EF20 2	50/300	0	2.7.2021	40	blocked
C4	2/7 EF20 2	80/140	4	2.7.2021	40	
C1	5/7 EF20	50/200	29	5.7.2021	40	
C3	5/7 EF20	50/300	3	5.7.2021	60	blocked
C4	5/7 EF20	80/140	1	5.7.2021	60	
C1	7/7 EF20 1	50/200	16	8.7.2021	40	curly
C3	7/7 EF20 1	50/300	24	8.7.2021	60	
C4	7/7 EF20 1	80/140	31	8.7.2021	60	curly
C1	7/7 EF20 2	50/200	0	8.7.2021	60	
C3	7/7 EF20 2	50/300	0	8.7.2021	60	
C4	7/7 EF20 2	80/140	0	8.7.2021	60	
C1	13/7 EF20 1	50/200	8	14.7.2021	60	
C3	13/7 EF20 1	50/300	0	14.7.2021	60	
C4	13/7 EF20 1	80/140	0	14.7.2021	60	
C1	13/7 EF20 2	50/200	22	14.7.2021	60	
C3	13/7 EF20 2	50/300	41	14.7.2021	60	
C4	13/7 EF20 2	80/140	36	14.7.2021	60	

C1	14/7 EF20 1	50/200	24	15.7.2021	40	
C3	14/7 EF20 1	50/300	28	15.7.2021	40	
C4	14/7 EF20 1	80/140	12	15.7.2021	40	
C1	14/7 EF20 2	50/200	35	15.7.2021	60	
C3	14/7 EF20 2	50/300	22	15.7.2021	60	half blocked
C4	14/7 EF20 2	80/140	16	15.7.2021	60	
C1	19/8 EF20 1	50/200	0	20.8.2021	40	blocked
C3	19/8 EF20 1	50/300	0	20.8.2021	40	blocked
C4	19/8 EF20 1	80/140	0	20.8.2021	40	blocked
C1	19/8 EF20 2	50/200	47	20.8.2021	60	
C3	19/8 EF20 2	50/300	0	20.8.2021	60	
C4	19/8 EF20 2	80/140	22	20.8.2021	60	curly?
C1	25/8 EF20	50/200	4	25.8.2021	40	
C3	25/8 EF20	50/300	0	25.8.2021	40	
C4	25/8 EF20	80/140	42	25.8.2021	40	
C1	13/10 EF20 1	50/200	18	14.10.2021	40	
C3	13/10 EF20 1	50/300	0	14.10.2021	40	
C4	13/10 EF20 1	80/140	39	14.10.2021	40	
C1	13/10 EF20 2	50/200	40	14.10.2021	40	
C3	13/10 EF20 2	50/300	47	14.10.2021	40	
C4	13/10 EF20 2	80/140	48	14.10.2021	40	
C1	13/10 EF20 3	50/200	45	14.10.2021	60	
C3	13/10 EF20 3	50/300	34	14.10.2021	60	
C4	13/10 EF20 3	80/140	47	14.10.2021	60	
C1	14/10 EF20 1	50/200	40	29.12.2021	20	
C3	14/10 EF20 1	50/300	23	29.12.2021	20	
C4	14/10 EF20 1	80/140	25	29.12.2021	20	
C1	14/10 EF20 2	50/200	47	29.12.2021	20	
C3	14/10 EF20 2	50/300	29	29.12.2021	20	
C4	14/10 EF20 2	80/140	20	29.12.2021	20	
C1	14/10 EF20 3	50/200	46	29.12.2021	20	
C3	14/10 EF20 3	50/300	0	29.12.2021	20	
C4	14/10 EF20 3	80/140	38	29.12.2021	20	open and undeformed!
C1	3/1 EF20 1	50/200	36	4.1.2022	20	
C3	3/1 EF20 1	50/300	1	4.1.2022	20	
C4	3/1 EF20 1	80/140	30	4.1.2022	20	curly
C1	3/1 EF20 2	50/200	5	4.1.2022	20	
C3	3/1 EF20 2	50/300	0	4.1.2022	20	
C4	3/1 EF20 2	80/140	30	4.1.2022	20	curly
C1	5/4 EF20	50/200	0	11.4.2022	20	
C3	5/4 EF20	50/300	0	11.4.2022	20	
C4	5/4 EF20	80/140	31	11.4.2022	20	
C1	26/4 EF20 1	50/200	44	26.4.2022	-	
C3	26/4 EF20 1	50/300	12	26.4.2022	-	
C4	26/4 EF20 1	80/140	32	26.4.2022	-	
C1	26/4 EF20 2	50/200	3	27.4.2022	-	
C3	26/4 EF20 2	50/300	0	27.4.2022	-	
C4	26/4 EF20 2	80/140	3	27.4.2022	-	
C1	26/4 EF20 3	50/200	0	27.4.2022	-	
C3	26/4 EF20 3	50/300	0	27.4.2022	-	
C4	26/4 EF20 3	80/140	16	27.4.2022	-	
C1	27/4 EF20 1	50/200	0	28.4.2022	-	
C3	27/4 EF20 1	50/300	0	28.4.2022	-	
C4	27/4 EF20 1	80/140	39	28.4.2022	-	
C1	28/4 EF20 1	50/200	44	2.5.2022	-	
C3	28/4 EF20 1	50/300	21	2.5.2022	-	
C4	28/4 EF20 1	80/140	20	2.5.2022	-	
C1	28/4 EF20 2	50/200	46	2.5.2022	-	
C3	28/4 EF20 2	50/300	5	2.5.2022	-	
C4	28/4 EF20 2	80/140	17	2.5.2022	-	

*Chips:

C1: Channel network with 50 µm wide channels and 200 µm thick walls
C3: Channel network with 50 µm wide channels and 300 µm thick walls
C4: Channel network with 80 µm wide channels and 140 µm thick walls